MASTER OF SCIENCE THESIS

DESICCATION, CRUST FORMATION & CONSOLIDATION OF SOFT, COHESIVE SOIL DUE TO ATMOSPHERIC CONDITIONS

A CASE STUDY OF THE MARKER WADDEN

L.H. SIJBRANDIJ

FACULTY OF CIVIL ENGINEERING & GEOSCIENCES: GEO-ENGINEERING

Boskalis
Dredging & Marine Experts

TU Delft

22 JUNE 2017

Visualization of the Marker Wadden

Cover image courtesy of Boskalis

DESICCATION, CRUST FORMATION & CONSOLIDATION OF SOFT, COHESIVE SOIL DUE TO ATMOSPHERIC CONDITIONS

CASE STUDY OF THE MARKER WADDEN

By

Lorraine H. Sijbrandij

In partial fulfillment of the requirements for the degree of

Master of Science
in Civil Engineering

at Delft University of Technology,
to be defended publicly on 26 June 2017

Committee Chair:	Dr. Ir. P. Vardon	TU Delft: Geo Engineering
Company Supervisor:	Ir. T. Vijverberg	Boskalis: Hydronamic
Thesis Committee:	Prof. Dr. Ir. J.C. Winterwerp	TU Delft: Hydraulic Engineering
	Dr. Ir. C. Chassagne	TU Delft: Hydraulic Engineering

Boskalis
Dredging & Marine Experts

TU Delft

This thesis is confidential and cannot be made public until 20-06-2019

An electronic version of this thesis is available at http://repository.tudelft.nl/

Preface

Completing a Master's thesis such as this is never, in reality, a one-woman job. There are so many people who have made this project and its completion possible, and so many people I would like to thank for their patience and assistance. First and foremost, I would like to thank Boskalis and Thomas Vijverberg, for taking a chance on me and giving me the opportunity to work on such a unique project such as the Marker Wadden. Thank you, Thomas, for proving to be one of the best thesis company supervisors I could have ever wished for; your constant presence, input, and willingness to be not only a sounding board but also guide me in the right direction was invaluable. I would also like to acknowledge my thesis committee chairman, Phil Vardon, for his patience and willingness to meet with me whenever and wherever in order to tackle one issue after another. Furthermore, I would like to recognize the efforts of my other committee members, Han Winterwerp and Claire Chassagne, whose invaluable expertise and advice during the (seemingly) countless meetings provided helpful insight into my research and offered ways to improve upon it.

I would also like to thank Roeland Lievens for sacrificing numerous cozy office days for windy and cold ones out testing at the containers with me. Of course, these containers and their setup would not have been possible without the assistance of Boskalis E&I, and I would especially like to thank Bert van Roon, Stefan Ordelman, and Tom Sparreboom for their assistance. In addition, I would like to thank Boskalis Environmental and especially Ivy Raeijmaekers, Johan van der Velden, Chantal van Bergeijk, and Jasper Visser for their help in brainstorming a lab testing plan and analyzing the various samples we collected. Furthermore, I would like to thank Deltares and both Miguel de Lucas Pardo and Marcel Busink for both providing and advising on the various test equipment utilized within the containers.

In addition, I would like to thank my parents, Angie and Arthur, who gave me the unceasing support and encouragement necessary for leaving one country and starting anew in another; this whole journey would not have been possible without them, both literally and figuratively. To my sister Emily, who kept me from missing home with endless care packages and life updates; you helped to keep me on track and provided endless entertainment during my late nights working. I'd also like to thank my Dutchie, who was always willing to put up with my crazy work schedule and indulge me during my stress-relieving rants, even when he might not have understood everything I was talking about. Finally, I would like to thank my friends and family —both near and far— for their support, understanding, and willingness to assist me in any way they could.

Lorraine Sijbrandij
09 June 2017

Abstract

Deterioration of the ecological quality within the Markermeer, due to the elimination of natural flushing and a resulting increase in turbidity, has created a need to revitalize the region for the benefit of the local wildlife. One major way in which this is being achieved is through the Marker Wadden, designed as a wetland area featuring a combination of islands, marsh-pond areas, mud flats, and sheltered shores which will serve as bird and wildlife spawning area. One of the primary innovations within the Marker Wadden project is the utilization of locally dredged material to form many of the wetland areas. This dredged material —often referred to as mud— is characterized as a soft, cohesive, fine-grained soil material with a mixed sediment composition of clay, silt, fine sand, organic material, water, and often gas (Winterwerp and van Kesteren, 2004). This material has a lot of inherent uncertainties in regards to its behavior and use in construction, stemming from its general non-homogeneity and less predictable/studied behavior. When considering the use of this material to construct areas with specifically designated elevation and strength ranges, there are three main processes involved in which the material's behavior and predicted development in varying parameters change significantly. First, the initial settlement of the mixture after it has been dredged, mixed with water, and deposited as a fill layer. Second, the primary consolidation of the material due to self-weight. And third, the additional strength and settlement effects due to desiccation and crust formation once the material surface has been exposed to atmospheric conditions. It is this third process concerning desiccation and crust formation which was assessed in more detail. The assessment includes the outlining of a conceptual model emphasizing two distinct stages of desiccation and crust formation, lab testing to define material behavior during this phase, large-scale testing with various conditions, and finally an evaluation of an existing numerical model for this process. The conceptual model was then compared and validated in part through both physical, in-situ measurements from a large-scale test setup, as well as to a numerical model developed at Delft University of Technology and further adapted for this process. In addition, the numerical model was further utilized as a prediction tool for the Marker Wadden, under various atmospheric conditions and surface water conditions, in order to assess the effects of atmospheric conditions on the desiccation and crust formation process in terms of water content, void ratio, settlement, and strength.

The large-scale test setups —representing three varying degrees of atmospheric conditions and surface water conditions— exhibited similar trends in both the in-situ measurements and modelled results, with increasing levels of active surface water removal and precipitation minimization correlating to increased void ratio profile reduction —and therefore increased desiccation and drying— especially at the surface. However, due to the short-term nature of the large-scale testing, none of the large-scale tests ever reached the second stage of desiccation, and it can be concluded that in the initial stage of desiccation, minimal shear strength development will occur in the surface material. This natural delay in significant shear strength development is also seen in the modelled results for the Marker Wadden, excluding any surface water removal measures. Modelling of variations in surface water conditions show that active removal of surface water promotes faster progression into the second stage of drying, and therefore faster initial development of shear strength. Other significant findings include the long-term stabilization in terms of total additional settlement, and that neither short-term re-submergence of the material surface nor initial seasonal start date will hinder this long-term settlement stabilization. Furthermore, the reality of the large-scale test material, including the presence of increased sand content layers, also highlights the importance of assessing the profile material variation, as deviation between the various in-situ measurement profiles and modelled "uniform" profile results show a high deviation. Modelling of this process is limited to the selection of the proper material input values utilized for the complete profile. During this modelling process, it was determined that the special consideration should be given to how the soil water retention properties are obtained, as well as the hydraulic conductivity relation and values utilized, as small deviations in these inputs impact the model significantly in comparison to other inputs.

Contents

List of Figures

List of Tables

DEFINITIONS

Consolidation— any process which involves a decrease in water content of saturated **soil** without replacement of water by air, and which generally results in a reduction in volume; in this thesis, refers to the additional self-weight consolidation which takes place after the desiccation process has been initiated

Self-Weight Consolidation— "the process whereby excess pore pressures due to the applied stress are allowed to dissipate, resulting in volume change" (Fredlund and Rahardjo, 1993); in this thesis, refers to the initial consolidation which takes place after the material has settled and a surface water layer is above it

Surcharge Consolidation— in this thesis, refers to the part of the consolidation due to the desaturated crust layer acting as an additional overburden upon the rest of the material

Crust— material with significant densification, as well as reduced void ratio, saturation, and permeability; quantified as the unsaturated region between the surface and initial void ratio inflection point in contrast to the expected void ratio profile in terms of depth

Density— ratio of mass to volume

In-situ (bulk) Density, ρ— ratio of total mass to total volume; including water

Dry, ρ_d— ratio of total mass solids to total volume ($\rho_d = \frac{\rho}{(1+w)}$)

Desiccation— "The drying of soils by evaporation and evapotranspiration" (Fredlund and Rahardjo, 1993)

Desiccated Soil— material whose properties have deviated from those at the end of primary self-weight consolidation due desiccation; also includes the material forming the crust

Effective Stress, σ'— portion of the normal stress which drives volumetric changes ($\sigma' = \sigma + u$)

Evaporation— loss of water from within the soil as it turns from liquid to vapor and is carried away from the soil; one component within net precipitation (see **net precipitation**)

Excess Pore Pressure, u'— increase in pore pressure (above hydrostatic conditions) due to sudden undrained loading

Free Water Table, *f.w.t.*— delineation between full saturation and partial saturation

Ground Water Table, *g.w.t.*— also typically known as the water table, it is the delineation between positive and negative pore pressures; pore pressure along the g.w.t. are therefore considered to be zero

Hydrostatic Pressure, u— pore pressure under no water flow conditions

Liquid Limit, LL (w_l)— the moisture content at which the soil transitions between plastic and liquid state (%)

Matric (Capillary) Suction— "the equivalent suction derived from the measurement of the partial pressure of the water vapor in equilibrium with the soil water, relative to the partial pressure of the water vapor in equilibrium with a solution identical in composition with the soil water." (Fredlund and Rahardjo, 1993)

Mud— soft, cohesive, fine-grained soil material with a mixed sediment composition of clay, silt, (fine) sand, organic material, water, and (sometimes) gas which has a water content above its liquid limit (Winterwerp and van Kesteren, 2004)

Net Precipitation— total overall value of precipitation (+) and evaporation (-), combined (see **precipitation** and **evaporation**)

Overburden Pressure— surcharge pressure exerted on the underlying material from newly unsaturated soil

Partially Saturated— soil with saturation less than 100%, but still considered to contain excess water

Plasticity Index, *PI*— the difference between the liquid limit and the plastic limit (PI = LL – PL)

Plastic Limit, *PL* or w_p— the moisture content at which the soil transitions between semisolid and plastic state (%)

Pore-Water Pressure— pressure on particles due to water within the voids

Precipitation— rain or additional water which is introduced to the exposed soil; one component of net precipitation (see **net precipitation**)

Saturated— material whose voids are filled entirely with water (i.e. no air or gas); includes the material within both the saturated and capillary zones

Saturation, *S* (degree of)— ratio of volume of water to volume of voids (%)

Shrinkage Limit, *SL* or w_s— the moisture content at which soil transitions between solid and semisolid state; moisture content where changes in soil mass volume (deformation) no longer occur.

Tension Crack— cracks due to the increase in negative pore-water pressures near the ground surface and resulting shrinkage of the material. (Fredlund and Rahardjo, 1993)

Unsaturated— soil considered to be completely "dry"

Void Ratio, *e*— volume of voids to volume of solids

Water (Moisture) Content, *w* or θ— ratio of the mass/volume of water to mass/volume of solids, respectively.

Nomenclature

A	log-linear hydraulic conductivity parameter	[--]
A_k	SIC effective stress/permeability parameter	[--]
A_{SH}	Shrinkage curve parameter: minimum void ratio	[--]
B	log-linear hydraulic conductivity parameter	[--]
B_k	SIC effective stress/permeability parameter	[--]
B_{SH}	Shrinkage curve parameter: slope defining	[--]
C_{SH}	Shrinkage curve parameter: transition defining	[--]
C1	Large-scale test container 1	[--]
C2	Large-scale test container 2	[--]
C3	Large-scale test container 3	[--]
c_u	Undrained shear strength	[kPa]
e	Void ratio	[--]
E_o	Open water evaporation	[m/s]
E_s	Soil evaporation	[m/s]
G_s	Specific gravity (particle density; excludes pores)	[--]
I_l	Liquidity Index	[--]
I_p	Plasticity Index	[--]
K_S	Saturated hydraulic conductivity	[m/s]
LI	Liquidity index	[--]
LL	Liquid limit	[%]
m_{WRC}	van Genuchten SWRC fitting parameter	[--]
n	Porosity	[--]
n_{WRC}	van Genuchten SWRC fitting parameter	[--]
PL	Plastic limit	[%]
PI	Plasticity index	[--]
q_{ult}	Bearing capacity (Terzaghi)	[kPa]
S	Saturation	[--]
SL	Shrinkage limit	[%]
SCC	Shrinkage (Characteristic) Curve	[%]
$SWRC$	Soil Water Retention Curve	[--]
u	Pore water pressure	[kPa]
w	Gravimetric water (moisture) content	[%]
w_l	Liquid limit	[%]
w_p	Plastic limit	[%]
w_s	Shrinkage limit	[%]
WCR	van Genuchten parameter: Residual water content	[--]
WCS	van Genuchten parameter: Saturated water content	[--]

α	van Genuchten SWRC fitting parameter	[--]
ϕ	Soil suction (matric potential)	[kPa]
θ	Volumetric water content	[--]
ρ	In-situ (bulk) density	[kg/m^3]
ρ_b	Dry density	[kg/m^3]
ρ_w	Density of water	[kg/m^3]
σ	Total stress	[kPa]
σ'	Effective stress	[kPa]
τ	Shear strength (in-situ vane)	[kPa]

1 Introduction

This section provides information regarding the Markermeer area, including an overview of the Marker Wadden project and its motivation. Included in this section is a brief discussion of previous relevant research work, as well as the motivation behind this research in regards to the Marker Wadden and its design. From this motivation, focused research objectives were formulated in order to establish the scope of this research.

1.1 The Markermeer

The Marker Wadden project, identified in Figure 1-1, is located within the Markermeer lake, which is part of the Ijssel region in the Netherlands. The Ijssel region was initially part of the Zuiderzee saltwater inlet of the North Sea before the construction of the Afsluitdijk and the creation of the freshwater Ijsselmeer lake area in 1932. With the original intention of further land reclamation, the Houtribdijk was constructed in 1976 by the Rijkswaterstaat, establishing and cutting off the Markermeer area from the Ijsselmeer. However, the Markermeer reclamation never took place, and today the Markermeer is a 700 km^2 lake situated between the provinces of Flevoland and North Holland with a depth ranging between two to four meters (Natuurmonumenten, 2014).

Figure 1-1: Map showing location of the Marker Wadden (www.nos.nl)

The Markermeer is part of a protected area designated as a Natura 2000 region (Atlantic). These Natura 2000 regions aim to conserve species and wildlife habitats throughout Europe (European Commission, 2016). The Markermeer region has been specifically designated as a bird directive site (European Environment Agency, 2011).

1.2 The Marker Wadden Project

Figure 1-2: Conceptual drawing of the Marker Wadden (courtesy of Boskalis)

After the Markermeer was cut off from the Ijsselmeer, natural flushing of the lake came to a halt. This —as well as partial land reclamation— has resulted in both the loss of natural banks as well as a built-up silt layer of fine sediments forming at the bottom of the already relatively shallow Markermeer. Not only does this 'fluffy' silt layer suffocate bottom-dwelling organisms, including plants and algae, but it also causes turbidity in the water column as a result of resuspension of this layer. This results in an increase of light attenuation within the lake due to floating sediments, further adversely impacting both the water and ecological quality within the lake. This issue affects not only fish and plant life in the lake, but also the birdlife within the area which relies upon the Markermeer as a food source provider. A decline of more than 75% in both the tufted duck and common goldeneye populations since the 1980s has been observed within the area (Natuurmonumenten, 2014).

To address this decline in wildlife and create a diverse habitat for birds within the Markermeer, the Marker Wadden project was developed by the Dutch Society for Nature Monuments (Vereniging Natuurmonumenten), supported by partners ANWB and VNO-NCW, and executed by the dredging contractor Boskalis. The Marker Wadden is an ongoing "Building with Nature" project which aims to utilize local natural materials and natural processes to create a bird and wildlife marshland area. A visualization of the Marker Wadden area can be seen in Figure 1-2.

1.2.1 Design & Construction

The Marker Wadden, is designed to be a wetland area and is meant to improve the ecological value of the Markermeer. This wetland area will feature a combination of islands, marsh-pond areas, mud flats, and sheltered shores which will serve as birdlife spawning area. This will be accomplished through the creation of artificial islands in the northeastern part of the Markermeer using locally dredged clay materials. Extended sand berms will outline sheltered main island areas which will be comprised of smaller basins. These basins will then be filled with locally dredged mud material taken from the lake bottom to form elevated land areas which can then be cultivated for vegetation and bird habitat areas (Natuurmonumenten, 2014).

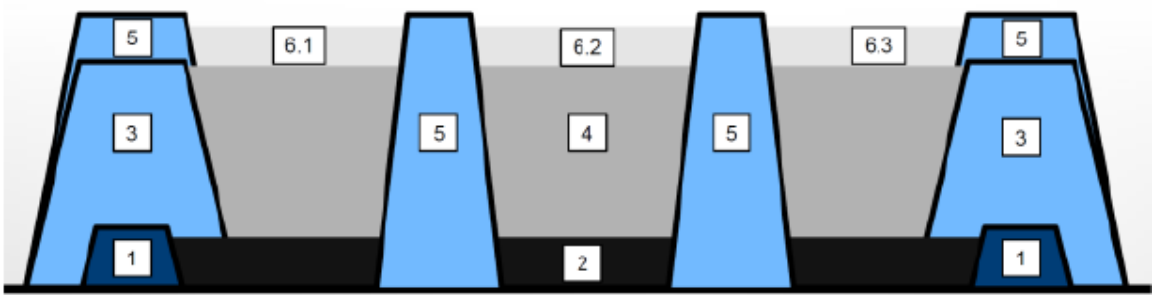

Figure 1-3: Sequential design & construction of Marker Wadden compartments (Vijverberg et al., 2016)

Figure 1-3 shows the distinct layering and construction sequence of the Marker Wadden project, and are as follows:

- **1** initial sandy berms are constructed
- **2** first clay-water mixture filling of main compartment
- **3** main sandy berms raised to water level
- **4** second clay-water mixture filling of main compartment
- **5** intermediate sandy berms constructed to create sub-compartments; all berms (including initial ones) are raised above water level
- **6** third clay-water mixture filling of sub-compartments (6.1, 6.2, and 6.3)

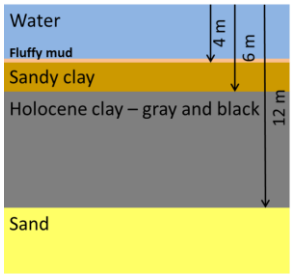

Figure 1-4: Soil profile of the Markermeer adapted from (van Olphen, 2016)

The clay-water mixture is comprised of material dredged from a Holocene clay layer within a borrow pit located nearby, and after dredging and being mixed with water has an initial density of approximately 1200 kg/m^3. A general soil profile of the Markermeer bed —including the Holocene clay layer in which the material is taken from— can be seen in Figure 1-4. The clay-water mixture is transported and pumped into the compartments, with a spreader pontoon being utilized within the compartments themselves in order to fill the compartments in more controlled, thin, layers (Vijverberg et al., 2016).

1.2.2 Current Progress

Construction of the first main section of the Marker Wadden commenced in March 2016, with the first main island's sand berms emerging from the lake in May 2016. This first phase of the Marker Wadden project can be seen in Figure 1-5 and Figure 1-6 (Boskalis, 2015). This area, which is approximately 4 km from the Houtribdijk, consists of a 5 km^2 nature island with a 10 km^2 marsh-pond area (Natuurmonumenten, 2014). Filling of the basins within the first main island is still taking place, with new fill layers being added over time (Roels, 2015). Some of this area is being designated as a testing

site for various future innovative aspects of the Marker Wadden, including things such as vegetation and further academic research.

Figure 1-5: Marker Wadden render outlining main compartment A (Roels and Jacobs, 2015)

(a) main compartment A construction

(b) sand berms and initial filling stage

Figure 1-6(a)(b): Progress photos of Marker Wadden (©John Grundlach) (Vijverberg et al., 2016)

1.3 Motivation & Problem Description

In the typical construction of artificial islands and land reclamation projects, sand is the preferred primary building material due to its beneficial and relatively predictable properties and behavior, as well as its relatively high bearing capacities. However, this sand must typically be imported and transported from other locations in order to meet the quantity required for construction, increasing project costs with minimal added benefits for the local region and ecology.

Because of this, as well as other ecological benefits, the possibility of utilizing locally dredged materials is now being considered more and more as a potentially viable alternative. However, the use of this typically soft, cohesive, and fine-grained material comes with its own difficulties and uncertainties, stemming from its general non-homogeneity and less predictable/studied behavior.

When considering the use of this mud material to create areas within a specified design requirements such as elevation, time, and strength, there are three main processes which must be evaluated, as conceptualized in Figure 1-7. These include 1) the settlement of the mixture after it has been dredged, mixed with water, and deposited as a fill layer; 2) the primary consolidation of the material due to self-weight; and 3) the additional strength and settlement effects due to desiccation and crust formation once the material surface has been exposed to atmospheric conditions.

Previous studies have been performed on dredged material and various aspects of atmospheric drying, such as crack formation, desaturation, and changes in volume. Additionally, studies on the dewatering and densification of dredged material have typically only studied the maximum amount of settlement which can be estimated in order to make space for additional fill layers. This results in a more general overview of the total settlement rather than a careful assessment of the effects of the crust, its strength, and its effects on the saturated underlying material. However, the Marker Wadden requires a careful balance between consolidation and strengthening in order to minimize the amount of material required while still meeting both strength and elevation requirements. Therefore, it is the unique surface elevation and strength requirements that generally drive this project, by highlighting the necessity for a careful desiccation and crust formation study.

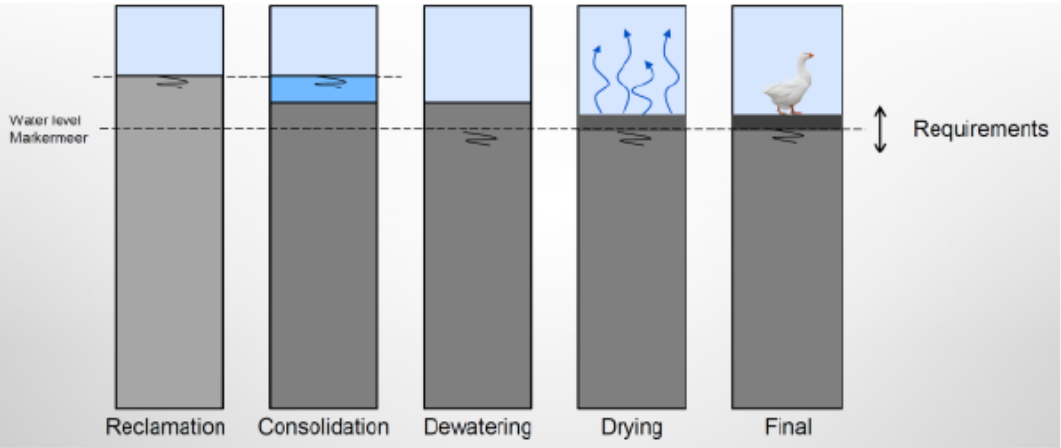

Figure 1-7: Complete process from reclamation to final conditions (Vijverberg et al., 2016)

1.3.1 Elevation Requirements

Dependent upon the area within the Marker Wadden being considered, there are different elevation requirements which have been established in reference to seasonal water levels. For the specific marsh-pond areas being considered (designated as 'plas-dras') in relation to this research, the following elevation requirements have been set:

- Based on a summer water level elevation of -0.20 m NAP, the surface elevation of the plas-dras area within the marsh must fall within +/- 0.2 m of the summer water levels. This means an acceptable elevation variation between -0.40 m NAP and 0.00 m NAP.
- At any given time, at least 50% of the total plas-dras area must be above the summer water level
- However, an additional restriction is that only 20% of this area can have an elevation higher than specifically required.
- All elevation requirements must be met by the end of 2020 as well as an additional 5 months later (Roels and Jacobs, 2015).

This means that both achieving the desired elevation and obtaining it by a certain time after filling are important priorities, especially when considering the effects of crust formation and consolidation. If too much deformation and consolidation of the fill material occurs, then the project elevation requirements will not be met and remedial design and construction modifications must take place, costing not only both money and time, but also potentially harming any initial vegetation development which may take place within the first years.

1.3.2 Strength Requirements

As the Marker Wadden is cited as a bird and wildlife habitat, it is important that the area be able to support that life, especially in the literal sense of the word. Therefore, it was designated by Natuurmonumenten that certain areas within the Marker Wadden must be able to support the landing and moving weight of a goose. From an approximate weight and footprint of a typical male goose, the required undrained shear strength was determined using the Prandtl failure mechanism and formula. The following strength specifications for the Marker Wadden have been established:

- 80% of the plas-dras area must be able to support the weight of a goose.
- Minimum undrained shear strength of 3 kPa
- Minimum bearing capacity of 15 kPa (Turnhout, 2016).

However, it should be emphasized that higher bearing capacities are allowed and encouraged, as long as it does not adversely affect the project, its construction, or in meeting other design requirements. The main focus of this study is to determine the shear strength values which can be met, and to assess approximately how long this development would need to take place in various atmospheric conditions.

1.3.3 Uncertainty

As mentioned previously, working with this dredged material comes with a multitude of uncertainties. One of the primary concerns to consider is that although it is generally assumed that the material is homogenously mixed during the dredging process to a uniform initial density, this is in fact not the case.

Initial densities of the material vary considerably, especially when considering the scale of the basins being filled and the limitations of the transportation and basin filling process. A visual confirmation of this can be seen in Figure 1-8, with the denser exposed material visible close to the fill pipe outlet compared to the further submerged material, which has a lower initial density in comparison due to the pumping and filling process. This variability in density is then further affected by the settlement process and additional fill layers atop the initial material. Additionally, other aspects such as potential sand segregation and variations of density profiles within an area also increase the uncertainty of final conditions.

Figure 1-8: A Marker Wadden filling (outlet) pipe, taken on 12-07-2016

1.4 Previous Research

Previous research concerning the Marker Wadden material initial settlement and self-weight consolidation was conducted by Emmeline van Olphen presented in her thesis entitled "Consolidation behavior of soft cohesive soils, the correlation between different scale model tests: case study of the Marker Wadden." In essence, van Olphen's research covers the development stages directly prior to those covered in this research, such as the settlement and primary consolidation of the material, just after filling the compartments (van Olphen, 2016). Because of the clear connections and correlations between these two subjects, certain aspects of van Olphen's project, such as her general findings and large-scale test setup, are utilized and will be referenced throughout this research.

A study of the effects of atmospheric drying on the dredged material of the Marker Wadden has been performed by Phil Vardon of TU Delft during the initial design phase, through the use of a numerical model (Vardon et al., 2015). This model will be further utilized within this research to validate the findings and conclusions of this research. In addition, sensitivity testing of the primary inputs required to run the model will be performed on varying soils in the laboratory. These input variations will then be put into the model to assess the effects and changes in predicted desiccation.

1.5 Research Objectives

Based on the existing literature and an evaluation of the design considerations of the Marker Wadden project and the necessity for knowledge concerning crust formation, the following research question has been posed for this research:

What are the effects of evaporation & precipitation conditions on desiccation and crust development in terms of time, strength, and consolidation?

In order to properly tackle and assess this question, the following sub-objectives have been defined in order to more accurately outline the approach which will be used to evaluate crust formation throughout this research:

What is the evolution of desiccation and crust formation in soft, cohesive, fine-grained soil material?

The aim of this sub-objective is to more clearly define and explain the desiccation and crust formation process as it occurs with this specific material, through the use of a conceptual model. This model will initially be outlined based on existing literature and studies, and then further refined. It will serve as the basis of understanding for further assessment of crust formation. This conceptual model will highlight the main factors of crust formation and will include theoretical simplifications and assumptions, which will be outlined and discussed. Furthermore, this model will be compared to both physical and modelled results for additional assessment.

How can this process be modelled, and which parameters significantly affect the model's output prediction —and therefore theoretically the desiccation, crust formation, and consolidation of the soil?

This objective will focus on assessing the numerical model utilized during the design phase of the Marker Wadden, beginning with a discussion of the challenges and limitations present when modelling this process. This model will then be used to compare the results seen in the large-scale tests to those output by the model, an in essence will serve as an analysis of measured results versus modelled results. Furthermore, the model's primary input parameters will be assessed in order to identify the material parameters whose variance result in the largest differences in model output during a sensitivity analysis of the model.

What is the effect of atmospheric and surface water conditions on desiccation, crust development, and consolidation?

Desiccation and crust formation of a soil is driven by the atmospheric conditions experienced once the surface has been exposed, including precipitation and evaporation. This sub-objective will focus on assessing the extent and influence of atmospheric conditions on the material in terms of time, strength, and consolidation of the material. These will be assessed through monitoring the soil in naturally exposed containers open to the atmosphere, with careful noting of changing environmental conditions. Moreover, this will be assessed by encouraging differences in development through test setup variations, including 'natural', 'assisted', and 'exacerbated' conditions to encourage the desiccation and crust formation process. Additionally, other influencing factors such as seasonal variations and surface water conditions will be assessed through the numerical model.

1.6 Approach & Limitations

The focus and scope of this research is somewhat constrained due to time limitations, but also in terms of what can be discussed in depth. The ideal culmination of this research and its research is to not only better explain and predict desiccation and crust development as well as its effects on consolidation of the underlying material, but to also provide practical recommendations for the Marker Wadden project in regards to crust formation, so that the proper strength and elevation requirements can be better achieved.

One aspect of this research consists of large-scale testing to observe and monitor changes in the soil profile under various natural and assisted atmospheric conditions. Furthermore, these conditions and results are used to compare and validate an existing numerical model for the consolidation and atmospheric drying of soft, fine grained, cohesive material. Both general and specialized lab tests are conducted in order to assess the variance of select material parameters. Moreover, a sensitivity analysis of the numerical model itself is compiled based on these lab tests, in order to determine the most optimal model conditions as well as the parameters which need careful consideration. Finally, based on the results and analysis, a discussion of desiccation and crust formation in terms of practical applications is presented.

As with many thesis projects, there are numerous practical limitations due to time, scope, and result goals. Excess consolidation of the underlying material is an important consideration which will be extensively discussed throughout this research; however, the secondary effects of the filling material and crust as an additional load on the Markermeer is not be addressed. While this is something which should be considered during realistic project design, the aim of this research is focused entirely on the desiccation of the filling material, rather than its additional influence on the supporting Markermeer bed.

Furthermore, while various potential organic and chemical effects on crust formation are discussed briefly, their exact amount of influence is not be investigated in detail during the testing period. Moreover, while wetting and drying cycles are experienced by the soil through natural precipitation and evaporation periods, only the overall effects will be assessed, rather than the detailed influence of each of these individual cycles on the desiccation of the soil and its properties.

Finally, it should be noted that as this research is especially limited in time, it is expected that full desiccation and crust formation and resultant long-term strength and settlement will not take place within the period of the large-scale testing. The testing timeline is therefore not a complete overview of the atmospheric conditions that will take place over the Marker Wadden's construction and lifetime.

1.7 Report Outline

Chapter 1 gives a brief overview of the Marker Wadden project, the motivation behind this research study, its research objectives, approach, and some practical limitations. Chapter 2 provides the relevant knowledge needed in the evaluation and analysis of desiccation and crust formation, including an overview of the soil characterizations; main properties used to observe changes which occur within the soil over time; and a discussion of the processes leading up to desiccation and later stages. This information is then brought together in Chapter 3 to provide a detailed conceptual model of the desiccation and crust formation process, including a discussion on the application of the model in this research. Chapter 4 then explains the methodology utilized in the current research, in terms of testing timelines, testing variations, and setup. Also included within this chapter are explanations of the tests and equipment utilized, as well as information regarding the numerical model and its usage for comparison and validation. Chapter 5 presents the findings and data from the testing period, initial lab test results, as well as the numerical model simulations. For ease, this section also includes an initial analysis of results from the large-scale testing, lab tests, and numerical model simulations. Chapter 6 provides a more comprehensive analysis of data and findings from the testing, as well additional remarks on data uncertainties, inconsistencies, and potential sources of error. Finally, Chapter 7 presents the final conclusions drawn from this research, practical applications and implications of the findings for the Marker Wadden. Also included in this chapter is a discussion of potential improvements of various testing aspects utilized within this research work, as well as a brief discussion of further research recommendations.

2 Literature Review

This section provides a theoretical background relevant to the research of desiccation and crust formation. First, an in-depth description of the dredged material, relevant properties, classification, and behavior is presented. Following this is a theoretical overview of the processes that typically take place prior to desiccation in relation to dredged material, as well as a further discussion on empirical parameters that can be used to map the behavior of, as well as changes within, the material. All of these aspects are brought together in Chapter 3 in the form of a more comprehensive, integrated, and sequential conceptual model of crust formation.

2.1 Dredged Material

This section serves to provide a more in-depth discussion of the dredged material being considered within this research and also offers insight into how this material, its properties, and behavior can be quantified and assessed.

2.1.1 Terminology & Composition

The colloquial term for the soil being considered in this project is "mud". However, this is a general term which does not accurately convey details about the material's properties and behaviors, and in fact can be used to describe a multitude of soil materials. In a geotechnical and hydraulic engineering context, this mud –which can also be referred to as a cohesive sediment- can more accurately be described as a soft, cohesive, fine-grained soil with a "mixed sediment composition of clay, silt, (fine) sand, organic material, water, and (sometimes) gas" (Winterwerp and van Kesteren, 2004). Within this research, the term mud, soil, and dredged material is used interchangeably.

This dredged mud material has many other properties that must be considered when assessing and predicting its behavior under various conditions, especially consolidation and crust formation. These include its granular, mineral, and organic composition, as well as the initial conditions of the material after it has been dredged, deposited, and consolidated.

2.1.1.1 Granular Composition

One of the main components that governs the mechanical behavior of a cohesive sediment is the specific granular soil types which are present within the mud. As explained before, mud sediment is comprised of varying amounts -or fractions- of clay, silt, and sand. These material fractions are generally differentiated based on particle size. The defined particle size limits that categorize clay from silt, and silt from sand can vary based on the standards being utilized.

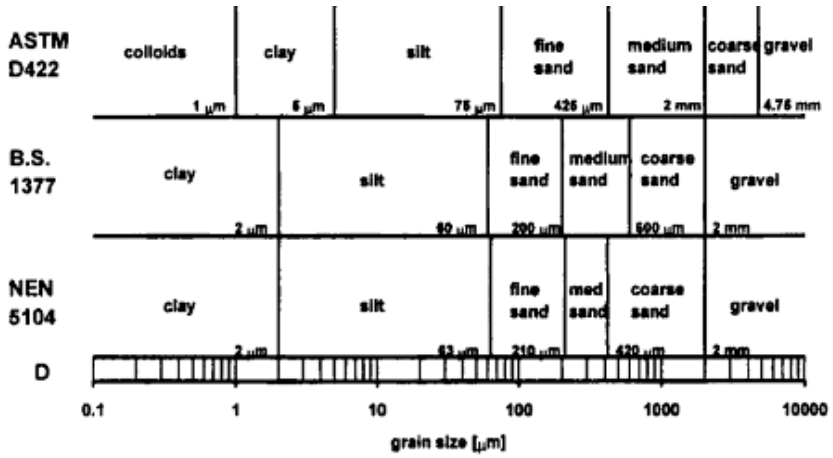

Figure 2-1: Grain size classification standards, adapted from (Winterwerp and van Kesteren, 2004)

A comparison of the three main standards used when classifying the material fractions present within the sediment can be seen in Figure 2-1. It should be noted that the primary classification which will be utilized within this research are the Dutch (NEN) standards unless otherwise indicated. This means that any particles with a grain sizes less than 2 µm will be considered part of the clay fraction, particle sizes greater than 63 µm will be considered part of the sand fraction, and any particles between 2 µm and 63 µm considered to be silt.

Identifying the fractions present within the dredged material is important in order to understand its mechanical behavior, especially with respect to the observed clay fraction. The clay fraction is the main determinant for the ductile, or cohesive, behavior of the material (Winterwerp and van Kesteren, 2004). Later sections will discuss the exact fraction distribution and composition of the dredged material being used in this research (as well as in the Marker Wadden).

Merkelbach and Kranenburg state that if at least 10% of the dredged material volume is comprised of clay, then it can be assumed that the presence of silt and sand can be considered as a passive presence, as the cohesive clay fraction will be the determining factor in terms of behavior. It is already known that this material has a clay fraction above the minimum 10% required to dominate the ductile and cohesive element of the total sediment behavior, therefore resulting in the usage of the term "cohesive sediment" when referring to the dredged material (Merckelbach and Kranenburg, 2004).

2.1.1.2 Mineral Composition

The term 'clay' generally refers to a material comprised of mineral particles, which in combination with varying water contents demonstrate ductile and cohesive properties (Murthy, 2003). Varying mineral compositions can play a role in determining not only the cohesive behavior of the sediment based on the properties of the minerals, but even its general permeability range. Because of this, it is important to assess not only the clay fraction, but also the mineral composition within the material itself.

Preliminary designation of the mineral composition includes determining the presence of silicates and non-silicates. Common silicates which can be present in a marine sediment include quartz, feldspar, and various clay minerals such as kaolinite, illite, smectite (montmorillonite), and chlorite. The presence of non-silicate mineral solids such as salt precipitates, oxides, and hydroxides are dependent upon not only the silicates present, but also the chemical conditions within the sediment (Winterwerp and van Kesteren, 2004).

2.1.1.3 Organic Composition

In addition to the determination of mineral composition, it is also important to ascertain the presence and degree of organic material within the sediment. Organic matter can be present through natural transportation and deposition, or as a result of biological processes and organisms within the sediment which can also be referred to as the detritus organic content. This organic matter can result in the formation of gases such as methane and carbon dioxide within the bed, which can become entrapped as gas bubbles within the sediment itself (Winterwerp and van Kesteren, 2004). Furthermore, the degree of organic matter present can affect the properties of the soil as well as the magnitude of consolidation which can occur.

While the organic matter and its influence on crust formation is not the primary focus of this research, it is nonetheless important to address and recognize the potential effects it can have upon the material and its properties.

2.1.2 Chemical Aspects

As mentioned previously, the mineral content within the material is an important characterization of the soil in terms of predicting its properties and behavior. The occurrence of the non-silicates aspect of the mineral content is highly dependent upon the chemical conditions within the soil and water present. This includes considerations such as the availability of oxygen, as well as the presence of iron (Fe), calcium (Ca), magnesium (Mg), and manganese (Mn) and their reduced states (Winterwerp and van Kesteren, 2004). Generally, the chemical (and even organic) state of the material can be assessed through the material's redox potential and pH.

A more detailed assessment of the effects of pH on fine, cohesive, sediment in regards to the Marker Wadden was performed by Erik Hendriks in his thesis entitled "The effect of pH and the solids

composition on the settling and self-weight consolidation of mud". It was determined that the effects of pH on the primary stages of settlement and consolidation were increased in soils with higher plasticity values. However, no large changes in pH are expected to take place within the context of the Marker Wadden (Hendriks, 2016).

2.1.1 Biological Aspects

There are a multitude of organisms which can be found within marine sediment –and that can influence the properties and behavior of the sediment– including animals, plants, and bacteria. The organisms most relevant to the discussion of crust formation are the fauna and bacteria which reside in the benthic layer, and are commonly referred to as part of the benthic community. The benthic layer encapsulates the seabed layer which is comprised of soft sediment. Some relevant examples of benthic life include meiofauna and tubifex. These organisms can also produce detritus material on and within the soil.

De Lucas Pardo remarks that Markermeer material with a significant benthic presence, exhibited increased permeability during the first consolidation phase in comparison to material without benthic life. This is due to the bioturbation caused by the meiofauna, resulting in holes, burrows, and tunnels within the sediment profile. Furthermore, it was found that sediment profiles with benthic organisms can show a 20% effective stress decrease in comparison to a sediment profile without benthic life after primary consolidation takes place. This is due to the irregular changes within the sediment matrix due to bioturbation (de Lucas Pardo, 2014).

2.2 Overview of Complete Process

Desiccation is only one stage of the complete settlement and overall consolidation process. This section focuses on providing a general overview of the complete process by breaking down and briefly discussing the distinctive stages leading up to desiccation and crust formation. However, for a more detailed investigation of desiccation and the development of the crust as well as the various drivers and state changes, see Chapter 3.

The overall process that takes place can be seen in Figure 2-2. This includes the hindered settlement phase, primary (or 1st phase) consolidation, desiccation and crust formation, and finally the additional surcharge (or 2nd phase) consolidation.

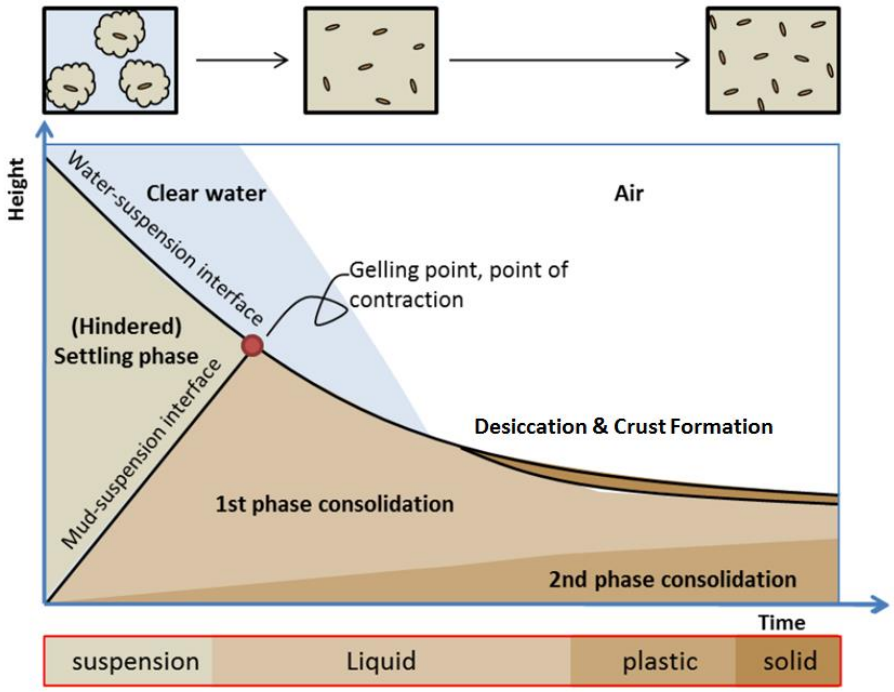

Figure 2-2: Evolution of deposited cohesive sediment over time, adapted from (van Olphen, 2016)

2.2.1 Hindered Settlement

Initially the dredged material is homogenously mixed and pumped into a contained area where minimal disturbance and turbulence occurs. At this stage, the dredged material is in a suspended state as the mud flocs start to settle, and aggregate to form a mud bed. As the mud flocs settle and begin to hinder one another, the concentration/density of the mud material begins to increase, until the gelling concentration is reached and a space-filling matrix is formed. The end of the hindered settlement phase is reached not only once this gelling concentration is reached and most of the material has separated and settled, but it also indicated by the presence of a clear mud-water interface between the mud bed and the water above it (van Olphen, 2016). This moment of gelling concentration can be seen in Figure 2-2.

2.2.2 Self-Weight Consolidation

After hindered settlement takes place, the material is considered to transition from a suspended state into a liquid state and the material will then start to consolidate under its own weight. As can be seen in Figure 2-2, this results in large vertical deformations throughout this phase, as water is essentially squeezed out of the matrix. During this stage, excess pore water pressures dissipate over time and the effective stresses are considered to be minimal. In general terms, the end of this stage is assumed to be reached once a stabilization of the mud-water interface occurs. The complete dissipation of excess pore pressures can also be observed if measured pore pressures reflect anticipated pore pressures under hydrostatic conditions.

It should be noted that even after this process takes place, excess water is still atop the consolidated material (which is not accurately conveyed in Figure 2-2). This inhibits desiccation —due to atmospheric conditions— from taking place, until the excess water evaporates or is actively removed and the mud surface is exposed. Furthermore, the effects of an additional fill layer atop an original layer of material, in which the self-weight process is ongoing, should also be considered. However, this was not considered to be within the scope of this research.

2.2.3 Desiccation & Crust Formation

Once the surface of the material is exposed to atmospheric conditions, the next stage in the process can commence. Cargill defines desiccation as a “removal of water by changing the state of the water near the surface from a liquid to a gas” and states that the primary drivers of this state change is evaporation and transpiration (Cargill, 1985). From previous studies, it has been determined that evaporation from a dredged material occurs in two identifiable stages, referred to as the first and second drying stages. In the first stage of desiccation, all of the material is considered to remain saturated and evaporation can take place at close to its full potential rate, or in other words, at full efficiency.

However, after a certain point the water being drawn up from within the soil can no longer meet the requirements of full evaporation efficiency. It is at this point that the second stage of desiccation begins and a crust begins to form on the surface of the material as the material finally begins to lose saturation and significantly densify. In addition, the evaporation efficiency is no longer constant, but reduces based on both the water table and crust thickness. It is also possible that “negative desiccation” may occur; this may take place- “if water is lost because consolidation exceeds potential evaporation desiccation” (Stark et al., 2005a). By this, it is meant that the water leaving the surface of the material builds up atop the material surface as it exceeds the maximum rate of evaporation which can occur.

As desiccation takes place, changes in the soil profile and its various properties also occur. These property changes are driven mainly by the changing water content and densification of the material. The way these changes can be characterized and defined is more clearly explained in section 2.4 Soil Profile Conditions & Relations.

2.2.4 Surcharge Consolidation

Prior to the start of the second stage of drying, the dredged material is considered to be buoyant and saturated. However, once the water table drops within the material and the top layer eventually desaturates, it becomes less buoyant and an increase in effective weight is observed (Haliburton, 1978). This increase in weight of the top material serves as an additional load atop the underlying material, causing further self-weight consolidation of the material as it ‘squeezes’ out water from lower material.

The total effect of the drying of the top layer and the consolidation of the lower saturated material can be seen in the vertical settlement of material (Stark et al., 2005b).

2.3 Environmental Conditions

There are many factors which can potentially affect the desiccation and formation of a crust layer, some of which can be seen in Figure 2-3. These include some of the following:

- Solar Radiation & Cloud Cover
- Temperature, Humidity, & Wind
- Precipitation & Evaporation
- Groundwater Table
- Vegetation & Root System
- Surface Drainage

This section of the literature review is aimed at providing a brief overview of each of these, as well as —for the more relevant influencers— how to generally quantify these effects.

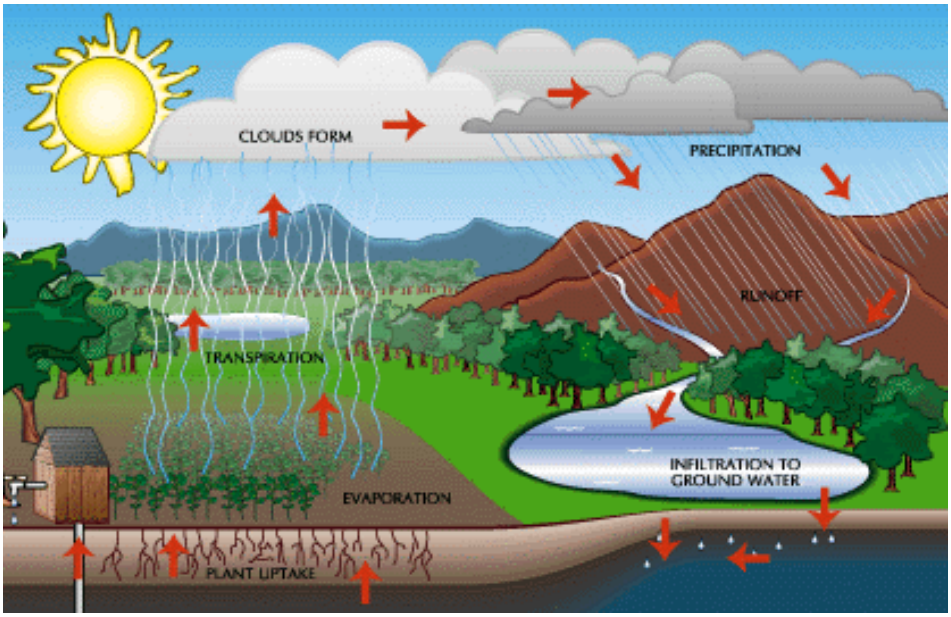

Figure 2-3: Environmental components, water cycle (www.fewresources.org)

2.3.1 Atmospheric Conditions

Perhaps the most obvious driver of desiccation and crust formation of dredged material are the atmospheric conditions present. While the main influencer of crust formation is the evaporation, an understanding of additional atmospheric conditions, such as temperature, precipitation, humidity, wind, and surface conditions is critical in order to properly assess the effects of evaporation as well as how desiccation and crust development will take place.

2.3.1.1 Evaporation

Evaporation is defined as the transfer of water from liquid state into gaseous state, and can occur through either direct evaporation or transpiration (Luxemburg and Coenders, 2015). Direct evaporation as it relates to crust formation occurs in primarily two ways, depending on the presence of free water above the mud surface. If excess surface water is present, the direct evaporation which takes place is considered to be 'open water' evaporation, E_o, in which the amount of water available for evaporation is not restricted in any way. The second type of direct evaporation is referred to as 'soil' evaporation, or E_s, in which the water which is being vaporized is considered to be moisture from within the soil itself. Hence, this type of evaporation is limited by the amount of moisture present within the soil (Luxemburg and Coenders, 2015).

Evaporation is driven primarily by energy from solar radiation, which itself is dependent upon multiple factors, including:

Atmospheric Conditions
- Wind Velocity
- Relative Humidity
- Temperature
- Solar Radiation

Surface Conditions
- Albedo
- Roughness
- Covered Fraction

The most common method used to calculate the potential open water evaporation in a specific location is the Penman equation, in which the evaporation is computed in meters per day [m/d]. The Penman equation is as follows:

$$E_p \approx E_o = \frac{\frac{sR_n}{\rho\lambda} + \frac{c_p\rho_a}{\rho\lambda}\frac{(e_s - e_a)}{r_a}}{s + \gamma} \qquad [\ 2\text{-}1\ ]$$

In which,

R_n	net radiation on the earth's surface [J d^{-1} m^{-2}]
λ	latent heat of vaporization≈ 2.45*10^6 [J/kg]
s	slope of saturation vapor pressure-temperature curve [kPa/°C]
c_p	specific heat of air at constant pressure≈ 1004 [J kg^{-1} K^{-1}]
ρ_a	density of air≈ 1.205 [kg/m^3]
ρ_w	density of water≈ 1000 [kg/m^3]
e_a	actual vapor pressure in the air at 2 m height [kPa]
e_s	saturation vapor pressure for the air at 2 m height [kPa]
γ	psychrometer constant≈ 0.066 [kPa/°C]
r_a	aerodynamic resistance [d/m]

For an in-depth look at how the daily evaporation is calculated, please see the Appendices in the section Evaporation Calculations. As transpiration is due to the presence of vegetation this aspect will be covered in section 2.3.3 Vegetation.

2.3.1.2 Temperature

Temperature plays an important role not only in determining the amount of potential evaporation that can take place, but can also effect the soil in additional ways. If the temperature drops to below freezing, evaporative drying of the soil is no longer possible due to the freezing of the pore water within the material. However, although the process of evaporation stops, the freeze-thaw effects due to temperature variations may result in additional densification of the soil (Haliburton, 1978).

2.3.1.3 Wind Conditions

Wind conditions above the surface of the soil will also influence the rate of evaporation. In general terms, it can be understood that air movement above the soil surface allows for more evaporation to occur. More specifically, this is due to the ability of the water vapor which transfers from the soil into the air above the soil to be carried away. If there is minimal to no air movement above the soil surface, the air will approach its water vapor saturation limit and evaporation will therefore cease to occur.

2.3.1.4 Precipitation

While evaporation drives the desiccation and formation of the crust, precipitation events can instead inhibit this process. If the precipitation is less than the evaporation for periods, desiccation can take place. However, if precipitation exceeds that of evaporation, it is likely that no desiccation and crust formation will occur without the aid of additional surface drainage measures. This is due primarily to the buildup of excess surface water atop the soil, which must then evaporate or be removed before the material surface is once again exposed to full atmospheric conditions.

Precipitation events also result in wetting and drying cycles of the soil throughout the desiccation process. While wetting due to precipitation may temporarily increase the evaporation rate to those seen during the first stage for a short period of time, this only serves to remove the precipitation runoff that is not removed from desiccation cracks or surface drainage (Haliburton, 1978).

Additionally, it should be noted that general precipitation can be different than net precipitation. Net precipitation refers to the combined value of both precipitation and evaporation into a single value, in which precipitation is generally taken to be a positive value and evaporation as negative.

2.3.2 Surface Drainage

Re-wetting events and the buildup of surface water can be mitigated through the use of surface drainage. Surface drainage measures can help to assist and promote the desiccation process by removing excess water from precipitation events, rather than letting it accumulate or deeply re-infiltrate the soil before. In realistic applications, this surface drainage can be implemented in the form of trenches which can collect and transport a majority of the rainwater away from the material surface. Studies have shown that strains, or volume changes, of 50% can occur within a dredged material, with even higher potential strains if additional surface drainage measures are put in place (Stark et al., 2005a).

2.3.3 Vegetation

Vegetation atop the soil can also affect the desiccation process and the properties of the material towards the surface. For instance, vegetation can help to promote the desiccation process through transpiration and the water which is drawn up from within the dredged material through their root systems. An established vegetation root system within the soil can also aid in strengthening the soil and providing extra stability. However, there can also be disadvantages to vegetation, as tall vegetation can provide shading and reduce the influence of wind, therefore inhibiting evaporation to an extent (Haliburton, 1978). Furthermore, when preventing unwanted plant growth, a common practice is to submerge the surface of the soil to hamper the implantation of seeds which are transported by wind. Submerging the surface of the soil either before, during, or after desiccation has occurred will affect the soil in various manners.

2.4 Soil Profile Conditions & Relations

Throughout the duration of the desiccation and crust formation process, the state, conditions, and properties of the soil change over time. Some of these aspects, such as pore pressure and water content can influence the desiccation process, while changes in others such as void ratio, permeability, and densification are a result of the desiccation process taking place. This section is aimed at providing background knowledge about each of these aspects, so that a more complex and involved conceptual model can be understood.

2.4.1 Soil Phases & Parameters

In engineering practice, a soil is considered to be comprised of either two or three phases, dependent upon its saturation conditions. These phases include the soil particles (or solids), the pore-water present between these particles, and any air or gas contained in the soil. As can be seen in Figure 2-4, if the soil is considered fully saturated, the space between solid particles in a sample volume is assumed to be exclusively occupied by pore water. However, the presence of air and gas must also be considered as the soil becomes partially saturated, eventually resulting in the pore water present being replaced by air as it enters the soil system.

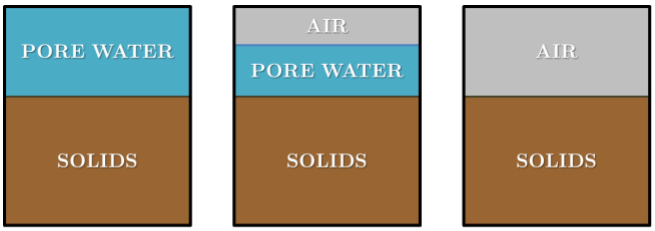

(a) *Fully Saturated* **(b)** *Partially Saturated* **(c)** *Completely Dry*

Figure 2-4: Representative soil phase compositions

The ratio and proportions of these phases in relation to one another influence the properties and behavior of the soil in its various states. These proportions and some general relations can be seen in Figure 2-5.

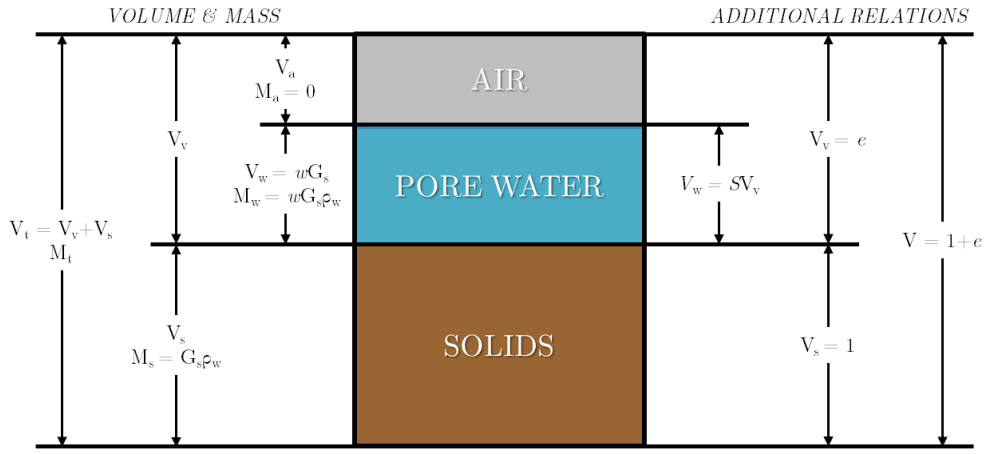

Figure 2-5: Soil phase relations

2.4.1.1 Water Content

One of the most commonly utilized proportions which help to assess the physical properties and behavior of soil is the ratio of water to solids. This ratio is defined as the water content, or moisture content, and is often expressed as either a dimensionless value or as a percentage. There are two ways the water content of a soil can be considered, either gravimetric or volumetric. The one most often used in basic geotechnical engineering applications is the gravimetric water content, or w. The gravimetric water content can be calculated using the following equation:

$$w = \frac{m_w}{m_s} \qquad [\ 2\text{-}2\ ]$$

Where m_w and m_s is the mass of water and mass of solids, respectively, and w is dimensionless.

The volumetric water content differs from the gravimetric water content in that it is the ratio of the volume of water to the volume of solids present. The volumetric water content can be calculated using the following equation:

$$\theta = \frac{V_w}{V_s} = wG_s \qquad [\ 2\text{-}3\ ]$$

In which,
V_w = Volume of water
V_s = Volume of solids
G_S = Specific Gravity

It is important to note that in some cases, volumetric water content can be calculated using the dry density, ρ_b, rather than the specific gravity, G_S. However, for this application, the volumetric water content will be used to calculate the pore space (for the void ratio), and therefore must not include the pore space itself, which is included in the dry density.

2.4.1.2 Void Ratio & Porosity

Another commonly referenced ratio of the phases present within a soil is the ratio between the volume of void space to the volume of solids, and is known as the void ratio, e. The void ratio is defined with the following equation:

$$e = \frac{V_V}{V_S} \qquad [\ 2\text{-}4\ ]$$

Where V_v and V_S is the volume of void space and solids, respectively.

As seen in Figure 2-5, the void space is the complete pore space present, which can be filled with either water, air, or a combination of both. When assuming that the volume of solids remains constant, the

void ratio is especially valuable in defining the volume state of a soil over time as drying and desiccation takes place. An additional note is that when the soil is considered to be fully saturated, the void ratio and volumetric water content are essentially equivalent, as all of the void space is filled with pore water, therefore making the volume of voids and volume of water equivalent.

Whereas the void ratio relates the void space and solids volumes, the porosity is instead the ratio of the former with the total volume of the soil rather than merely solids. The porosity, n, is typically expressed as a percentage and can be related to the void ratio through equation [2-5].

$$n = \frac{e}{1+e} \qquad [\ 2\text{-}5\ ]$$

2.4.1.3 Saturation

As observed in Figure 2-4 previously, the saturation conditions give an indication to the phases considered to be present. The saturation of the soil can be characterized by the degree of saturation, or S, which is commonly represented as a percentage and is the ratio of the volume of water to the volume of voids. The degree of saturation can be related to the void ratio and water content through the following equation:

$$S = \frac{wG_s}{e} \qquad [\ 2\text{-}6\ ]$$

The specific gravity, or G_S, is defined as the ratio of the particle density to the density of water, and can be obtained through lab testing or assumed based on soil expertise. The degree of saturation can range anywhere between 1 and 0, in which a value of 1 (100%) indicating a fully saturated soil and 0 (which is difficult to obtain) classifying the soil as completely dry (Budhu, 2011). In addition, it should be noted that for cases when the soil is considered to be fully saturated, the volumetric water content is considered to be equivalent to the void ratio, based on the relation proposed in equation [2-6].

2.4.2 Pore Pressure

The pressure of the pore-water present within soil can provide a good indication of the conditions present within the soil, such as saturation, groundwater elevation, and whether the soil is in an equilibrium state. Under hydrostatic conditions —when the soil is considered to be in equilibrium conditions with no water flow— the pore pressure increases linearly with depth and can be determined using the following equation:

$$u = \rho_w h_w \qquad [\ 2\text{-}7\ ]$$

In which u is the pore-water pressure, ρ_w is the density of water and h_w is the depth below the groundwater table.

Pore-water pressures under hydrostatic conditions in relation to the groundwater elevation and soil saturation can be seen in Figure 2-6. In the instance where the pore water pressure is negative, this can be designated as suction pressure, and can occur in saturated and partially saturated soil conditions, i.e. the capillary zone.

However, as the soil is exposed to seasonal and climate conditions, such as precipitation and evaporation events, the pore pressure profile deviates from hydrostatic conditions. These effects can be seen in Figure 2-7. During dry periods where excessive evaporation can occur, the pore pressures within the capillary zone increase, and vice versa in wet periods (Fredlund and Rahardjo, 1993).

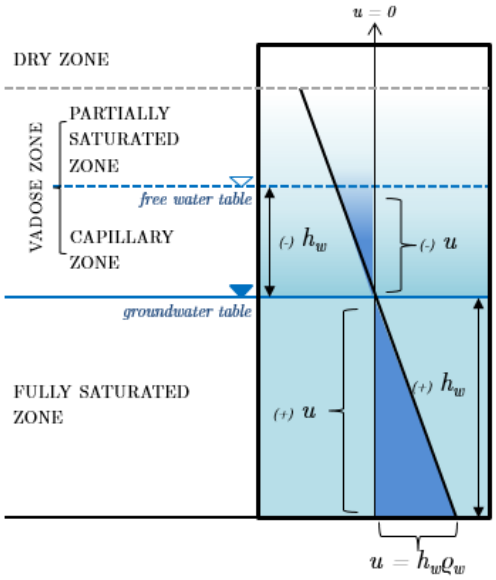

Figure 2-6: Hydrostatic pore pressure profile showing saturation zones

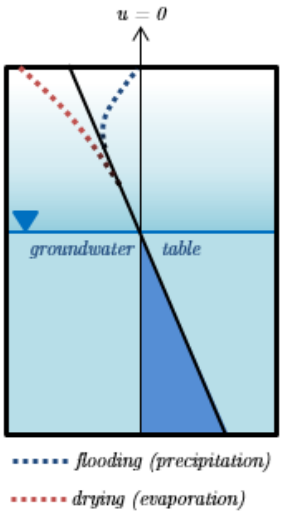

Figure 2-7: Seasonal effects on pore pressure

2.4.3 Capillarity & Suction

As mentioned previously, there is a zone above the groundwater table in which the soil is still considered to be completely saturated. This is due to capillary forces, which allow for the upward flow of water from the groundwater table (Fredlund and Rahardjo, 1993). This is best understood through a capillary tube idealization, in which the tube represents the void/pore space between particles, and can be seen in Figure 2-8.

The height of the capillary zone, z_c, is inversely proportional to the pore size, and can be determined by the following equation:

In which D_{10} is the average particle diameter after which only 10% of the soil particles are smaller in size (Budhu, 2011). Typical capillary zone height ranges based on soil type can be seen in Table 2-1. It is also important to note that the effective stress within the soil increases with increasing capillary pressure, as can be seen in the equation below:

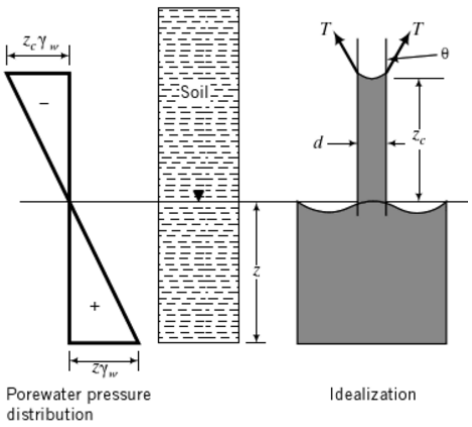

Figure 2-8: Capillarity idealization (Budhu, 2011)

$$z_c = \frac{1}{0.1D_{10}}[m] \qquad [\ 2\text{-}8\ ]$$

$$\sigma' = \sigma - (-z_c\gamma_w) = \sigma + z_c\gamma_w \qquad [\ 2\text{-}9\ ]$$

Capillary pressure can also be referred to as matric suction, which serves as a component of the total soil suction, ψ, as seen in the following equation:

$$\psi = (u_a - u_w) + \pi \qquad [\ 2\text{-}10\ ]$$

In which,

ψ = total soil suction
$(u_a - u_w)$ = matric suction
u_a = pore-air pressure
u_w = pore-water pressure
π = osmotic suction

When the total suction is quantified in terms of relative humidity, the matric suction component contributes to a reduction in relative humidity, while the osmotic suction incorporates the effects of dissolved salts within the pore-water on the total soil suction. This is because the presence and degree of dissolved salts will also result in a decrease in relative humidity (Fredlund and Rahardjo, 1993).

Soil Type	Capillary Rise [m]	Capillary Pressure [kPa]
Sand	0.1-1.0	1.0-10.0
Silt	1.0-10.0	10.0-100.0
Clay	Over 10.0	Over 100.0

Table 2-1: Capillary rise & pressure based on soil type, adapted from (Bell, 2004)

2.5 Classification & Characterization

Soil can be characterized using a variety of standards and properties. These can then often be empirically correlated to describing additional aspects of the soil, including additional soil properties as well as predicting the behavior of the soil.

2.5.1 Particle Size Distribution

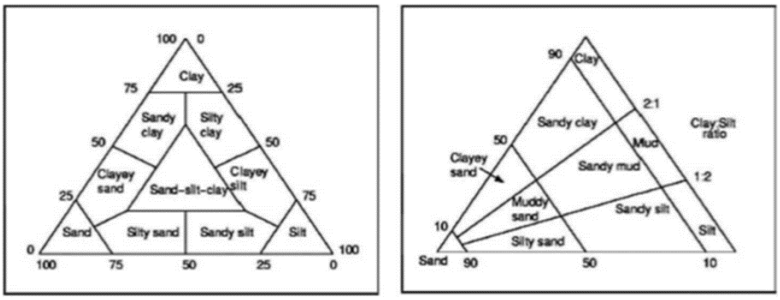

Figure 2-9: Shepard and Folk sediment classification diagrams (Winterwerp and van Kesteren, 2004)

As mentioned previously, the granular composition of the sediment is one of the most important aspects when classifying and characterizing soil. The complete granular composition can be determined by compiling a particle size distribution, or PSD, of the material. Then based on the PSD and particle size classification system used, the general classification of the material can be determined using either of the triangular diagrams seen in Figure 2-9 (Winterwerp and van Kesteren, 2004).

2.5.2 Atterberg Limits

The Atterberg limits are used to define the properties of cohesive soils in terms of consistency, state and plasticity, which is defined as "the property of cohesive soils which possess the ability to undergo changes of shapes without rupture" (Murthy, 2003). There are three main limits which have been defined, and these include the liquid limit (LL or w_l), plastic limit (PL or w_p), and shrinkage limit (SL or w_s) which are all typically expressed as percentages of water contents. The various states, limits, and relating consistencies can be seen in Table 2-2 (Murthy, 2003). It is also generally regarded that the strength of the soil while at its plastic limit is approximately 100 times stronger than its strength at its liquid limit (Wroth and Wood, 1978).

State/*Limit*	Consistency	Volume
liquid	very soft	changes take place due to water loss/addition
liquid limit	*soft*	
plastic	stiff	
plastic limit	*very stiff*	
semi-solid	very-extremely stiff	
shrinkage limit	*extremely stiff*	*change stops*
solid	hard	no changes

Table 2-2: States, limits, and consistencies of cohesive soils, adapted from (Murthy, 2003)

The liquid limit is the water content at which the cohesive soil transitions between the liquid and plastic state. Next, the water content at which the transition between the plastic and semi-solid states takes place is defined as the plastic limit. The final limit, the shrinkage limit, is defined as the water content after which water loss from within the sample does not result in further volumetric decreases within the soil (Murthy, 2003).

The shrinkage limit also represents the designation between saturated and partially saturated soil. Up until the shrinkage limit, the soil is considered to be fully saturated, however after the shrinkage limit the soil is assumed to become partially saturated or unsaturated (Murthy, 2003).

Two other direct parameters which are often used to characterize cohesive soil include the liquidity index, LI or I_l and plasticity index, PI or I_p. The values and their meanings in relation to soil characteristics can be seen in Table 2-3 and Table 2-4.

The plasticity index highlights the range of water contents between the liquid and plastic limits, which can help to further describe the plastic behavior of the soil. It can be determined using the following equation:

$$I_p = LL - PL = w_l - w_p \qquad [\ 2\text{-}11\ ]$$

Value of Plasticity Index, I_p	Plasticity
$\boldsymbol{I_p > 17}$	Highly plastic
$\boldsymbol{7 < I_p < 17}$	Medium plastic
$\boldsymbol{I_p < 7}$	Low plastic
$\boldsymbol{I_p = 0}$	Non-plastic

Table 2-3: Plasticity index guide to soil plasticity, adapted from (Murthy, 2003)

The liquidity index is often used to help indicate the state of the soil in undisturbed conditions (e.g. in the field) and can also be related to the shear strength of the material. This value can be determined using the following equation, in which w and $w_{natural}$ is the in-situ or natural water content:

$$I_l = \frac{w - PL}{LL - PL} = \frac{w_{natural} - w_p}{I_p} \qquad [\ 2\text{-}12\ ]$$

It should be noted that the liquidity index ranges from values less than zero (negative) to values greater than 1. A general guide for relating the liquidity index to consistency and in-situ state can be seen in Table 2-4 below (Murthy, 2003).

Value of Liquidity Index, I_l	State/Limit	Consistency
$\boldsymbol{I_l > 1}$	Liquid State (when disturbed)	Liquid - Very Soft
$\boldsymbol{I_l = 1}$	Liquid Limit ($w = w_l$)	Very Soft
$\boldsymbol{0 < I_l < 1}$	Plastic State	Soft
$\boldsymbol{I_l = 0}$	Plastic Limit ($w = w_p$)	Very Stiff
$\boldsymbol{I_l < 0}$	Semisolid – Solid State	Very Stiff - Extremely Stiff

Table 2-4: Liquidity index guide to state and consistency, adapted from (Murthy, 2003)

2.5.3 Soil-Water Retention Curve

The soil-water characteristic curve (SWCC) characterizes the relationship between the water content of a soil and the suction the soil experiences. The SWCC can also be referred to as the soil-water retention curve (SWRC), in which the curve represents the amount of water which can be retained by a specific soil at equilibrium conditions when experiencing a certain suction value. In this research, the term SWRC will be used, but in other literature may be termed as SWCC. The SWRC of a soil is heavily influenced by a multitude of soil properties, including type and structure. It can be used to empirically determine both the permeability and shear strength functions of an unsaturated soil, especially for modelling water distribution within a partially saturated soil (Tuller and Or, 2003).

The water content can be expressed either in terms of volumetric water content, θ, or as gravimetric water content, w. The type of suction value used can also vary, with either the matric or total suction being utilized. A typical SWRC for a soil can be seen in Figure 2-10. A more detailed description of the zones designated in Figure 2-10 can be seen in Table 2-5.

It is typically understood that the engineering properties of unsaturated soil are influenced by the suction present within the soil. It is also important to note that the SWRC cannot be used to directly estimate the in-situ suction values based on natural water content readings, as additional hysteresis affects due to adsorption and desorption must also be taken into consideration. However, the SWRC is still an important characterization of the soil which can be used to estimate other properties of the soil, especially in unsaturated conditions (Fredlund, 2006).

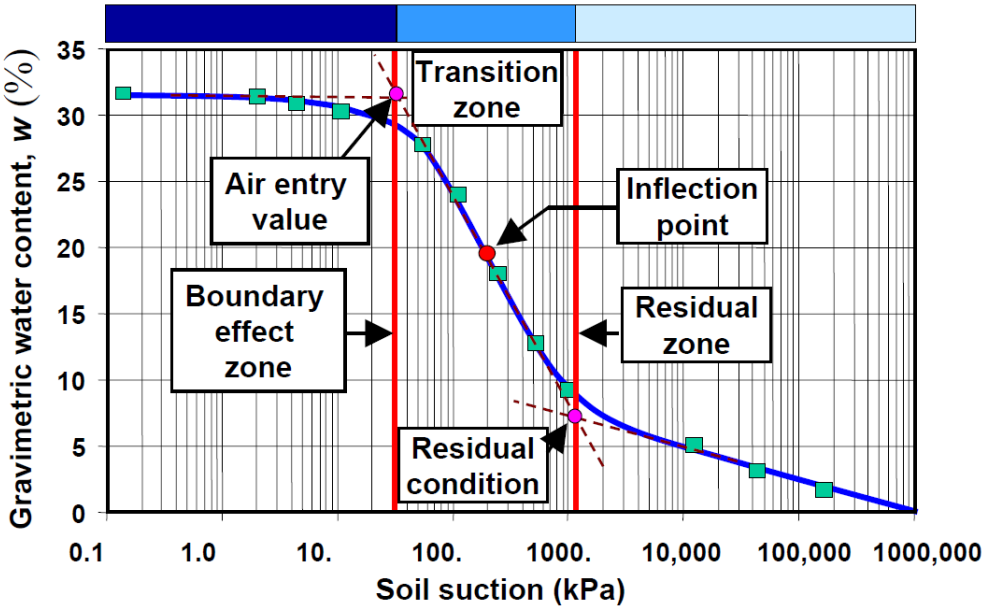

Figure 2-10: Typical SWRC with zones of saturation (Fredlund, 2005)

SWRC Zones	In-Situ Zone Equivalent	Description
Boundary effect zone	Capillary zone	Zone where although the soil is saturated, it can be subjected to negative pore-water pressures.
Transition zone	Two phase fluid flow	Continuous water and air occurs within this zone, with mixture of air and water filling the voids
Residual zone	Dry (vapor transport of water)	Mainly air filling the voids, rather than water

Table 2-5: SWRC saturation zones & in-situ zones, adapted from (Fredlund, 2006)

2.5.4 Soil Shrinkage Characteristic Curve

In addition to the SWRC, another characteristic curve called the soil shrinkage characteristic curve (SCC), is often utilized to anticipate volume changes in relation to water content. In place of the volume of the sample, this curve can be also typically generated by relating the void ratio to the water content with the same output shape.

A typical SCC is shown in Figure 2-11, with the Atterberg limits and their relation to volume and state change also detailed. As can be observed, much of the volume change is linearly proportional to the reduction in water content. However, this trend ceases once the water content approaches that of the soil's shrinkage limit, after which further volume change no longer occurs.

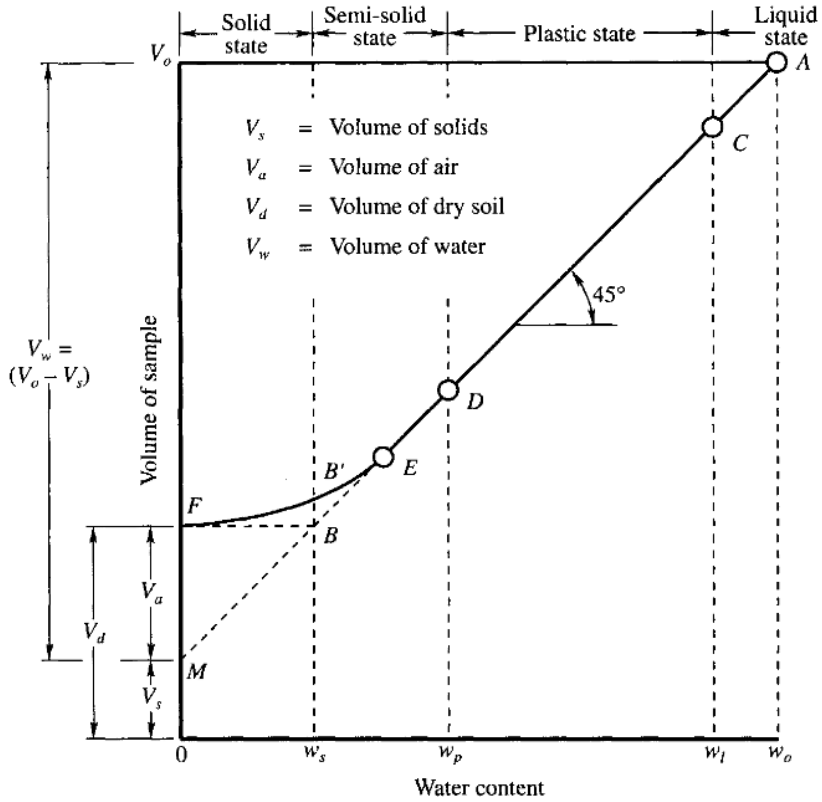

Figure 2-11: Typical SCC including state transition relations (Murthy, 2003)

3 Conceptual Model

This section serves to provide a more comprehensive, integrated, and sequential conceptual model of the desiccation and crust formation process. This includes a breakdown of relevant soil profile property changes throughout the process, as well a discussion on the simplifications and assumptions utilized in the formation of this conceptual model and its application to the rest of this research.

3.1 Process Description

The desiccation and crust formation process can be described with three main components: water movement, pore-water pressures, and void ratio profiles. Changes of these components have been graphically described in Figure 3-1, Figure 3-2, and Figure 3-3, respectively.

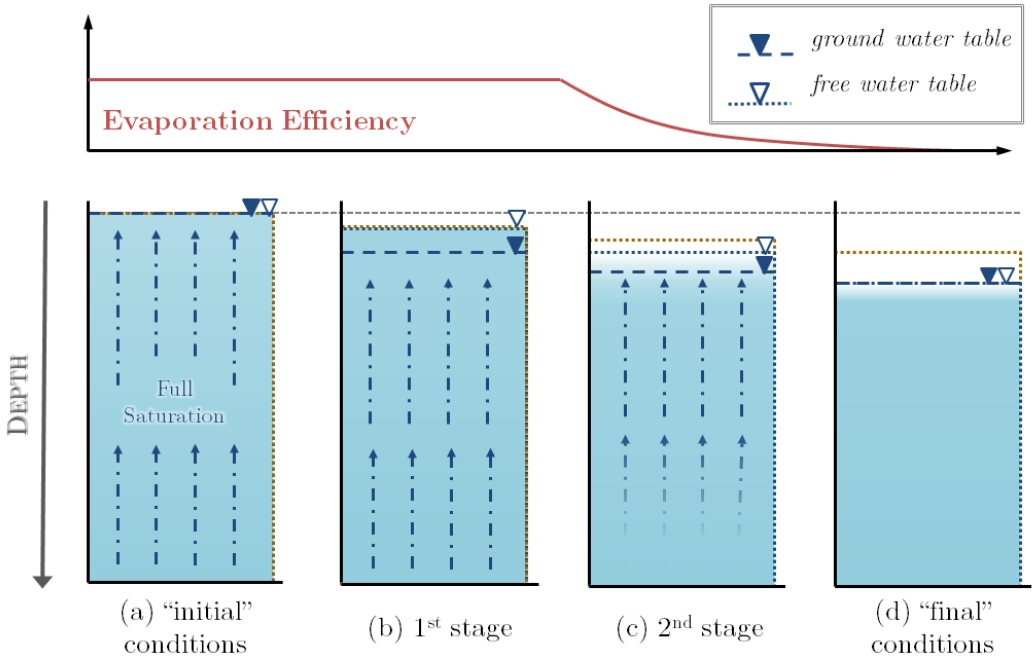

Figure 3-1: Conceptual Model – Water movement, evaporation, and saturation

Figure 3-1 displays the water conditions over time during the desiccation and crust formation stages, including blue to white shading which represents full saturation to dry conditions, respectively, as well as both the free and ground water tables. These two differing water tables have been designated due to the capillarity of the soil mentioned previously. An additional point of note are the arrows shown in profiles (a), (b), and (c). This is meant to represent the water being drawn up from within the complete profile. The effects of this can be further observed in Figure 3-2, in the overall void ratio profile development. Also provided in this part of the conceptual model is a relative evaporation efficiency chart which serves to show the changes in potential evaporation rates based on the stage of desiccation and drying.

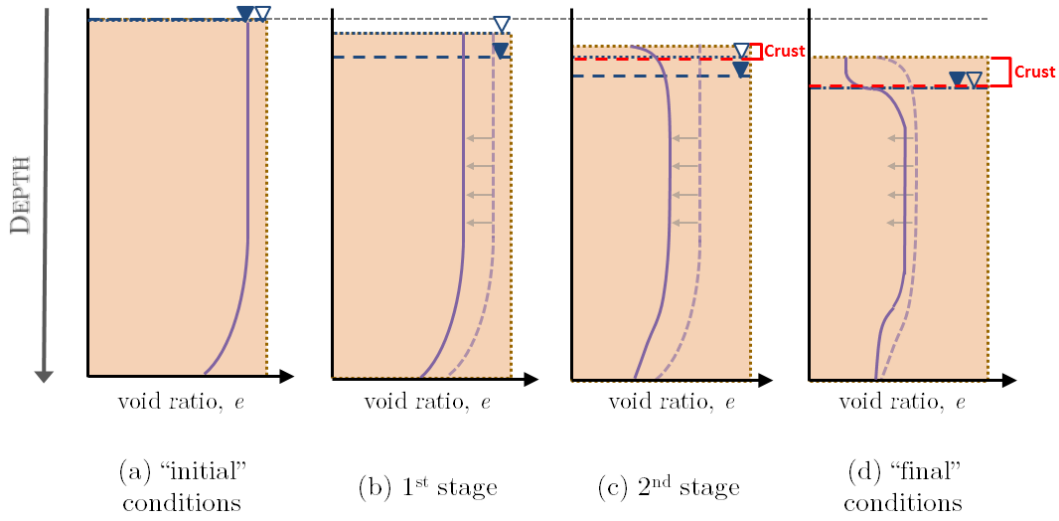

Figure 3-2: Conceptual Model – Void ratio profile and crust development

Figure 3-2 shows the development of the soil profile's void ratio, including the assumed initial void ratio profile for a single, homogenous fill layer after initial self-weight consolidation has taken place. As a result of the water movement upwards to meet the demands of evaporation, the complete void ratio profile exhibits a general reduction and therefore a leftward shift. These complete shifts of the profile are shown with the gray arrows, and the previous stage's void ratio profile is shown in the next stage with the lighter, broken, purple line. Also shown in red is the approximate crust edge and thickness. The definition of crust varies based on perspective and respective opinions but in this instance, it has been defined as the material with both significantly reduced void ratio and saturation; quantified as the unsaturated region between the surface and initial void ratio inflection point in contrast to the expected void ratio profile in terms of depth. In contrast, all of the material which has a differing void ratio in comparison to the initial conditions is considered to be "desiccated" soil. This desiccated soil therefore also includes the crust layer.

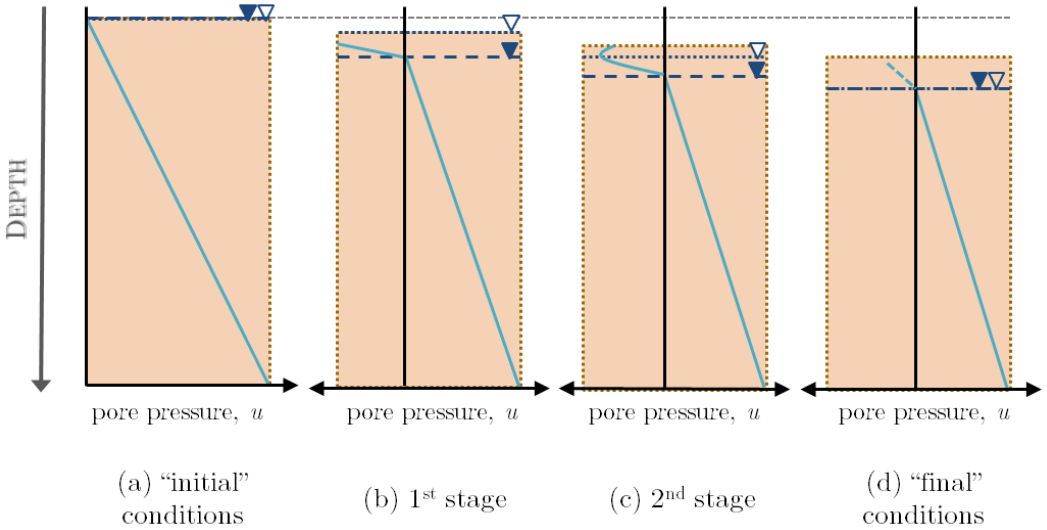

Figure 3-3: Conceptual Model – Pore pressure profile development

One final type of profile development shown is that of pore pressure, as seen in Figure 3-3. Under the assumption that the self-weight consolidation phase has concluded, all excess pore pressures have dissipated and the profile is under hydrostatic conditions, the pore pressure profile at initial conditions increases linearly with depth. As the groundwater table drops, negative pore pressures build up between the surface and the groundwater table. Water below the groundwater table is considered to remain hydrostatic. Once the soil desaturates, these negative pore pressures reduce, due to air entry.

3.1.1 First Stage: General Desiccation

Desiccation of the dredged material —after the initial self-weight consolidation has taken place— can only commence once the free surface water is removed, either by passive or active means. Once the free water above the material has been removed and the mud surface is exposed, the first stage of drying, can begin. During this stage, it is assumed that the free water table remains at the surface of the material even as evaporation and soil water loss occurs, due to capillarity. With this assumption, the material is also assumed to remain saturated and therefore buoyant, resulting in no excess consolidation of the underlying material taking place. The rate of evaporation proceeds at a constant rate related to the full potential evaporation, as the water is drawn up from within the full profile to meet the demand of the evaporation potential (Stark et al., 2005a). During this stage however, the ground water table (g.w.t.) is assumed to drop, as negative pore pressures develop between the surface of the material to the g.w.t., where the pore pressure is presumed to be 0. This stage is determined to be "governed primarily by capillary resupply potential of the soil"; due to the high clay and silt content, this potential is quite high (Cargill, 1985).

Initially, the void ratio profile is the same as that of the profile at the end of self-weight consolidation. This indicates that the permeability at the surface is higher than that of the permeability deeper within the material. However, as the first stage of drying takes place, this distribution will generally exhibit a complete shift and overall reduction in values.

After a certain point, it is assumed that water from within the soil can no longer be supplied at a rate fast enough to maintain the constant rate of evaporation, and is generally observed to occur at a point related to the liquid limit, or *LL*, of the material. After this saturation limit is reached, it is assumed that the first stage of drying has concluded. This designated saturation limit is often linked to the material's LL (Haliburton, 1978), or as a function of the plasticity index, or PI, based on various experimental site data (Stark et al., 2005b).

3.1.2 Second Stage: Crust Formation

During this stage, the material begins to desaturate from the surface downwards and form a dense crust layer, and the free water table shows this with a downward movement. The depth of crust from this stage determines the additional surcharge load which is applied to the underlying dredged material (Stark et al., 2005b). While the material was assumed to remain buoyant during the first stage, this is no longer the case during the second stage of drying. As the material de-saturates, an increase in effective weight of the top material is observed. This new overburden load of the heavier crust results in excess consolidation and 'squeezing' out of water from the underlying material, resulting in further reduction in void ratio distribution of the underlying material. This crust can be visually determined by observing the significantly reduced void ratio values which occur from the surface downwards, until the void ratio becomes generally the same as that expected with the void ratio distribution profile.

The rate of evaporation during the second stage drying is affected by not only by the permeability and thickness of the crust, but also as a function of depth along the material to the water table and the capillarity of the soil (Cargill, 1985; Haliburton, 1978). As a result, the evaporation rate proceeds at a much slower non-constant rate than that experienced during the first stage of drying. Eventually, the effects of second stage drying slows as the material reaches either the desiccation limit at a certain depth, or the natural surrounding water table depth. The desiccation limit of the material is based on the plastic limit of the material, or additionally the PI once again (Stark et al., 2005b; Haliburton, 1978).

The depth of crust layer is typically physically observed by bisecting the dredged material between desiccation cracks and revealing a vertical profile of the dredged material beneath the crust, to confirm the depth of the desiccation cracks and desaturation of the material from the surface inwards. However, the crust can also be graphically determined by observing the significantly reduced void ratio values which occur from the surface downwards, until the void ratio becomes generally the same as that expected with the void ratio distribution profile. This can also be termed as the region between the surface and the first major inflection point in the void ratio profile, in which the region exhibits significantly reduced void ratio values in comparison to the rest of the profile.

As mentioned previously, the void ratio profile —in comparison to that at the end of self-weight consolidation— reduces in value all throughout the profile during the first stage of drying. However, the profile is affected additionally towards the surface of the material during the second stage of drying as the crust layer develops. The crust layer exhibits a significant reduction in void ratio which continues throughout the layer, deviating from the normal void ratio profile. This results in low permeability values at the surface of the material (within the crust layer), with higher permeability values present within the underlying material. This crust layer, due to its significantly reduced permeability, then inhibits further evaporation of the lower material.

3.2 Additional Factors

There are numerous other factors and parameters in addition to the water, void ratio, and pore pressure that can be discussed in relation to the desiccation and crust formation process. While they can't all be addressed here, some of the additionally relevant factors include settlement, strength, cracking, influence of re-wetting, and time scale.

3.2.1 Settlement & Surcharge Consolidation

As water is removed from within the material due to evaporation, the material densifies and gradually reduces in volume, first in the vertical direction and later in the horizontal direction as well. The vertical reduction can be seen in the total settlement of the layer over time. Another tell-tale characteristic of this process is the formation of cracks within the material, which appear as a result of the horizontal reduction in size and the tension caused within the material due to the water loss.

During the first stage of drying, the reduction in volume and settlement is directly related to the amount of water loss which has occurred. However, during the second stage of drying there is no exact correlation between water loss and settlement due to the formation of a crack network, as well as the loss of saturation within the crust layer (Stark et al., 2005a). The amount of volume loss as the water content decreases is best characterized by the soil shrinkage characteristic curve, and it is important to note that most of the volume shrinkage can be linearly correlated to volume loss, as stated similarly when describing the changes which occur during the first stage of drying. However, after the shrinkage limit is reached, the volume change slows and eventually comes to a halt even as the water content continues to reduce.

3.2.2 Strength Development

The shear strength of the material —especially the upper crust layer as it becomes unsaturated, densifies, and develops matric suction— will also increase, with some literature showing a bilinear relationship between shear strength and matric suction (Elsharief et al., 2015). This matric suction in turn, is related to the water content within the material, and the relationship between water content and matric suction is best characterized by the soil water retention curve introduced previously. Again, based on this characterization, it can be clearly understood that water content and shear strength are inversely related. That is to say, that after a certain point, as the water content decreases the shear strength will increase, and vice versa.

3.2.3 Desiccation Cracking

During the first stage —even while the material is still considered to remain saturated— due to the water loss, the top layer of the material shrinks and densifies as the particles come into close contact and the pore space reduces in size. Any cracks that form during this stage are considered negligible, especially in comparison to those formed during the second stage of drying.

The cracks which result from the shrinkage experienced during the second stage of drying are considered to be the primary desiccation cracks. These cracks occur when considering 3-D shrinkage effects. The lateral stress increase due to the horizontal shrinkage of the material will at one point overcome the tensile strength of the material, resulting in a crack formation. The depths of these cracks can also be utilized to observe the depth of the crust layer. It should also be noted that the presence of a crust layer with a significant desiccation crack network formation will increase both the rate and magnitude at which excess consolidation of the underlying material occurs (Stark et al., 2005a).

3.2.4 Re-Wetting Events

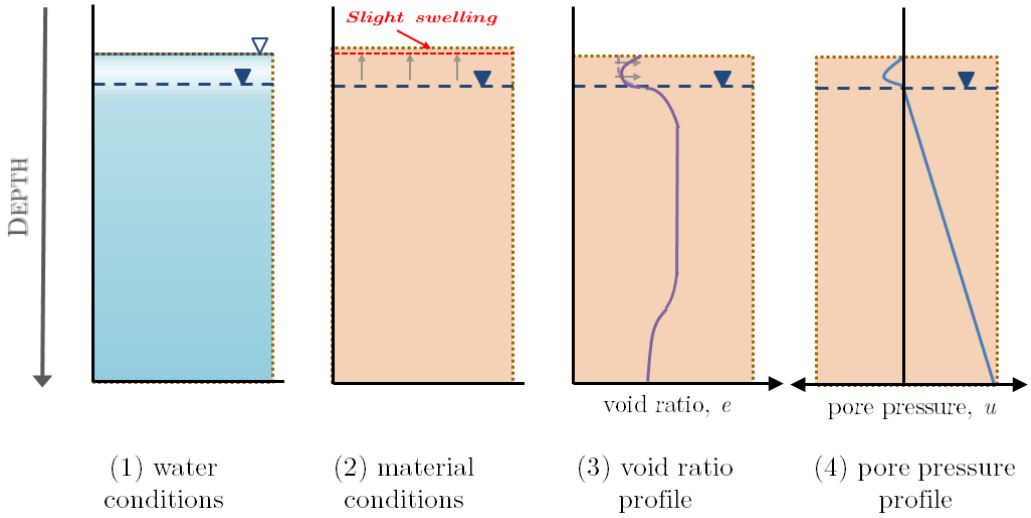

Figure 3-4: CONCEPTUAL MODEL – Profile changes due to re-wetting events

Re-wetting of the material during the drying stage is likely to occur due to precipitation events, or even intentional re-submergence of the surface. This results in temporary fluctuations in both the pore pressure and void ratio profiles at the surface of the material, and can inhibit the drying process if significant amounts of water remain above the surface of the material or is left to infiltrate. However, it should be noted that the excess water will then temporarily allow the evaporation to commence at full potential, until the water evaporates or is removed through other means (Haliburton, 1978). The rewetting of the soil may result in some swelling of the surface material which has previously shrunk. Furthermore, the rewetting and drying of the soil in terms of soil water retention is best characterized by a hysteresis effect which varies depending on the number of re-wetting and drying cycles the soil experiences. The effects of precipitation events on the soil after desiccation has taken place is summarized in Figure 3-4.

3.2.5 Time Scale

The desiccation and crust formation process and its timescale are highly dependent upon a variety of aspects, including:

- General climate conditions
- Atmospheric conditions
- Material properties
- Surface water conditions, including any active and/or passive maintenance

Because of this, it can be hard to predict an exact timeframe of desiccation and crust formation progression. However, to gain a general idea of the time frame involved, general time estimates specifically for the Dutch climate have been provided for context, and were taken from the numerical model provided by Phil Vardon and Delft University of Technology. Desiccation itself starts almost immediately once the initial surface water is removed; however, significant changes such as settlement and crust formation can begin taking place anywhere from 3 months to 2 years, with stabilization and the end of the second stage of drying occurring around the 5th year.

3.3 Assumptions & Application

There are numerous assumptions and simplifications in this conceptual model. For instance, it is assumed that the material is homogenous and shows similar, consistent properties throughout the profile. This means that no stratifications (or layering) has been taken into account in this model to allow for ease of comprehension and theorization. Moreover, the conceptual model is 1-D based, in that water and soil movement is characterized only in the vertical direction. This is a broad assumption, as a 3-D interpretation including desiccation cracking, and ground water flow would be more realistic.

In terms of its valid application to the large-scale test containers, two important assumptions were made. First, the assumption that the initial self-weight consolidation phase has fully taken place. This means that all possible consolidation which can occur under submerged self-weight consolidation has occurred, and all excess pore pressures have dissipated. This assumption forms the foundation of the start of the drying and crust formation process by assuming that any changes in properties after initial pumping is directly the result of the desiccation process. In reality, the desiccation process can occur once the material has settled and the resultant distinct water layer above the material is removed or evaporated. However, this was not the case for the anticipated Marker Wadden construction procedure, and therefore was not considered. Second, as mentioned previously, the conceptual model is 1-D based and therefore any interpretations of the conditions within the containers is assumed to be 1-D as well. This is an unrealistic assumption, as 3-D effects will be seen even within the large-scale test containers. Mitigation of this will be attempted by testing only towards the center of the container, and careful examination of the results.

Many of the aspects addressed in relation to the large-scale testing are also applicable to the Marker Wadden. But one must also keep in mind the scale of the Marker Wadden, as well as the construction process, which requires multiple fill layers and spreading, resulting in even greater heterogeneity in both the vertical and horizontal.

4 Methodology

This section focuses on describing the methods and test setups utilized as well as providing further background information about the experimental and modeling aspects of this project. Figure 4-1 has been provided in order to more clearly distinguish the various testing and modelling aspects of this research, as well as to indicate how these aspects relate to one another in regards to the larger scope of this research.

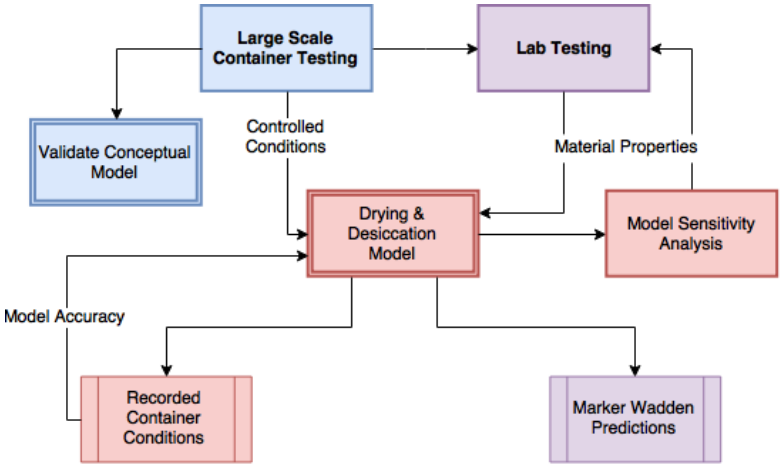

Figure 4-1: Thesis approach & methodology

4.1 Large-Scale Container Testing

Three large-scale shipping containers were utilized in order to observe the desiccation and crust formation process under varying conditions. These containers were used prior to this research in order to study the settlement and consolidation process of dredged material with varying filling methods. A brief overview of how the containers were initially designed and filled –as well as the end results which serve as this project's initial conditions– will be provided; however, for a more comprehensive understanding please see van Olphen's MSc thesis: "Consolidation behaviour of soft cohesive soils, the correlation between different scale model tests: case study of the Marker Wadden" (van Olphen, 2016).

4.1.1 Initial Conditions

The Holocene clay material was directly dredged from the same area where the borrow pit was set to be located for the main Marker Wadden project, in order to recreate soil conditions as closely as possible to that of the Marker Wadden project. This slurry mixture was then transported to the Papendrecht test site and deposited in the containers in either a single or two-fill layer process (dependent on the container), as seen in Figure 4-2[1]. This material was then monitored and tested over time as it was allowed to settle and consolidate.

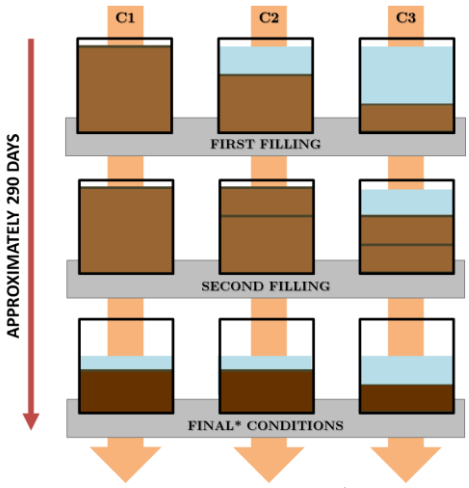

Figure 4-2: Initial container fill process

The "final" conditions of these processes were obtained at the start this research through the use of an echosounder, to determine the elevation of the mud-water interface without having to remove the surface water remaining atop the mud bed or disturbing the mud bed itself. The material surface elevation within each container was

[1] "Final* conditions" in Figure 4-2 is meant to represent the end conditions of van Olphen's thesis, which in reality are the initial conditions of this thesis project.

measured at 3 points along a longitudinal cross section using an Echotrac CV200/300 single beam transducer. The estimated material elevations from the bottom of the containers are listed in Table 4-1.

Container	Initial mud bed height [m]
C1	0.83
C2	0.82
C3	0.46

Table 4-1: Surface elevations after self-weight consolidation

An additional note of importance regarding the initial conditions of this setup was the observation made by van Olphen of sand segregation occurring at the bottom of each fill layer. This observation was confirmed with various tests throughout the duration of this project as well, and had to carefully be taken into account during test calibration and result analysis, as sand content fluctuations have a significant impact on the results. However, it should be noted that initial tests of the material used in the actual fill layers within the Marker Wadden had significantly reduced sand content values in comparison —excluding the samples taken from close to the sand berms.

4.1.2 Test Condition Variations

Each of the three containers utilized for testing attempted to vary the effects of evaporation and therefore the rate of desiccation experienced within the material. First, the initial free water layer remaining above the mud bed in each container was pumped out at the start of the testing period. Then, the conditions and active maintenance within each of these containers were varied in order to bring about varying amounts of desiccation. C3, the container with the least amount of consolidated soil served as the control, and after initial pumping only passive monitoring and in-situ testing took place. C2 represented "surface drainage" conditions, in that any excess water accumulated atop the surface of the mud bed was removed as consistently as possible after major rain events throughout most of the testing period. C1 served as the "extreme" evaporation case, in order to increase the likelihood of observing visible effects of desiccation within the project timeline, and utilized the same setup as C2 with additional measures in place. Table 4-2[2] summarizes the conditions simulated in each of the containers as well as the active measures taken to achieve these representative conditions.

Container	Conditions Simulated	Rain Events	Dry Periods
C1	Dry (Extreme)	cover*; ventilator*	ventilator*
C2	Surface Drainage (Assisted)	excess water removal	--
C3	Natural (Control)	--	--

Table 4-2: Large-scale test container conditions & setup variations

4.1.3 Container Timeline

The testing timeline is considered to begin on the first day of initial pumping and removal of the excess surface water from each of the containers. It should be noted that although these containers are a continuation of van Olphen's testing timeline, for the purpose of this research the initial start is considered to be the day of initial pumping and removal of the excess water, rather than the initial filling of the containers. This commenced on 16 September 2016, and the testing period with weather monitoring and running ventilator concluded on 4 January 2016, lasting 110 days.

Active removal of excess surface water in C2 concluded in November, after it was determined that a high level of active manual labor was required to continue the testing, with minimal observable effects as of that point in time. In the hopes of obtaining viable long-term data in a more passive manner, C1 remained covered with the ventilator on after November; however, it should be noted that this cover failed at least twice at two distinct points in time, resulting in significant amounts of additional surface water to enter the C1. Main testing days and remarks can be seen in Table 4-3; however, for a more detailed log of events and additional information, please see the section Container Testing in the Appendices.

[2] Use of the " * " symbol within Table 4-2 indicates only partial usage. For more details about the exact duration of usage, please see the Appendices for the detailed large-scale test log.

	Day	Date	Remarks
T1*	-4	Sept. 12, 2016	Initial Beeker core testing (still submerged)
T1	4	Sept. 20, 2016	Vane and densimeter testing
T2	10	Sept. 26, 2016	Vane and densimeter testing
T2*	19	Oct. 05, 2016	Beeker core testing
T3	31	Oct. 17, 2016	Vane and densimeter testing
T4*	46	Nov. 01, 2016	Beeker core testing
T4	51	Nov. 06, 2016	Partial vane and densimeter testing
T5	152	Feb. 15, 2017	Vane testing (C1 and C2 only)

Table 4-3: General testing dates and remarks

4.1.4 Container Setup

The various equipment and setups utilized throughout this testing, and the parameters involved, have been summarized in Table 4-4[3]. For a more detailed description of the equipment and setup, see section 4.1.4.2 Implemented Setup.

		Measured Parameter	Equipment	Frequency/ Usage
Constant	**surface/water level**	ultrasonic pulse (distance)	Milltronics XPS-15 transducers	15 minutes
	surface changes	surface images	Sony Bullet HD cameras	15 minutes
	saturation & pore pressure	pore-water pressure at specified depths	Piezometers (Deltares)	5 minutes
	weather & climate	precipitation, temperature, wind, humidity, atmospheric pressure	Vaisala Weather Transmitter WXT520	15 minutes
	evaporation	open water evaporation	Class A evaporation pan	daily*
Interval	**surface elevation**	complete interior area surface scan	Leica Nova MS50	2 times*
	density profile	acoustic variations, calibrate to density	UHCM densimeter (Deltares)	4 times*
	Beeker core	undisturbed profile sample	Beeker sampler setup	3 times*
	shear strength	undrained in-situ shear strength	Haake vane rheometer M1500	5 times*

Table 4-4: Large-scale test equipment & usage breakdown

4.1.4.1 Initial (Pre-Existing) Setup

The original design process of the containers took place during van Olphen's thesis, where the primary aim was to monitor the settlement and consolidation processes, with some general design input related to the next phases of the complete process. Because of this, the side compartments were designed as an area through which water from the main compartment would drain into, and consequently be pumped out of the container. This design included a geotextile and steel grid barrier between the compartments, theoretically allowing the water to pass through the permeable geotextile, while mitigating soil deformation with the implementation of a stiff steel grid system with holes.

[3] Use of the " * " symbol in Table 4-4 is used to indicate that the amount of times performed in each container deviates from the stated value, due to unexpected equipment errors, failure, and/or discontinuation of testing.

Based on the pre-existing side compartment design, preliminary test setups for this testing period included the use of automated pumps situated in the side compartments which would be activated by pressure transducers becoming submerged in 3 cm of excess surface water which had drained into the compartments. However, during initial pumping it was found that water was not draining from the main compartments due to a clogging of the steel grid and geotextile on both sides, as the dredged material had also been pumped into the side compartments and allowed to consolidate. This clogging effect can be seen in Figure 4-3.

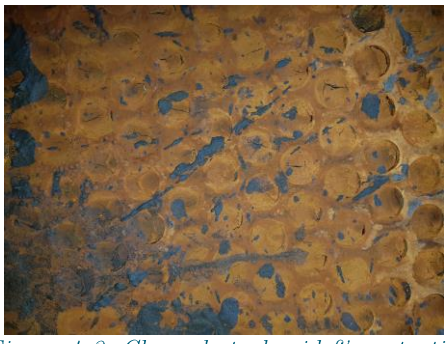

Figure 4-3: Clogged steel grid & geotextile

Subsequent designs attempted to place the pumps along the inner wall of the main compartment; however, it was determined that the amount of disturbance this would cause in combination with the fact that there was a substantial amount of surface water still remaining in the middle of the container, (even after pump activation) made an automated pump system no longer feasible.

Another modification from the pre-existing setup of the containers included the movement of C3. Container 3 was shifted horizontally using hydraulic equipment to allow for full access to the containers for testing. This was done before the initial removal of the free water above the material, but may have still have had an unquantifiable impact on the results obtained in C3. Furthermore, the piezometers installed at the beginning of van Olphen's testing were left within each of the containers for continual monitoring of the pore pressure and eliminate the possibility of soil disturbance during removal.

4.1.4.2 Implemented Setup

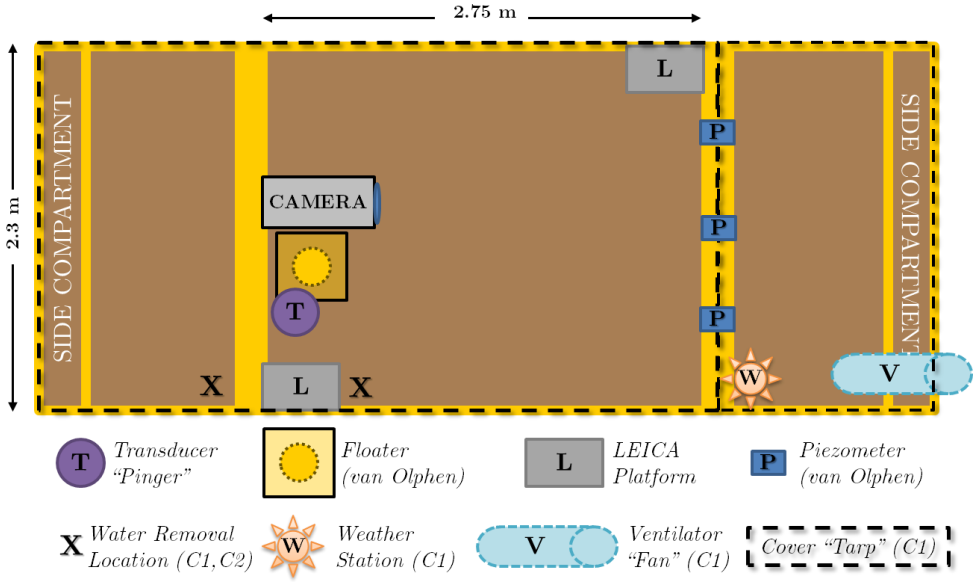

Figure 4-4: Large-scale test container setup schematic

As seen in Figure 4-4 —in addition to the equipment remaining from van Olphen's project— each container was outfitted with a camera, transducer, and welded Leica connection platforms. The camera was set to take pictures of the mud surface at fifteen minute intervals throughout the testing period in order to assess the presence of surface water as well as potential changes of the mud surface, such as crack formations. In addition to the camera, Milltronics XPS-15 transducers were utilized to record the mud surface/water levels within the three containers at 15 minute intervals. Furthermore, two small steel platforms with bolt connections were fitted on opposing corners of the main compartment. This was done so that the Leica Nova MS50 surface scanner would have fixed points of measurement throughout the container testing phase.

The setup of C1 also incorporated a ventilator and tarp cover design. A ventilator with an estimated airflow of 3900 m^3/hr and IP42 rating (weatherproof) was installed along with a 0.30 m diameter hose.

The hose was horizontally positioned approximately half a meter above the mud bed in order to promote airflow across the surface as well as the removal of water vapor to encourage maximum evaporation. The tarp cover was installed and secured in two separate pieces which were connected around the protruding piezometer pipes to minimize disturbance of the piezometers and for ease of installation.

Lastly, a mobile steel scaffolding was designed in order to access to the central areas within the containers. Various tests sensitive to tilting or movement were performed from atop the scaffolding in designated areas, and to reduce to amount of sidesway (side-to-side movement) experienced, the scaffolding was secured to the container side with a tie-down prior to any testing.

4.1.4.3 Environment & Climate Monitoring

In addition to the in-situ container monitoring, a meteo-station (Vaisala Weather Transmitter WXT520) was installed approximately one meter above C1 to record climate and weather conditions. The meteo-station monitored the following weather parameters directly above the container site:

- Wind speed and direction
- Rainfall (accumulation, duration, and intensity)
- Air temperature
- Barometric pressure
- Relative humidity

Any further required weather information not collected onsite by the meteo-station was inferred from the closest Koninklijk Nederlands Meteorlogisch Instituut (KNMI) weather station, which was chosen to be station 344 Rotterdam. The data obtained —as well as any resulting calculations made with them— from the onsite meteo-station were validated by that of the KNMI's weather data for the same day (KNMI, 2017a).

As the main necessity of the weather data was for the calculation of evaporation and net precipitation, a secondary direct evaporation measurement system was setup. This setup involved the use of a "Class A" open water evaporation pan, seen in Figure 4-5. Daily measurements within 0.01 mm of the water level fluctuations in the pan were recorded and subsequently compared to the values calculated empirically from the weather data and global container location using the Penman evaporation equation. After it was deemed that the calculated values fell within the same range of the evaporation pan's direct measurements, the evaporation pan was no longer maintained.

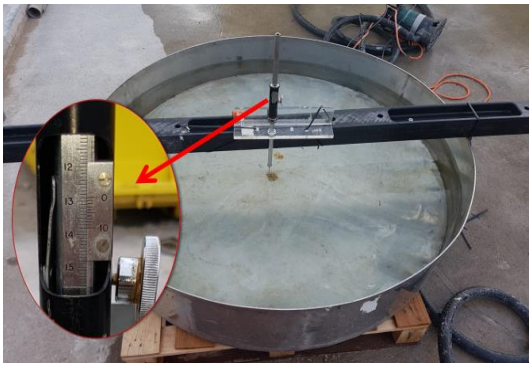

Figure 4-5: Class A evaporation pan setup

4.1.5 In-Situ Testing

A main concern when testing soil profiles within a contained environment is that all tests are performed in "undisturbed" soil locations, which is a requirement for most in-situ testing. Because of this, a grid system was implemented, in order to reduce the risk of testing in an area which had already been disturbed. Figure 4-6 shows this grid system.

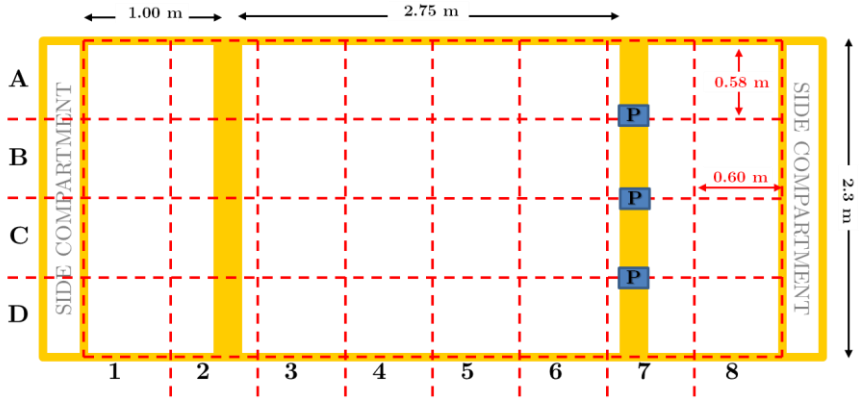

Figure 4-6: Container test grid schematic

4.1.5.1 Beeker Core

Figure 4-7: Beeker core sampler

A Beeker core sediment sampler was used to obtain relatively undisturbed soil profile samples from within the containers (as well as at the Marker Wadden site) at multiple points in time. The Beeker core sampler consists of a special head component which is secured to a transparent tube and can be seen in Figure 4-7. The Beeker core sampler is vertically lowered into the material until the required profile depth. A membrane within the end piece can then be pressurized, essentially inflating it, resulting in the closure of the opening at the bottom of the transparent tubing. After this, the Beeker core sampler can be lifted out from the material and the end piece can be removed from the transparent tube containing the undisturbed sediment profile. Additionally, the material can be pushed out of the tube and partitioned into 10 cm segments which can then be analyzed for its various material and chemical properties.

4.1.5.2 Densimeter

In order to assess the changes in density within the container over time, a densimeter was adapted for field use. The type of densimeter used was an Ultrasonic High Concentration Meter, or UHCM, which uses transmitter probes situated 10-20 mm apart and can be seen in Figure 4-8. An acoustic (ultra sound energy) signal is sent between the two probes and through the soil particles between them. A voltage output can be determined which is dependent on the volume of the particles as well as the size of the particles. The densimeter probes can then be incrementally lowered within a soil profile to determine the voltage changes at various depths within the soil. For profiles within the containers, the densimeter was lowered in either 1 cm (or 5 cm in initial testing) increments.

Figure 4-8: UHCM densimeter setup

Based on a calibration procedure which utilizes the same soil with variations of known densities, the voltage readings can then be related to their density values, and an in-situ density vs. depth profile can be generated. It is important to note that changing soil particle sizes as well as increasing sand contents along the depth can influence the voltage-density calibration procedure. This is because the voltage-density relationship is a linear trend, with increasing sand contents setting a new linear trend to be used in determining the density.

As mentioned previously, sand segregation occurred in all three containers —in C2 and C3 especially, as sand segregation also occurred in the middle of the container material. Additionally, it was conjectured that entrapped air and gas was present between the fill layers within C2 and C3. As the densimeter encountered these areas, the resultant output readings were presumed to be unrealistic and unrepresentative of the actual density at that depth and location. For a more comprehensive overview of how the calibration and generation of the density profiles for the various containers were conducted, see the section Densimeter Measurement Calibration in the Appendices. Furthermore, section 6.1.4.2 Densimeter Inconsistency remarks upon some of the issues encountered when utilizing this device and interpreting the results.

4.1.5.3 Vane Test

In addition to in-situ density measurements, in-situ shear strength tests were also conducted within the containers to evaluate the development of strength over time. These tests were performed using a Haake M1500 rheometer which served as the torquemeter component, equipped with a vane and extension rods

to allow various depths within the container to be reached. A variety of vanes are available, as the anticipated soil strength factors into the size of vane necessary for strength testing. The vane —which is attached to the torquemeter via extension rods, is lowered into an undisturbed portion of soil and rotated at a constant rate while the torque required is measured and recorded. Eventually the soil gives way and both a peak and residual torque measurement can be made, which determines the peak and residual shear strength of the soil, respectively. This is done by relating the specific vane's dimensions to the peak torque required for shear failure of the soil.

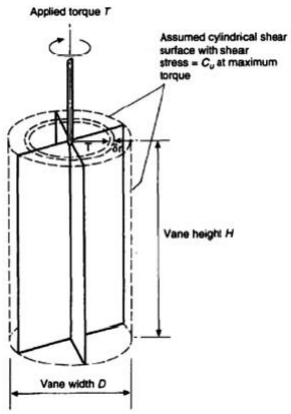

(a) vane end piece

(b) Haake M1500 interface

Figure 4-9(a)(b): Vane shear strength setup

For the strength profile generation within the containers, the vane was first inserted until the top edges of the vane blades disappeared within the material, which based on the initial vane used was typically 6 cm. After this initial vane test, the vane was lowered in 10 cm increments to assure that the vane would test in completely undisturbed conditions. Dependent on the vane being utilized —as the vane dimensions were reduced to account for the increase in strength due to depth— a buffer zone of 4-6 cm was maintained.

Even while assuring that the shear strength was determined in undisturbed conditions, problems still arose in the initial peak and torque readings. Ideally, a smooth increase to peak and then significant reduction in torque readings (as shown in Figure 4-10) would be recorded. However, due to possible interference of the vane movement with embedded objects (such as shells, clay clumps), the equivalent peak and residual torque values were not always easily interpretable from the readings.

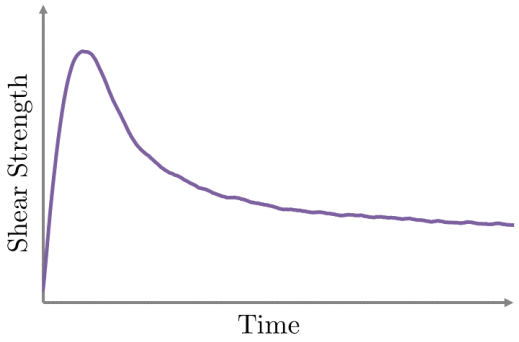

Figure 4-10: Typical vane test result

4.1.5.4 Surface Elevation Scanner

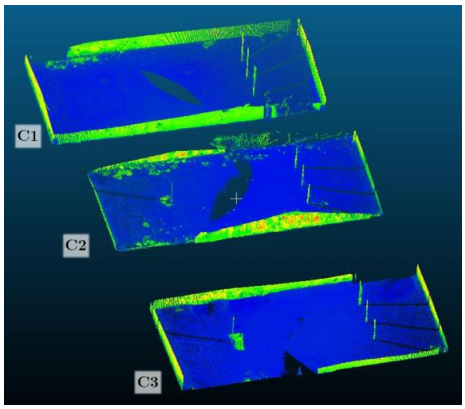

Figure 4-11: Initial Leica container scan

In addition to the individual transducers installed in each of the containers that would constantly measure the water/soil elevation, complete surface elevation scans were also planned over the course of the testing period. This was to account for any discrepancies and elevation variations within the containers. The first complete initial scan using the Leica MS500 scanner can be seen in Figure 4-11 and was generated based on establishing fixed points of measure for reference and by scanning the interior of each container twice from opposing corners.

Unfortunately, after the difficulty in obtaining the first initial scan, it was decided that due to the limitations of this equipment within these test constraints —mainly the presence of water above the material, reflectivity of the mud, and angle required for scanning— it was decided to abandon future scans.

4.2 Lab Testing

Various lab testing was performed using samples collected over time via Beeker core from both the containers and the Marker Wadden itself. This lab testing has been broken into two distinct types of testing: a) general material property characterization, and b) more specialized Hyprop testing to obtain the soils' SWRCs.

4.2.1 Soil Characterization

Table 4-5 summarizes the various lab analyses performed on the container and Marker Wadden material, as well as the test standards followed.

Property	Method	Test Standard
Particle size distribution, PSD	Sieve	NEN-EN
Clay content	Lutum	NEN
Water (moisture) content	--	NEN-ISO
Density: in-situ & dry	Volume Ring	NEN
Atterberg limits: LL, PL, PI	Casagrande	ASTM
Shrinkage limit, SL	Linear	BS*
Specific gravity, G_S	Pycnometer	BS
Organic content	Loss on Ignition	NEN
pH, EC (electrical conductivity)	--	NEN-ISO
Shear strength	Fallcone	Inhouse

Table 4-5: Soil lab analysis methods & test standards

4.2.2 Hyprop Testing (SWRC)

One important material input parameter for the numerical model and beneficial property to research when considering the desiccation and crust formation process is the SWRC of the material. The Hyprop utilizes the extended evaporation method, or EEM, first proposed by U. Schindler, and essentially monitors the soil tension and weight change over time (Chin A Moei, 2016). This is typically done through the setup seen in Figure 4-12, through which both the SWRC and the unsaturated hydraulic conductivity can be determined.

(a) Typical setup

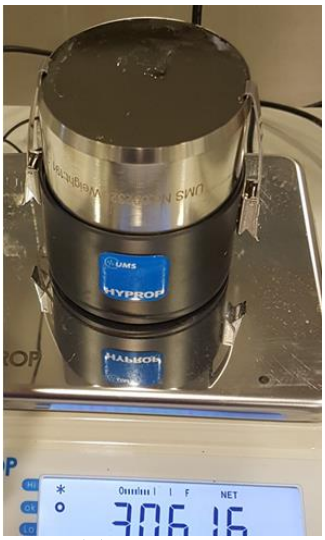

(b) Initial setup

Figure 4-12(a)(b): Hyprop setup

The suction pressure within the soil samples is measured typically with two small tensiometers placed at different levels within the soil, approximately 37.5 and 12.5 mm from the bottom of the sample. As the water evaporates from within the soil, the water from within the tensiometers is also pulled out through their porous tips, creating a vacuum pressure that can then be recorded. These pressures can range anywhere from +100 kPa to -85 kPa. In addition, the weight of the sample is continuously recorded as the water in the soil evaporates and the material eventually desaturates.

Due to the significant volume reduction exhibited by this type of soft, cohesive material, it was decided to remove the longer tensiometer from the setup, as significant soil shrinkage would result in its exposure to the air and potential breakage of the tensiometer shaft. One disadvantage of removing the second tensiometer is that the pressure head (or the difference in tensions at varying vertical points in the material) required in order to estimate the material's unsaturated hydraulic conductivity, as based on Darcy Buckingham's law, was not computable. However, the SWRC is still a valuable material characterization, and through the recorded soil suctions and weight can still be estimated with just one tensiometer.

The SWRC can then be determined by relating the water content and soil suction over time, however it is important to note that the SWRC can then further be fitted by a number of equations proposed by various academics. In this case, the SWRC fitting equation utilized in the numerical model is the van Genuchten equation, which is fitted to the data through the use of three mathematical fitting parameters. The calculation process of the SWRC data and fitting of the van Genuchten equation to the data is discussed in more detail in the section SWRC Calculations in the Appendices.

Figure 4-13 shows the connections and reasoning behind the six Hyprop tests conducted. This was done to evaluate the Hyprop sensitivity as well as material variation in both the Marker Wadden and the containers. Further information about the testing material can be found in Chapter 5.

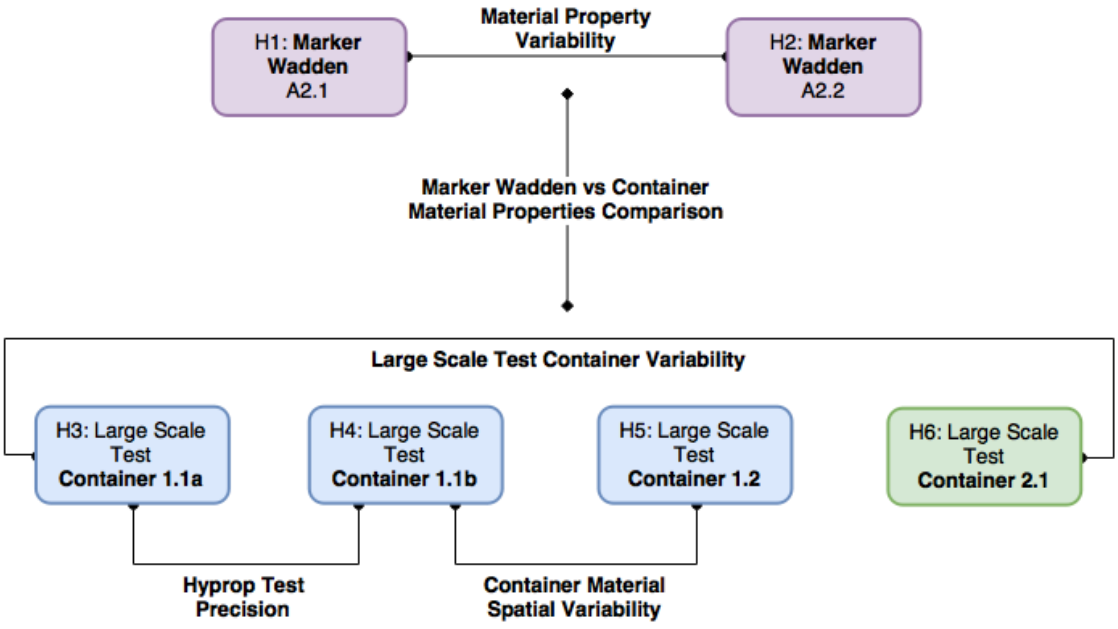

Figure 4-13: Hyprop test & sample approach

4.3 Numerical Modelling

In addition to the large-scale tests performed, an existing (inhouse) numerical model was used. This model, coded in MATLAB, was developed at Delft University of Technology to model the drying of oil sand tailings. The model has been used previously in for the Marker Wadden project in order to predict the long-term soil conditions. The same model was used to validate the findings from the large-scale tests. Furthermore, the Marker Wadden predictions and estimations will be updated with more accurate priority input parameters based on a sensitivity analysis conducted on the model.

4.3.1 Theoretical Foundation

This model, at its core, utilizes a one-dimensional finite difference approach to determine changes within the soil profile based on the overburden, gravity, and suction potentials. This has been modelled based on the following main equations and principles:

- Darcy's Law
- Principle of mass conservation
- Modified van Genuchten SWRC equation (1980)
- Modified Fredlund SC equation (2002)
- Saturated and unsaturated hydraulic conductivity defined by Kim, Diels and Feyen (1992) and Brooks and Corey (1964), respectively

For the sake of brevity, only the fundamental theoretical components, equations, and input parameters directly touched upon within the scope of this research will be outlined. For a more detailed explanation of the model as well as additional computing aspects, please see (Vardon et al., 2015) and (Vardon and van Tol, 2014).

The general van Genuchten soil water retention equation and the specific fitting parameters required as model input can be seen below

$$\theta = WCR + \frac{WCS - WCR}{(1 + (\alpha * \varphi)^{n_{WRC}})^{m_{WRC}}} \qquad [\ 4\text{-}1\ ]$$

In which,

WCR	residual water content [-]
WCS	saturated water content [-]
θ	volumetric water content [-]
a	van Genuchten fitting parameter [-]
φ	matric potential (suction) [kPa]
n	van Genuchten fitting parameter [-]
m	van Genuchten fitting parameter ≈1-1/n [-]

As this equation predicts infinity high suction values for lower water contents, an additional modification parameter was introduced within the model to serve as a cutoff point for the inputted SWRC (Vardon et al., 2015). This modification parameter has been designated as a.

In addition to the SWRC inputs, there are multiple inputs required which are based on the shrinkage characteristic curve, or SCC. The general shrinkage curve equation is shown below, and graphically can be understood through Figure 4-14.

$$e = A_{SH}\left(\frac{\theta^{C_{SH}}}{B_{SH}^{C_{SH}}} + 1\right)^{\frac{1}{C_{SH}}} \qquad [\ 4\text{-}2\ ]$$

In which,

e	void ratio [-]
θ	water content [-]
A_{SH}	minimum void ratio [-]
B_{SH}	shrinkage curve slope defining parameter [-]
C_{SH}	shrinkage curve transition defining parameter [-]

The slope of the shrinkage curve is approximated to lie directly on the saturation line, S =1 (Fredlund et al., 2002). C_{SH} was determined visually to smoothen out the transition. The re-wetting curve parameters can be seen in Figure 4-14 as the dotted blue line.

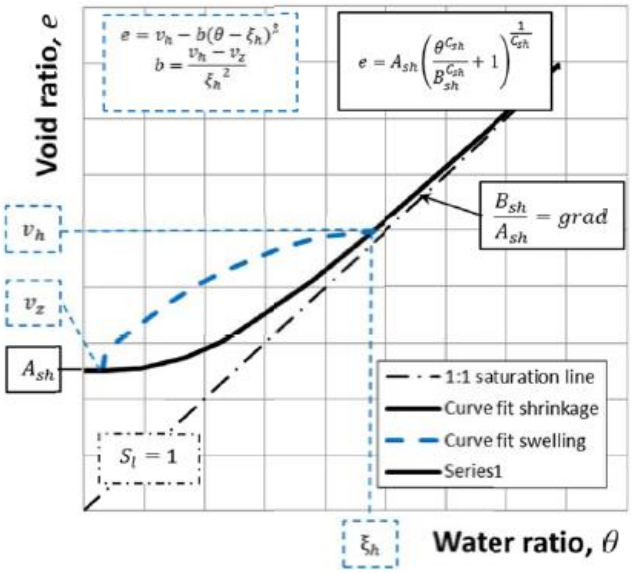

Figure 4-14: Shrinkage curve parameter interpretation (Vardon et al., 2015)

Finally, the permeability is incorporated using functions which relate the hydraulic conductivity to the void ratio. The primary saturated hydraulic conductivity equation utilized in the model can be seen below:

$$K_S = 10^{A*e-B} \qquad [\ 4\text{-}3\ ]$$

In which,

K_S	saturated hydraulic conductivity [cm/d]
e	void ratio [-]
A	hydraulic conductivity material parameter [-]
B	hydraulic conductivity material parameter [-]

However, there is a secondary hydraulic conductivity equation which is typically used in DELCON models, which utilizes parameters obtained by a Seepage Induced Consolidation (SIC) test or a settling column test[1]. This can be seen below:

$$K_S = A_k e^{B_k} \qquad [\ 4\text{-}4\ ]$$

In which,

K_S	saturated hydraulic conductivity [m/s]
e	void ratio [-]
A_k	hydraulic conductivity SIC material parameter [-]
B_k	hydraulic conductivity SIC material parameter [-]

Initial findings by Vardon stated that results varied primarily due to the wide difference in these values and resulting hydraulic conductivities. Additionally, specially determined permeability parameters[2] for the Marker Wadden were not available at the time, so effort was made to compare the two equations and input parameters and their resulting values.

A multitude of simulation and material input parameters are required to run the model; these have been summarized in Table 4-6 and Table 4-7, respectively.

[1] The power-log relation also requires two input parameters, as seen in equation [4-4]. For ease of comprehension, these have also been referred to as parameters A and B, but with subscript "k" to designate that these values are not directly comparable to the A and B parameters used in equation [4-3], and are determined using either settling column or SIC tests..

[2] SIC3 parameters as designated by Deltares; designated hereafter as SIC_New

4.3.2 Simulation & Atmospheric Input

The main scope of this research was to determine the effects of atmospheric conditions on the desiccation and crust formation of soft, cohesive, material. The primary way these differing conditions were simulated within the model was through modifying the recorded atmospheric input. Because of this, priority was placed upon properly differentiating the differing conditions not only in terms of design (as in the case of the various large-scale containers), but also in terms of accuracy, and duration.

Input Parameter		Explanation
Layer Thickness	[cm] *value/matrix*	Initial thickness of slurry layer
Drying Period	[days] *value/matrix*	Time from deposition to required end time
Sublayer Thickness	[cm] *value*	FDM layer size
Initial Water Content	[-] *value*	Initial water content for complete slurry layer
Time Step	[days] *value*	FDM time step size
Days	[day] *matrix*	Days with recorded data
Net Average Precipitation/Evaporation	[cm/day] *matrix*	Recorded average values for the days specified above; "+" for precip. & "–" for evap.

Table 4-6: Model simulation input parameters, adapted from (Vardon and van Tol, 2014)

In terms of the containers –although the atmospheric data at the containers' site was collected– additional modifications were made in order to generate distinct atmospheric conditions that would best represent each of the containers. In general, however, a significant reduction in windspeed was utilized due to the presence of the container walls and their nullifying effects on full wind movement across each of the soil surfaces. Exact graphs of the container variations and modifications made to each of their net precipitation timelines can be seen in section 5.1.3 Container Conditions Timelines.

In the case of the large-scale tests, any missing atmospheric data which was not obtained on site was procured through the KNMI database, specifically the Rotterdam station, as it was the closest located weather station. Initially, it was proposed to utilize the KNMI database once again to obtain weather data from a station as close as possible to the Marker Wadden site and this was determined to be the Lelystad station. However long-term climate data from this station was not available and instead, average monthly values were utilized and were obtained from KNMI LN-15, which averaged the data from 15 major weather stations all across the Netherlands (KNMI, 2017b). The approximate daily values based on each month can be seen in Figure 4-15.

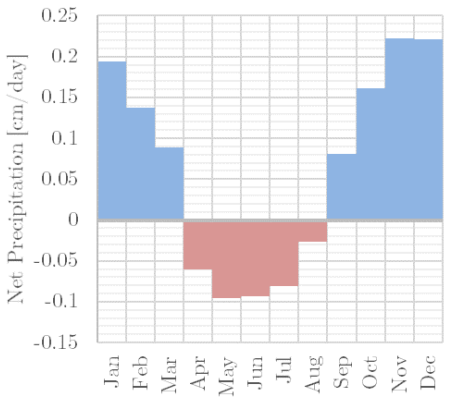

Figure 4-15: Average net precipitation values across the Netherlands, adapted from (KNMI, 2017b)

In addition to predicting the general behavior of the Marker Wadden soil over time, an additional aspect investigated was the initial start season in which a majority of the surface free water was to be removed. This included rotating the starting values based on seasonal variations within the Netherlands, with the corresponding first summer, autumn, winter, and spring months taken to be June, September, December, and March. This was to not only realistically model the initial behavior of the desiccation and crust development, but to also assess the both the short and long-term effects of initial season variations.

4.3.3 Material Properties Input

The model requires various material properties and parameters to be externally determined either through laboratory testing, equation fitting, or using pre-existing knowledge of the soil and its properties. Table 4-7 provides a summary and explanations of the main model material input parameters.

Both the SWRC and permeability fitting parameters are meant to be experimentally determined. The SWRC parameters were initially estimated based on an odeometer test; however, for this research updated SWRC parameters which were determined using the Hyprop as discussed in previous sections were utilized instead, with a brief comparison between the two assessed.

Input Parameter		Explanation
Solid Density	[g/cm^3] *value*	Specific gravity of slurry solid particles
Fluid Density	[g/cm^3] *value*	Density of water; 1
Liquid Limit	[-] *value*	Liquid Limit of the slurry
Plastic Limit	[-] *value*	Plastic Limit of the slurry
Plasticity Index	[-] *value*	Plasticity Index of the slurry
	Shrinkage Curve	
A_{SH}	[-] *value*	Minimum void ratio; SL
B_{SH}	[-] *value*	Slope defining parameters; equal to A_{SH}
C_{SH}	[-] *value*	Transition defining parameter; 3
	Soil Water Retention Curve	
Minimum Water Content	[-] *value*	Residual water content
Maximum Water Content	[-] *value*	Full saturation water content
α	[-] *value*	Van Genuchten SWRC fitting parameter
n_{WRC}	[-] *value*	Van Genuchten SWRC fitting parameter
m_{WRC}	[-] *value*	Van Genuchten SWRC fitting parameter
Modified	Y or N	Y
a	[-] *value*	10000
	Permeability/Hydraulic Conductivity	
A	[-] *value*	Dependent upon relation used
B	[-] *value*	Dependent upon relation used
Unsaturated Permeability	Y or N	Y
delta	[-] *value*	3

Table 4-7: Model material input parameters, adapted from (Vardon and van Tol, 2014)

The permeability relation and parameters must also be determined, either based on existing data and literature, or through experimental testing. In the case of the log-linear relation expressed in equation [4-3], the values were estimated using previously published material concerning experimental estimations for specific clay mineral types, and were modified based on varying sand contents expected in the Marker Wadden and in the large-scale containers. For the other power-log relationship expressed in equation [4-4], settling columns and a seepage induced consolidation (SIC) test had been performed specifically for the Marker Wadden. However, the SIC determined values were not yet available during the initial modeling; because of this, only the initial settling column determined values were utilized in the initial Marker Wadden estimations.

Relation	A [-]	B [-]
Settling Col (Orig)	$1x10^{-18}$	13
SIC (New)	$5.373x10^{-17}$	15
TUD (excl. sand)	0.9	6
TUD (containers)	0.9	5

Table 4-8: Various Permeability Relation Parameters

Table 4-8[3] provides the actual inputs used within the model. All of these relations and their values can be seen graphically in Figure 6-13.

4.3.4 Limitations & Assumptions

As this is meant to be a fast working model, there are many assumptions and limitations in place to simplify modeling. First and foremost, the model assumes a single homogenous initial density across the complete vertical profile. This is especially important when considering the modelling of the large-scale containers, as the density varies throughout the depth, especially due to the presence of sand layers. Furthermore, as the Marker Wadden is filled in layers, each layer will have varying densities that cannot be accounted for within this model.

Another important long-term component of the desiccation and crust formation are the cracks which occur as well any chemical changes which could inhibit or exacerbate the process. However, cracks form as a result of the increase in lateral tension, which cannot be modelled in a one-dimensional context. Instead, the model implements a single representative factor to try and take these more complex and intricate processes into account, but only serves as a general estimation of these effects (Vardon et al., 2015).

Additionally, the initial conditions within the model assumes that the material has just been uniformly deposited in layers. This is an important limitation, as the measured results of large-scale containers begin only at the end of the initial self-weight consolidation phase. Therefore, the prior settlement and self-weight consolidation phases must be accounted for when modelling the large-scale test conditions.

4.3.5 Additional Model Modifications

In addition to modifying the input values of the model, minor modifications were made in order to further assess the results of the model for the large-scale containers and in general for other properties. This included the additions of estimated shear strength relations throughout the profile over time, in addition to the expected bearing capacity. The following equations were utilized in the model in order to determine shear strength and bearing capacity, respectively.

$$c_u = \left(\frac{1.167}{LI}\right)^{2.44} \qquad [\ 4\text{-}5\ ]$$

$$q_{ult} = 5.14 c_u \qquad [\ 4\text{-}6\ ]$$

The shear strength, c_u, is in kPa and LI is the liquidity index, which is calculated using the gravimetric water content and Atterberg limits. This equation was determined based on a correlation by Locat & Demers in addition to a study of Dutch marine clays performed at TU Delft. The bearing capacity, or q_{ult}, is determined by the Terzaghi bearing capacity equation (Vardon et al., 2015). In order to determine the liquidity index, additional material input parameters were established to include the estimated plastic and liquid limits of the slurry.

As previously mentioned, the saturated hydraulic conductivity can be modelled using two distinct equations. Dependent on the model run and the input parameters, the required equation was chosen, and therefore the difference in equations and their influence in the model results could be assessed. Because of this, both equations were added into the model, and one was selected at the beginning of each run. It is important to note that while equation [4-3] gives the saturated hydraulic conductivity in cm/day, equation [4-4] results in m/s, and must be converted into cm/day within the model, before being utilized in additional model computations.

[3] Settling Col (Orig) refers to the initial parameters which were determined using material from initial settling column tests and are the values used in the original model assessment of the Marker Wadden. SIC (New) refers to the newly determined parameters obtained from SIC tests performed with actual Marker Wadden material, referenced in Boskalis and Deltares documents as SIC3. Two sets of TUDelft parameters were used in the original model assessment. However, it was determined that the parameters representing primarily clay material and excluding sand contents was closest in representing the Marker Wadden, and an additional modification was made to these parameters for the large-scale test conditions to account for the higher sand fractions present.

5 Results & Initial Analysis

This chapter presents the relevant results of both main aspects of this research: the large-scale testing, Hyprop SWRC fitting, and numerical modeling, including initial analysis. These results will then be further analyzed and discussed in a larger scope in Chapter 6.

5.1 Large-Scale Tests

A detailed assessment of the exact properties and existing variability was conducted before assessing any changes which occurred within each of the containers over the timeframe of the current research. This included a generation of vertical fraction profiles, the changes in Atterberg limits, as well as a general chemical and biological analysis. In addition to these, more detailed property profiles were generated at various points throughout the testing period. These have been collected in order to compare and establish any trends which occur over time, and will be further used to validate the conceptual model outlined in Chapter 3. A more direct discussion of this conceptual model validation in regards to the large-scale tests can be found in section 6.1.1 Conceptual Model Validation.

5.1.1 Material Properties

The following sections provide a detailed overview of the material properties within each of the containers. All required tests were executed by Boskalis Environmental (unless otherwise stated) for highest accuracy and to limit possible procedural errors. As stated previously, due to differences in the filling procedures, each container exhibited variations in material properties. Representative property values were established to allow for more precise analysis process and overall trending hypotheses to be concluded within each of the containers, although a high variance in properties with depth was observed.

5.1.1.1 Clay, Silt, & Sand Fractions

Based on the final conclusions presented in van Olphen's thesis, the first material assessment conducted was a profile breakdown of the fractions present within each of the containers. This was done by collecting a vertical profile using a Beeker core, separating the profile into 10 cm sections, and assessing each section for the clay, silt, and sand contents.

Figure 5-1 shows each of the three containers' main fraction distributions, including the gradual increase of sand content towards the bottom of all three containers and, in the case of C2 and C3, towards the middle of the profile. For reference, the fraction assessment of a sample taken from van Olphen's initial container filling slurry can be seen in Figure 5-2.

In comparison to the material used in the filling layers of the Marker Wadden itself, the material utilized in the large-scale

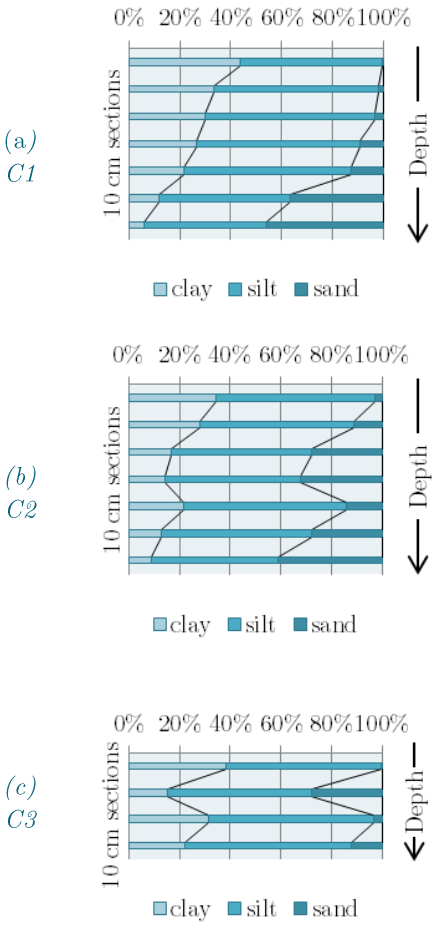

Figure 5-1(a)(b)(c): Measured clay, silt, and sand fractions

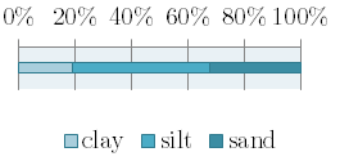

Figure 5-2: Initial container slurry fractions (van Olphen, 2016)

testing exhibits higher sand contents due to the dredging method. This is important as it influences density and shear strength results, because varying fraction ratios will exhibit different properties and this must be taken into consideration during both calibration and analysis. However, it is important to note that in terms of general ductile behavior, the 10% minimum clay fraction is present within all profile sections of the containers. Furthermore, in an attempt to replicate material utilized in the Marker Wadden, the material collected for Hyprop testing was taken from the top of the container material in order to reduce the unrealistic inclusion of elevated sand fractions.

5.1.1.2 Atterberg Limits

As anticipated, due to the variations in the fractions throughout the containers, the Atterberg limits of each section also vary along the profile depth. Table 5-1 shows the Atterberg limits obtained for the large-scale containers, with an emphasis on the limits for the topmost material, and the range of values exhibited throughout the vertical profiles.

Container		PL [%]	LL [%]	PI [%]
C1	**surface**	**64**	**196**	**132**
	profile	32-64	55-196	23-132
C2	**surface**	**62**	**155**	**92**
	profile	29-62	64-155	34-92
C3	**surface**	**63**	**155**	**92**
	profile	36-63	74-167	38-104

Table 5-1: C1, C2, C3 measured Atterberg limits

Due to the nature of the Casagrande method when obtaining the Atterberg limits of a material, there is an inherent variability of the values. This issue, in combination with the natural variability of the material (even at the same depth within the container) can be seen in the difference in the limit values between those of the container top material, and the material collected for the Hyprop testing, which can be seen in Table 5-4.

5.1.1.3 Organic, Biological, & Chemical Analysis

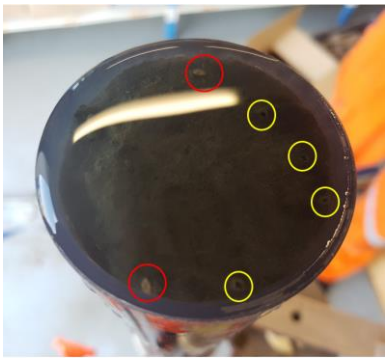

Figure 5-3: Biological presence

Only very basic organic, biological, and chemical analyses were performed in order to get a general overview of the conditions within the container. When retrieving relatively undisturbed vertical profile samples of the material within each of the containers, a clear biological presence was observed. This can be seen in Figure 5-3, with the organisms identified by the red circles, and some burrow holes identified in yellow.

Table 5-3 shows the approximate organic matter present within each section of the three containers, while Table 5-2 is a compilation of the both the pH and salinity within not only the containers at various depths, but also general values for the Marker Wadden samples obtained for additional laboratory (Hyprop) testing. The salinity values of the pore water present within both the containers and the Marker Wadden indicates the total concentration of dissolved salts present. This can be of importance as the salts can then form precipitates on the surface of the material as it dries.

Depth [m]	LOI [%] C1	C2	C3
0.0-0.1	19	15	15
0.1-0.2	15	13	7
0.2-0.3	14	10	12
0.3-0.4	13	12	11
0.4-0.5	11	3	
0.5-0.6	8	11	
0.6-0.7	5	10	
0.7-0.8	3	6	

Table 5-3: C1, C2, C3 organic matter

	C1		*C2*		*C3*	
Depth [m]	**pH [-]**	**Salinity [ppt]**	**pH [-]**	**Salinity [ppt]**	**pH [-]**	**Salinity [ppt]**
0.0-0.1	7.15	1.461	7.40	1.313	7.41	1.008
0.1-0.2	7.29	1.376	7.32	1.149	7.32	0.827
0.2-0.3	7.26	1.263	7.39	1.159	7.13	1.099
0.3-0.0	7.30	1.225	7.34	0.640		
0.4-0.5	7.22	1.201	7.20	0.899		
0.5-0.6	7.19	0.967	7.27	0.768		
0.6-0.7	7.26	0.781				

(a)

Marker Wadden Hyprop Samples	pH [-]	Salinity [ppt[
MW A2-1	6.93	1.546
MW A2-2	6.98	1.539

(b)

Table 5-2(a)(b): pH and salinity values for C1, C2, C3 and Marker Wadden samples

5.1.2 Project & Environment Timeline

The weather conditions throughout the testing period were monitored and recorded, and the main components can be seen in Figure 5-4, including markers of when the testing days took place for reference. While Figure 5-4(a) shows the general decreasing trend of the temperature over time, Figure 5-4(b) shows the pure daily precipitation values over the course of the project, as well as the calculated Penman daily evaporation. It can be observed that the decreasing daily potential evaporation trend reflects that of the seasonal change from dry summer to fall and winter.

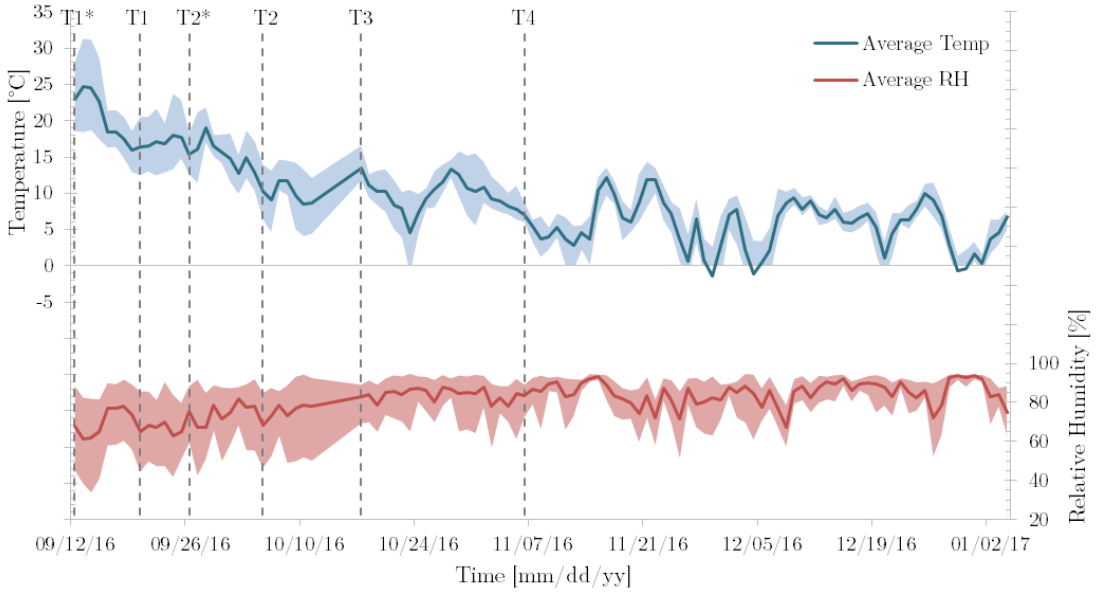

(a) Daily temperature and relative humidity

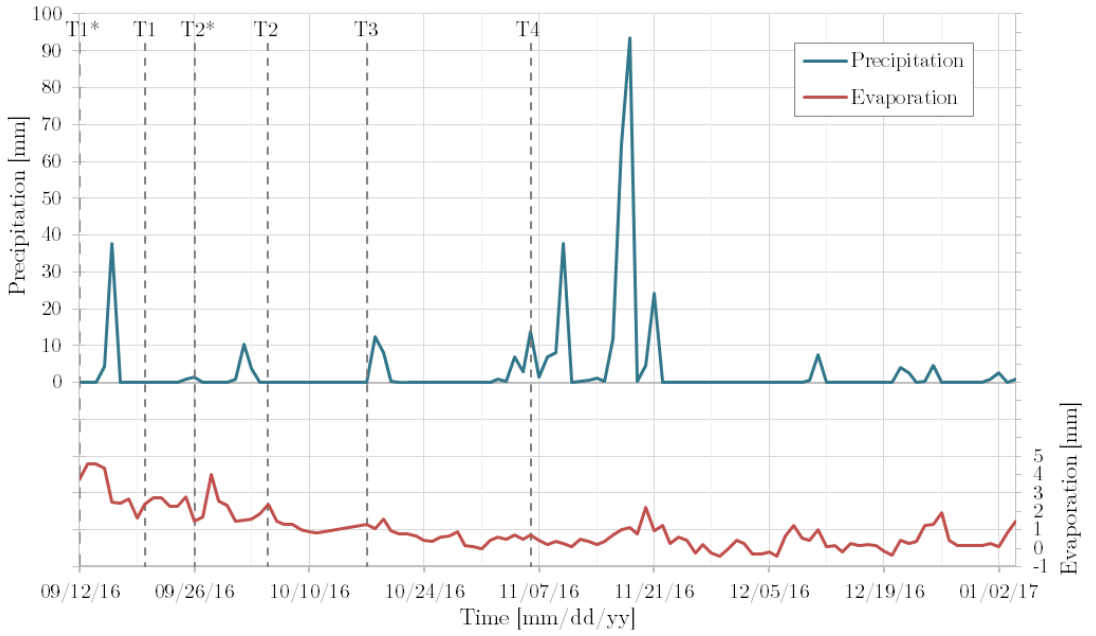

(b) daily precipitation and evaporation calculations

Figure 5-4(a)(b): Large-scale testing project timeline conditions

5.1.3 Container Conditions Timelines

While Figure 5-4 shows the actual recorded conditions for the large-scale testing, each of the containers experienced variations of the precipitation and evaporation conditions, which combined are represented through a net precipitation value, and can be seen in Figure 5-5, Figure 5-6 and Figure 5-7. The net precipitation has also been plotted above the recorded levels within the container. The level reading within the container is indistinguishable between the soil surface and excess surface water level, so care should be taken when interpreting these readings in relation to the net precipitation variations. Additionally, although measures were taken in C1 and C2 to prevent/remove surface water buildup after the initial water removal, the pore water pressure readings show that this was not always effective, as surface water buildup results in an increase between dated pore pressure profiles, which theoretically should only have stayed either constant or a decrease as time progressed. Attempts were made to distinguish water and soil using the pore pressure profiles generated from the three in-situ piezometers within each of the containers. Unfortunately, these were not detailed enough to confirm which surface reading was water and which was soil; however, these pressure profiles can be seen in the section Complete Pore Pressure Readings in the Appendices.

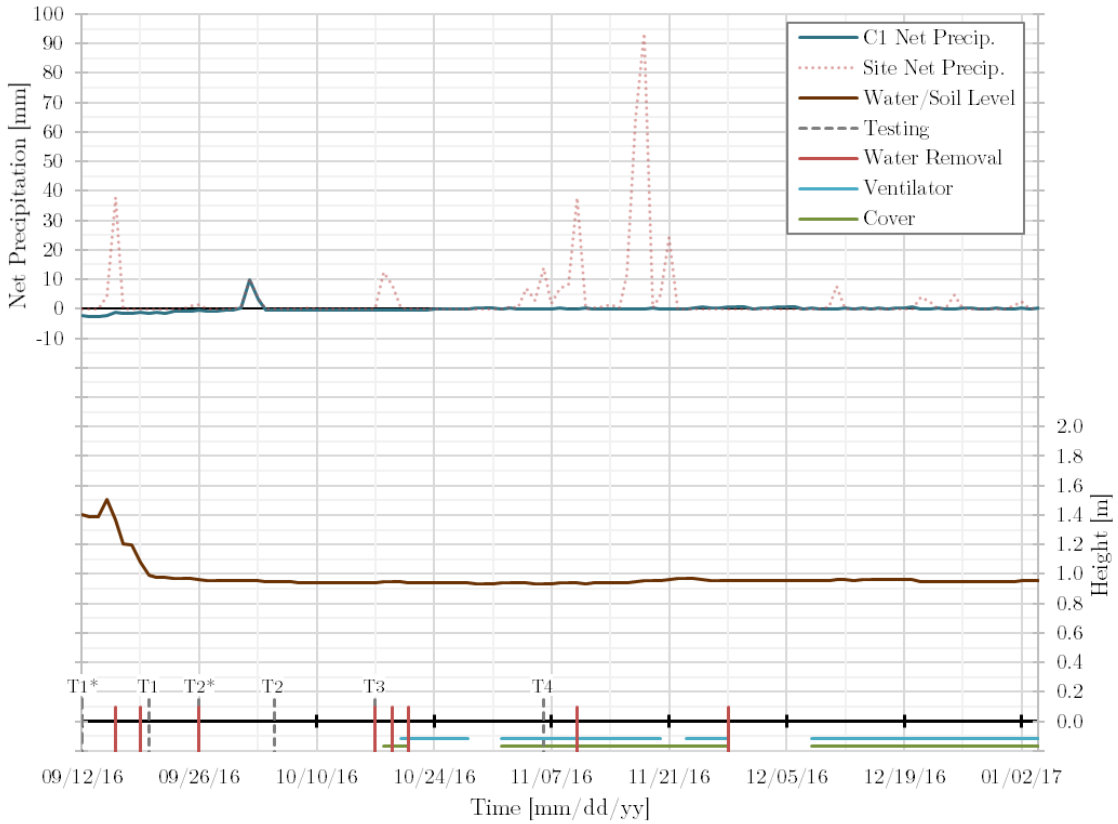

Figure 5-5: C1 modified net precipitation timeline with water/soil level

As described in section 4.1.2 Test Condition Variations, C1 represented the 'extreme' dry conditions and utilized not only a cover and ventilator at times, but also manual water removal. A specific timeline of what was done in C1 can be seen at the bottom of Figure 5-5 for reference. Additionally, due to these factors the estimated net precipitation has been modified for each of the containers, including C1. At times where the C1 was covered and the ventilator was operational, the wind speed used to calculate the estimated daily evaporation was modified to that of the wind speed generated by the ventilator within the container. Furthermore, any precipitation events which occurred while C1 was covered was taken out of the net precipitation calculations, as none of this water is assumed to have reached the soil inside the container. It should be noted that this was unrealistic expectation and therefore not a completely accurate assumption to make when modifying the conditions, which may influence the modelling output in comparison to the measured results.

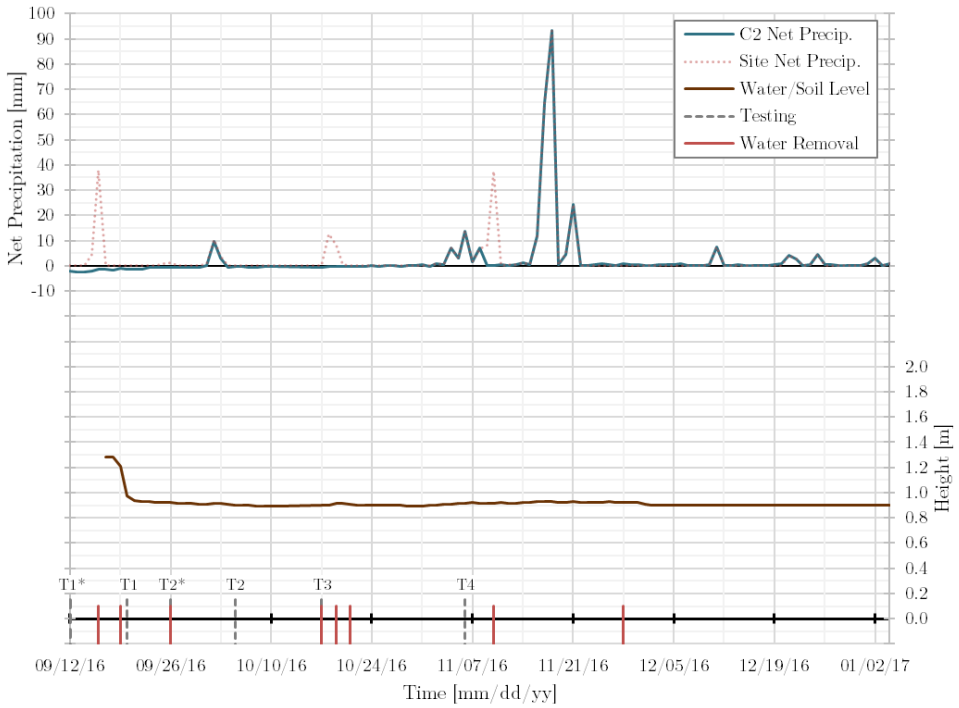

Figure 5-6: C2 modified net precipitation timeline with water/soil level

For reference, Figure 5-6 and Figure 5-7 have also been compiled for C2 and C3 and their respective modifications and timeline moments. The net precipitation of C2 was modified by eliminating precipitation which occurred before the manual water removal, to reflect that any water which built up as a result was no longer assumed to be present within the containers. This was also done at the same water removal points in C1. C3's net precipitation was modified by eliminating any potential evaporation which could have occurred due to water buildup of preceding rain events.

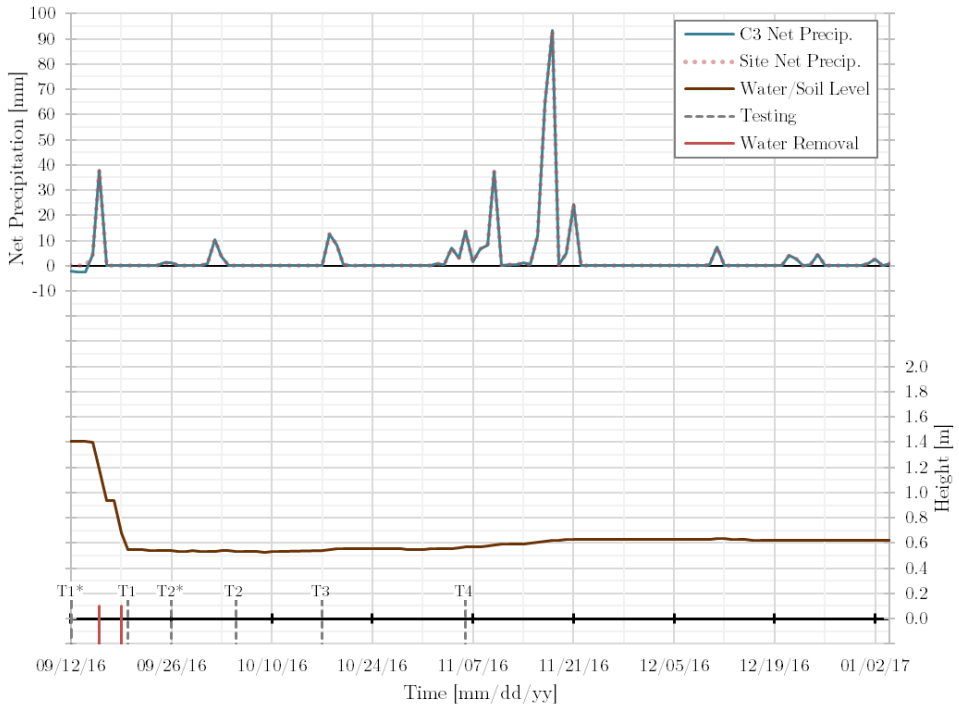

Figure 5-7: C3 modified net precipitation timeline with water/soil level

5.1.4 Water Content & Void Ratio Profiles

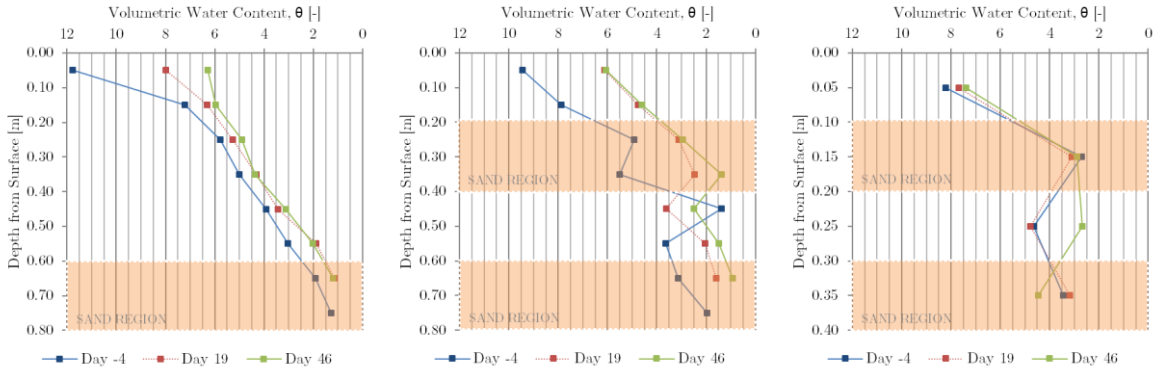

(a) C1 (b) C2 (c) C3

Figure 5-8(a)(b)(c): Measured water content profiles over time

As Beeker cores were taken throughout the testing period, these samples were analyzed for water contents, in addition to other specific properties. Each color within these graphs represent a distinct testing period, and the general areas with increased sand contents have been highlighted. An overall reduction in water contents throughout the container profiles can be observed in Figure 5-8, especially in (a) and (b). When assessing the reduction in water contents, these results do indicate an increased reduction over time based upon the extremity of the container conditions, as C1 shows a higher reduction in comparison to C3 which was exposed to completely natural conditions, and was essentially submerged under a layer of a water for the majority of the testing period an shows minimal changes over time.

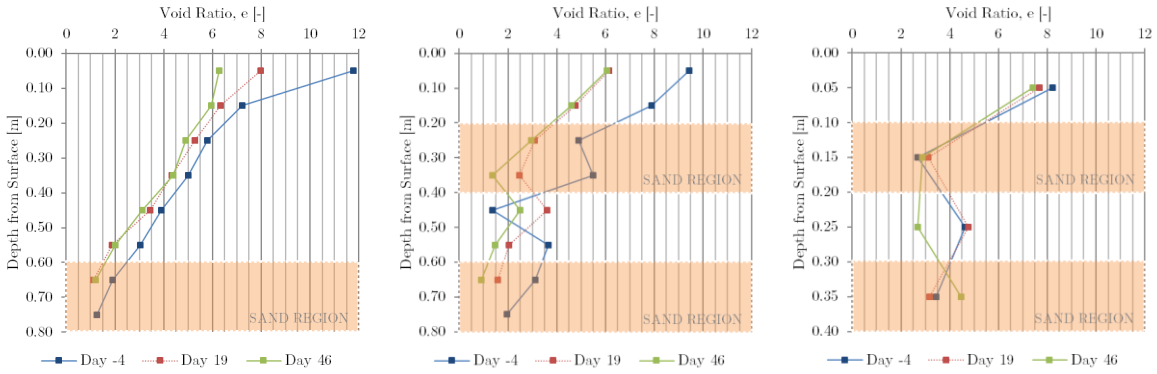

(a) C1 (b) C2 (c) C3

Figure 5-9(a)(b)(c): Measured void ratio profiles over time

In addition to the in-situ water contents, the void ratio profiles within each of the containers over time have been plotted, as the void ratio was the main parameter utilized in the conceptual model of desiccation and crust formation. The void ratios determined were equivalent to the water content, as the material was always saturated and were calculated using the relation proposed in equation [2-6]. As with the in-situ water contents, a general reduction throughout the entire profile, especially C1 can be seen in Figure 5-9.

5.1.5 Density Profiles

The results from the densimeter tests and Beeker core density measurements were compiled into one figure to determine the evolution of the density profile within each container over time. Abridged versions of these graphs can be seen in Figure 5-10 for C1 and C2, with solid lined trends for the initial and final generated density profiles.

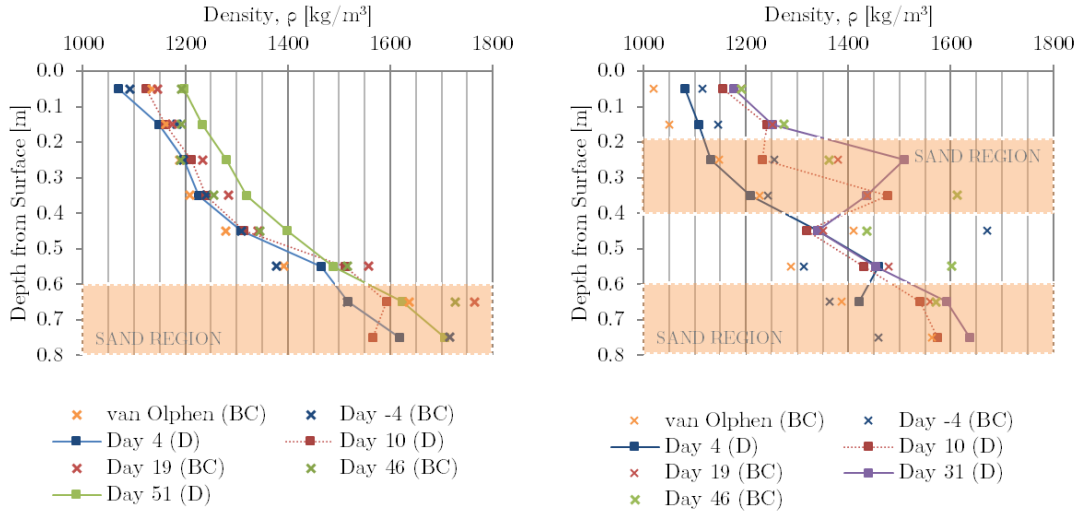

(a) C1 *(b) C2*

Figure 5-10(a)(b): Measured density profiles over time

It should be noted that any densimeter readings falling within the shaded "sand region" areas should not be taken into consideration. This is because further calibration with increased sand contents was not performed. Additionally, although original densimeter measurements were typically taken in one centimeter increments throughout the containers, these measurements were averaged into 10 cm sections in order to more concisely compare them to subsequent Beeker core density profiles. A general densification trend (shift towards the right) can be seen. This falls in line with the trends seen in both the in-situ water content and void ratio profiles, where water loss due to evaporation has taken place during the first stage of drying. However, these measurements, and especially those obtained with densimeter should be considered carefully, due to inconsistencies in output. Issues with the densimeter and its calibration are discussed in further detail in section 6.1.4.2 Densimeter Inconsistency.

5.1.6 Shear Strength Profiles

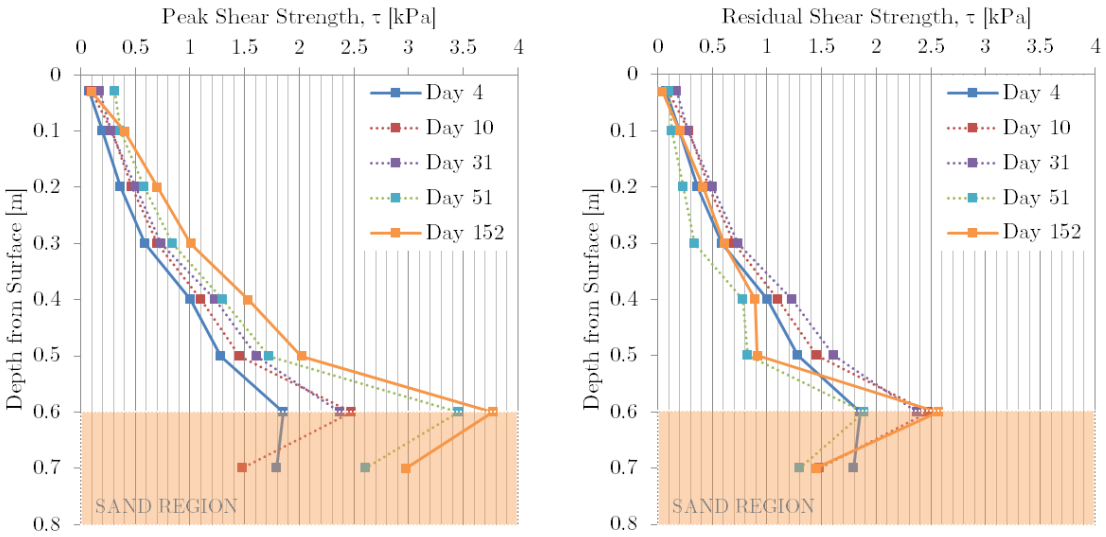

(a) C1 Peak *(b) C1 Residual*

Figure 5-11(a)(b): Measured C1 peak and residual shear strength profiles over time

Based on the data obtained through the in-situ vane tests, the shear strength development was broken into two distinct aspects: the peak and residual shear strength values. The development over time of each of these value profiles has been plotted for C1 and C2 in Figure 5-11 and Figure 5-12, respectively. While the increase in shear strength along the depth of the profile was to be expected due to the increase

in effective stress, there are some deviations within the profile due to the presence of the sand layers. Figure 5-11 shows a distinct increase in the peak shear strength profile over time, except at the surface. A similar increasing trend can be clearly seen in Figure 5-12, however the intermediate sand layer region impacts the clarity of this overall trend. It was expected that as the shear strength is related to the water content, that a more observable development in the surface shear strength would occur, however this was not the case, as evident in the figures.

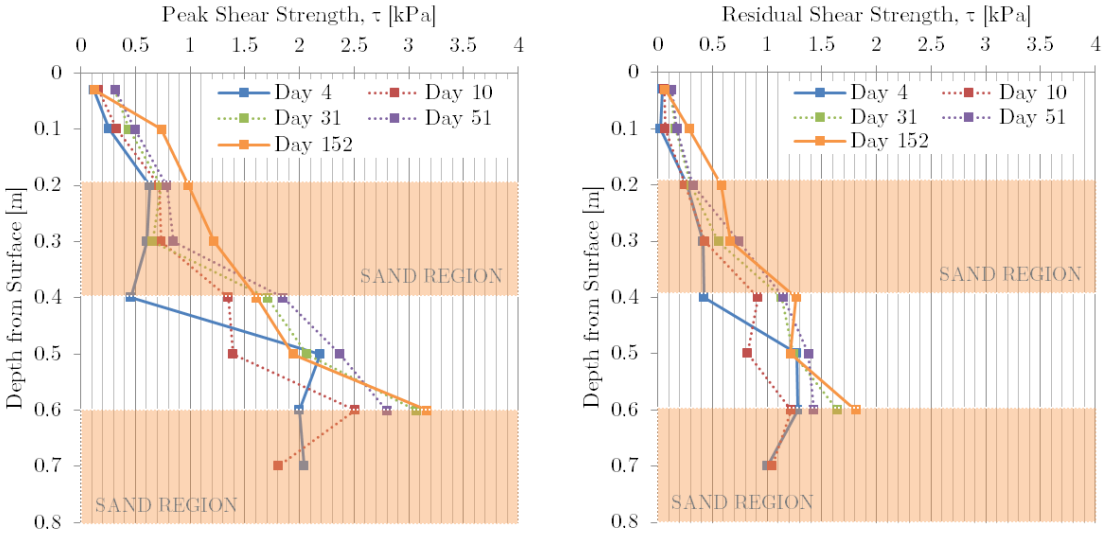

(a) C2 Peak *(b) C2 Residual*

Figure 5-12(a)(b): Measured C2 peak and residual shear strength profiles over time

5.2 Hyprop Results

The Hyprop testing aspect of this research consists of two main parts. The first is to confirm and compare the properties of the material being tested to the properties determined in the large-scale testing and Marker Wadden. The second is interpreting the results of the Hyprop testing in determining the parameters of the SWRC's for the various soil specimens.

5.2.1 Material Properties

Figure 5-13 shows the fraction distribution variations for each of the materials tested with the Hyprop. Note that that there are significant variations between not only the two containers sourced for sampling, but also within the Marker Wadden itself. While some of this may be due to sampling method, a large portion can be attributed to the natural heterogeneity of soil, but it should be noted that all of the samples have minimal sand fractions. It is important to recognize these variations when considering its effects on the fitting of the SWRC. These property variations can also be seen in Table 5-4, as well as the variation in initial water contents, which plays a role in the vertical positioning of the SWRC.

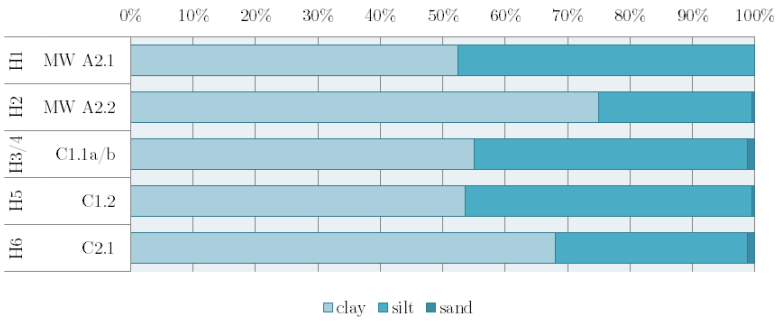

Figure 5-13: Hyprop test material clay, sand, and silt fractions

Hyprop Test	Sample Material	ρ [kg/m³]	*w* [%]	*LL* [%]	*PL* [%]	*PI* [--]
H1	MW A2.1	1187	291.7	175	61	114
H2	MW A2.2	1175	299.6	192	63	129
H3/4	C1.1a	1160	326.8	220	73	148
H5	C1.2	1146	359.0	222	70	152
H6	C2.1	1190	272.4	185	62	123

Table 5-4: Hyprop test material general properties

5.2.2 SWRC Fitting Parameters

The raw suction and weight data points obtained through the Hyprop test and final oven-drying was refined and corrected to account for initial negative tension values as well as any inconsequential readings after the peak tension reading took place and air entry occurred. As a sample, **Figure 5-14**(a) shows the complete data points obtained from the H3 Hyprop test, without correction or valid data isolation. For more details on how these calculations and refinements were performed please see the section SWRC Calculations in the Appendices.

As mentioned in section 4.3 Numerical Modelling, the SWRC is represented in the model through the Van Genuchten fitted equation. The corrected data points were then input into a pre-existing open source fitting model for various SWRC fitting equations (Seki, 2007). A sample of the corrected and isolated data points obtained by the H3 Hyprop test can be seen in **Figure 5-14**(b), with the relevant Van Genuchten equation fitted through the data. The fitting parameters of this equation for each of the Hyprop samples have been compiled in Table 5-5.

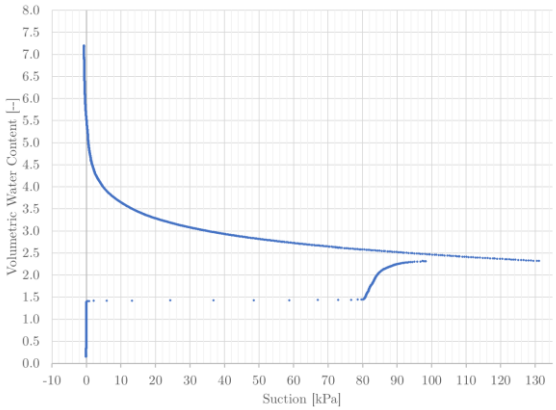

(a) raw Hyprop SWRC data points

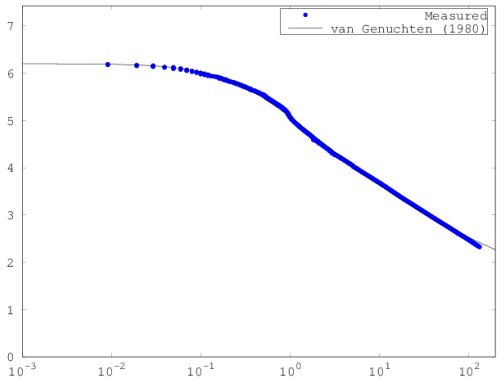

(b) corrected SWRC data points (log scale)

Figure 5-14(a)(b): Sample Hyprop SWRC data and equation fitting

One aspect to note is that the Hyprop maps only one part of the complete SWRC due to the tension range limitations of the tensiometers, and the WCS computed is generally restricted to a range near the initial (highest) water content exhibited by the sample. The impact of this as well as sampling will be discussed in further detail in Chapter 6.

Hyprop Test	Sample Material	WCS [-]	WCR [-]	α [-]	n_{WRC} [-]	m_{WRC} [-]	R^2
H1	MW A2.1	8.166	0.862	3.93	1.24	0.19	*0.9974*
H2	MW A2.2	6.839	0.000	4.33	1.15	0.13	*0.9982*
H3	C1.1a	6.200	0.000	2.84	1.16	0.14	*0.9984*
H4	C1.1b	7.063	1.307	1.81	1.30	0.23	*0.9944*
H5	C1.2	8.754	1.025	4.24	1.26	0.20	*0.9963*
H6	C2.1	6.069	0.000	1.95	1.20	0.17	*0.9907*

Table 5-5: Van Genuchten fitting parameters based on Hyprop data

5.3 Numerical Model Results

This section provides a condensed summary of the results obtained through the numerical modeling, including a discussion of the changes which were implemented in each of the model runs in order to generate optimal outputs. These results will then be further analyzed and discussed in tandem with both the available physical results (in regards to the large-scale testing) and additional model runs throughout Chapter 6.

A careful assessment of the model and its sensitivity had to take place as the model was highly susceptible to numerical oscillations based on the inputs provided, as well as other errors. While most of the major oscillations were eliminated by carefully assessing the sensitivity of the main input parameters, it is important to note that some oscillations within the results remained. However, this did not impede the interpretation or comparison of the overall results. In order to create optimal model runs, the main changes and modifications have been summarized below in their respective sections.

5.3.1 Large-Scale Test Modelling

The first portion of the modelling involved attempts to accurately replicate the measured results obtained over time from each of the containers. This included not only a determination of the optimum input parameters, but also an assessment of the potential discrepancies which could occur between the measured and the modelled profiles. In essence, these comparisons will then be used to further validate the numerical model and assess its applicability towards additional Marker Wadden predictions and estimations. An assessment of the model's validity is more directly discussed in the next chapter, in section 6.1.2 Numerical Model Validation.

5.3.1.1 Container Modelling Refinement

One of the main changes made for modelling the container conditions in order to compare the model results to those determined in-situ was the introduction of a pre-run period. This was done in order to mimic the filling, settling, and self-weight consolidation phases which took place in the containers prior to this project, as the model starts under the assumption that the material has yet to undergo these processes. As the focus of this project was on the subsequent desiccation stages rather than those which took place prior to initial water removal, minimal effort was made to ensure that the model properly represented the initial process stages. However, the pre-run time was based upon the approximate time between initial container filling and the start of this project (i.e. 290 days).

One of the primary limitations of the numerical model is that it assumes the layer to be homogenous throughout the vertical profile. This includes utilizing a single uniform initial water content value along the complete vertical soil profile. This became an issue in terms of modelling the containers due to very obvious presence of sand within the containers. This means that the material within the container cannot be easily assumed as homogeneous in nature, regardless of the natural variance in density throughout the profile which would take place due to the filling, settlement, and self-weight consolidation stages. Nonetheless attempts were made to increase the model accuracy based on the estimated initial density, which has an estimated initial void ratio value of 8.3 (and therefore initial volumetric water content, as S = 1) based on an assumed specific gravity of 2.4.

This proposed initial water content was higher than the maximum water content determined by the Hyprop, and attempts to use the original Hyprop SWRC with the proposed initial water content resulted in a highly deviating initial water content profile after the pre-run. In an attempt to resolve this, the volumetric water content and effective stress at various depths were assessed and compared to the Hyprop SWRC, and can be seen in Figure 6-3. Attempts to both modify the existing Hyprop data and utilize the effective stress and water contents as a rough SWRC still resulted in model errors. Therefore, the original Hyprop-obtained SWRC parameters were utilized with the highest allowable initial water content of 10 (beyond which the model failed).

5.3.1.2 Large-Scale Test Model Runs

After determining the optimal parameter settings and pre-run setup, primary model runs were performed for each container based on their specific characteristics. Model runs were performed for each of the three containers and their respective conditions, and their water content profiles over time can be seen in Figure 5-15. The days during which physical testing took place were extracted in order to directly compare the trends seen in the physical results, shown in Figure 5-8, to those produced through modeling. An assessment of the measured vs modelled results will be discussed further in Chapter 6, but for now only extreme differences will be addressed.

In general, one can see the same trends exhibited by the physical in-situ testing, including the correct initial height after the initial self-weight consolidation phase and associated pre-run. However, there is a clear discrepancy between the measured and calculated water contents. This was due in part to the limitation in the initial slurry conditions and soil water retention properties. Due to the lower initial water content profiles calculated at the start of the desiccation process, the model predicts an earlier crust formation, which is not seen in the physical results. Therefore, these model results can only be compared in trend, rather than direct values.

At first glance, it seems that C1 and C2 are on par in terms of desiccation; however, the model predicted thicker initial crust formation in comparison to C2. Additional profile properties were generated, a raw sample of which can be seen in the section Modelling Data in the Appendices. However, for brevity most of these have not been included in the main report, and only relevant graphs will be shown in Chapter 6, where necessary.

In addition to a straight comparison of the physical and model results, an isolated atmospheric influence assessment was made by using the material properties of C1 and running the model with three atmospheric timelines: uncorrected conditions, and both C2 & C3 net conditions. The results of C1 material conditions with recorded site values, and both C2 and C3 net precipitations can be seen in Figure 5-16.

While there is no significant deviation between C1 modelled with C1 net conditions and C2 net conditions (Figure 5-15(a) and Figure 5-16(b), respectively), it can be seen that the moderate surface water mitigation measures put in place had a moderate impact on the desiccation process, especially in comparison to the general site conditions (Figure 5-16(a)) and significantly in comparison to allowing surface water buildup, as was done in C3 (Figure 5-16 (c)).

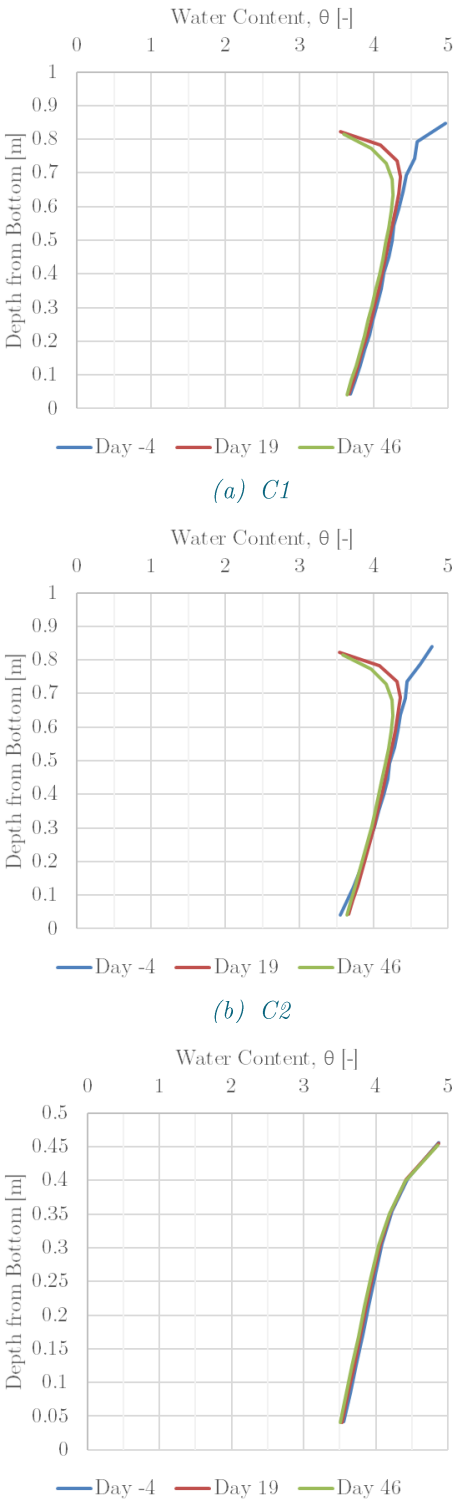

Figure 5-15(a)(b)(c): Modeled large-scale test water content profiles

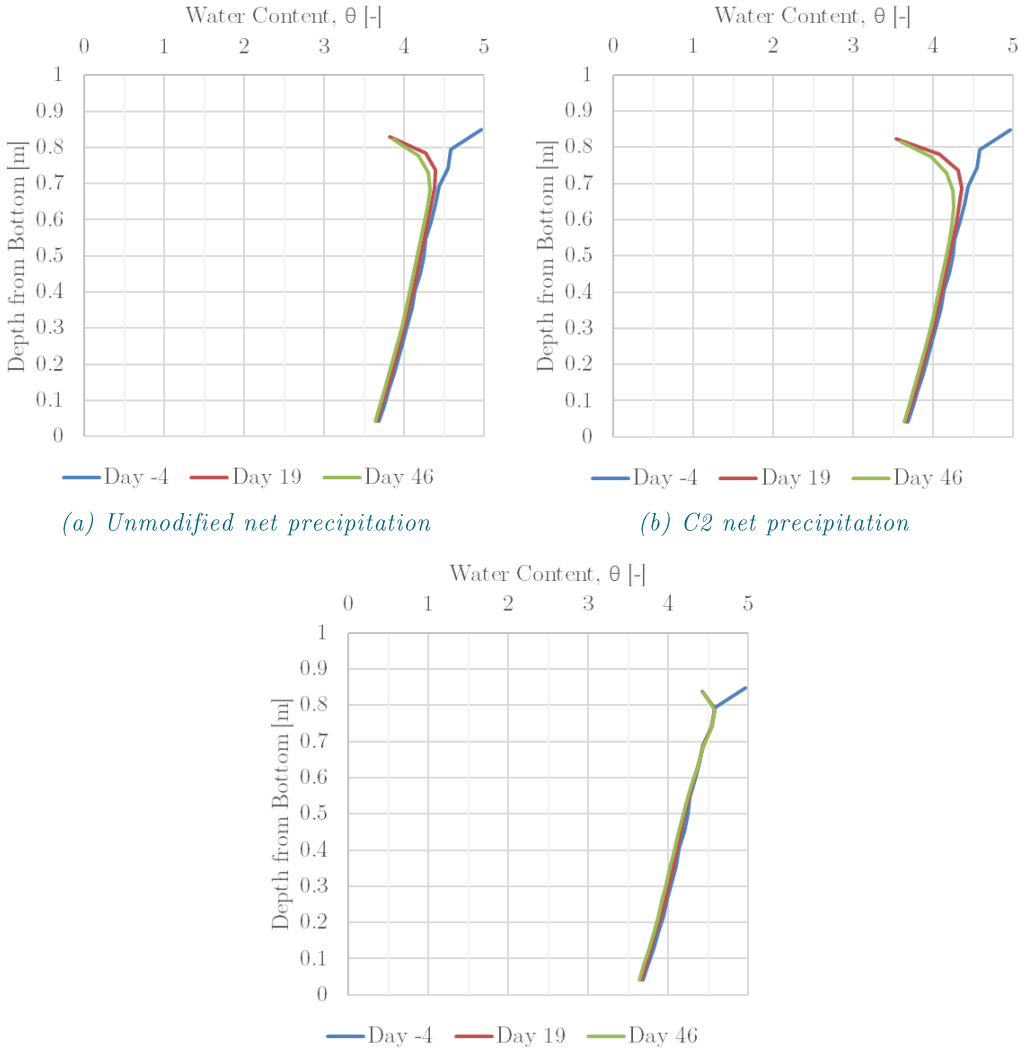

(a) Unmodified net precipitation

(b) C2 net precipitation

(c) C3 net precipitation

Figure 5-16(a)(b)(c): Modelled water content profiles of C1 material with varying net conditions

5.3.2 Marker Wadden Modelling

Further model runs were performed for the Marker Wadden and have been categorized into three main types of analysis: baseline, initial seasonal variation, and surface water measures. The baseline models –including the simulation of unaltered, average, net conditions– serve to provide the extreme possibilities of the desiccation and crust formation process. In addition, the updated, baseline average model run will serve as a comparison model to all other runs. The initial seasonal variations are meant to realistically consider the effects of starting in a specific season on the short and long-term development of the crust. The final portion of modelling is meant to mimic the potential effects of varying surface water mitigation measures, and again its effects on both the short and long-term development of the crust.

5.3.2.1 Original Marker Wadden Model Estimations

Table 5-6 summarizes the relevant predictions generated from the first model assessment, after two years. These will then be compared to the results from a newer, updated model with varied input parameters. It should be noted that the closest model run in terms of conditions is the model designated as run 8 in Table 5-6.

Ref. No.	Starting Season [month]	ATM Input Conditions	Surface Height [m]	Crust Thickness [m]	Bearing Capacity [kPa]
4	Winter (Jan)	Evap Only	3.62	0.22	0.55
5	Summer (July)		3.61	0.20	0.82
7	Winter (Jan)	Net Precip	3.63	0.35	0.35
8	Summer (July)		3.59	0.45	0.34

Table 5-6: Original modelling results for Marker Wadden, adapted from (Vardon et al., 2015)

5.3.2.2 Marker Wadden Modelling Refinement

Some of the input parameters for the Marker Wadden portion of modelling utilized the previously established material parameters from the original assessment performed by TU Delft on behalf of Boskalis. However, an analysis of varying SWRC parameters and hydraulic conductivity parameters and relations was performed at the start of this model portion. This was done in order to determine an "optimum" baseline model which would be used for a further analysis of varying atmospheric conditions.

As mentioned previously, there were two possible permeability relations which could be utilized, both of which required two fitting parameters each and relate the permeability to the void ratio in either a log-linear or power-log manner (see equations [4-3] and [4-4]). The plotted relations and resulting model outputs can be seen in Figure 5-17.

After assessing the model runs and the variations between these relations, it was decided to utilize the original log-linear relation for the main atmospheric runs. This was in part due to the closer estimation of the parameters to those of the clay minerals present within the Markermeer, but also because the estimation in both settlement and crust formation seemed balanced in comparison to the runs which implemented the power relation with the SIC-determined parameters. A further analysis of the variations in permeability relations can be found in the next chapter.

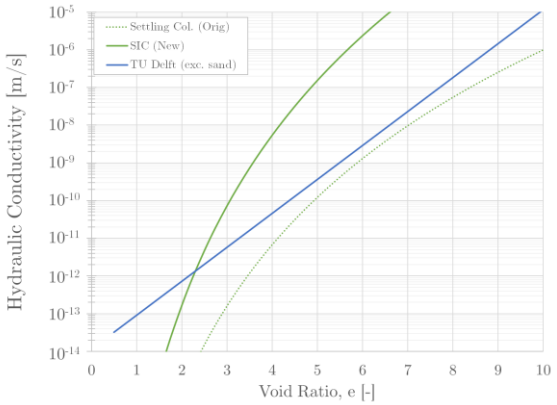

(a) initial permeability relations

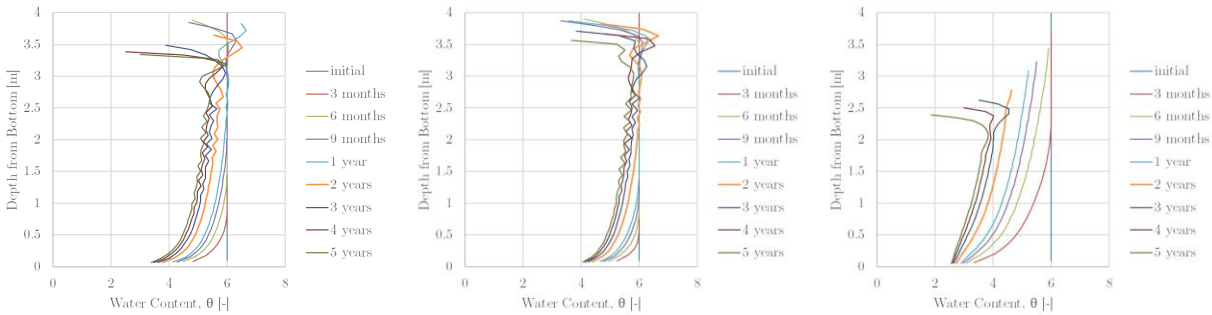

(b) TU Delft A=0.9, B=6

(c) Settling Col. (Orig) $A_k=10^{-17}$, $B_k=13$

(d) SIC (New) $Ak=5.373^{-13}$, $B_k=7.097$

Figure 5-17(a)(b)(c)(d): Marker Wadden permeability variations and initial results

In addition to the possible variations in the permeability inputs, an additional variation was possible in terms of the soil water retention input parameters. The initial SWRC parameters were estimated based on an oedometer relationship. As can be seen in Figure 5-18, there are minimal differences in results between the two different SWRC methods; however, the oedometer-based SWRC results show some numerical oscillations in the results, while the Hyprop-based SWRC does not. Because of this, it was decided to use the SWRC parameters which were determined by fitting the van Genuchten equation through the data points obtained by the Hyprop tests performed earlier in this project. For a more detailed assessment of the variations between the Hyprop and Oedometer obtained SWRC, please see section 6.3.1.2 Oedometer vs Hyprop.

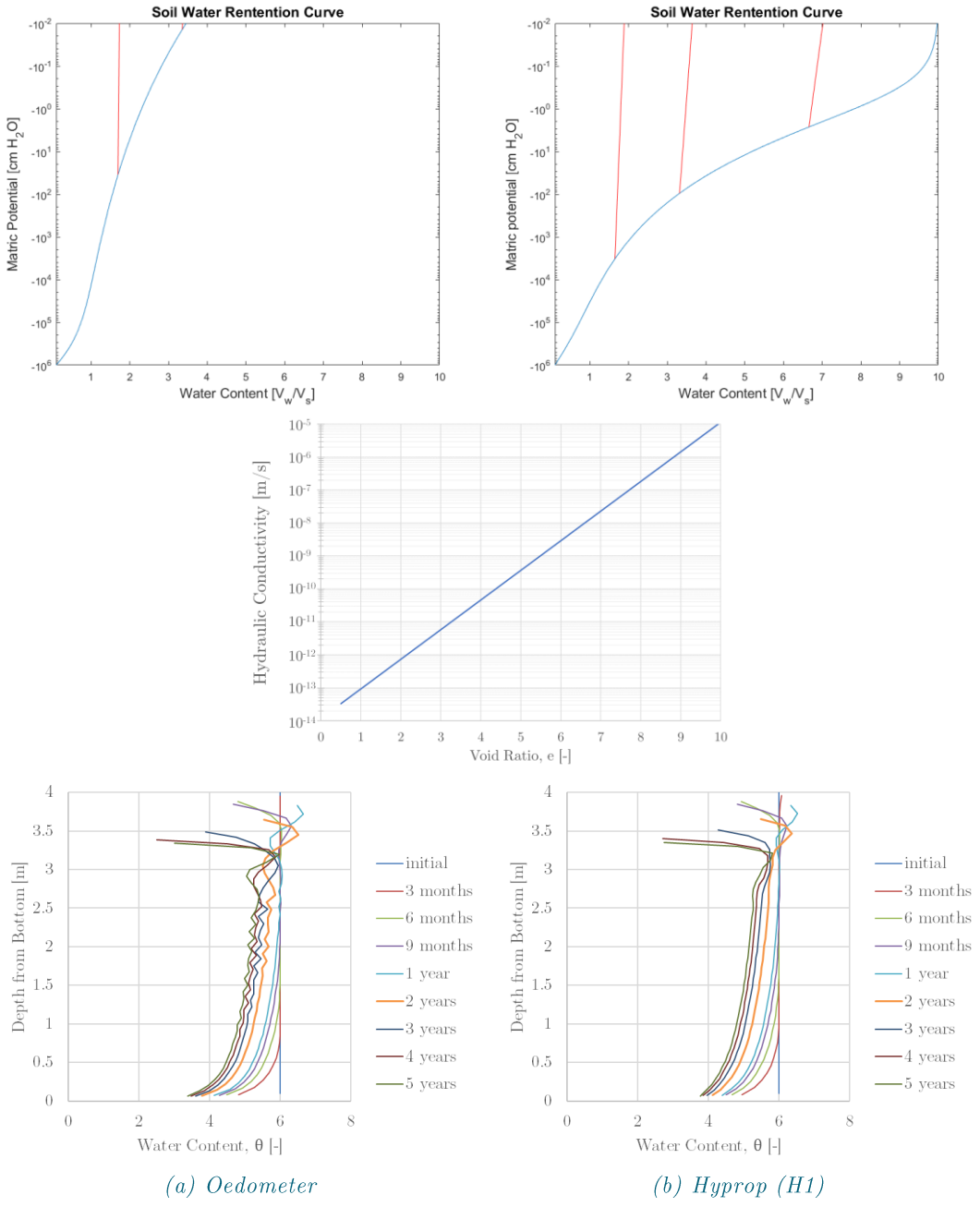

(a) Oedometer *(b) Hyprop (H1)*

Figure 5-18(a)(b): Marker Wadden SWRC variations and initial results

5.3.2.3 Variations in Marker Wadden Permeability Relations

In addition to assessing the influence of differing SWRC inputs, an additional modified model run was performed with newer/experimentally determined permeability input parameters. The original baseline model and its results were then compared to those of the newer model. Main parameter changes involved the SWRC and permeability inputs. The initial model's SWRC and permeability inputs were based on odeometer and theoretical estimates, respectively, while the newer model parameters were determined through the Hyprop and SIC testing. Therefore, Figure 5-19 shows not only the resultant water content profiles, but also the main SWRC and hydraulic conductivity functions.

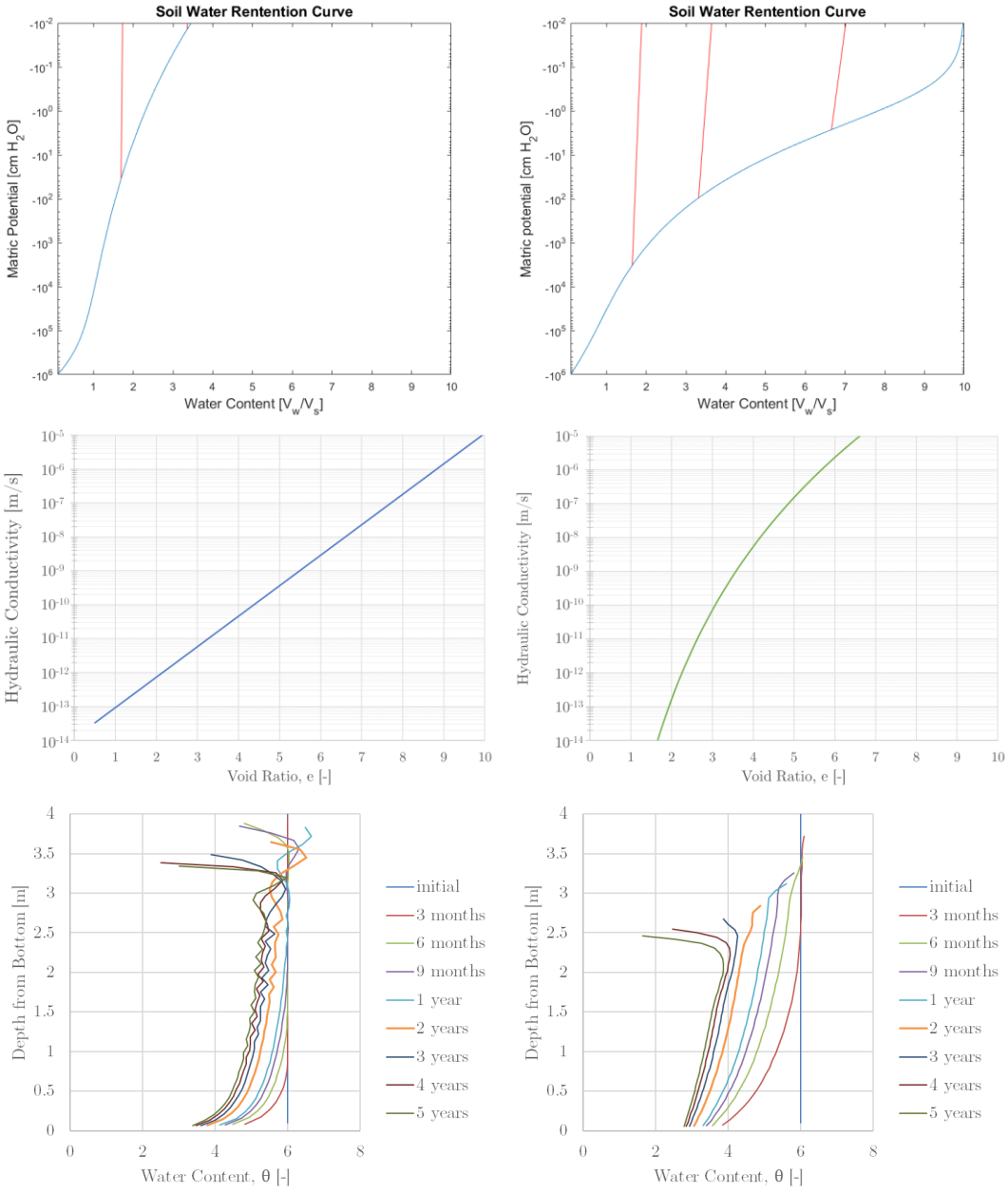

(a) Original *(b) Modified*

Figure 5-19(a)(b): Comparison of original and modified SWRC and permeability

As seen in both the sensitivity analysis and the modified permeability model seen next to the original in Figure 5-19, there is a significant variation in results. This is due to the fact that the power-log relationship estimates much higher permeabilities and high void ratios in comparison to the hydraulic

conductivity calculated with the original log-linear relationship. Further discussions about these variations and effects on other output parameters is presented in Chapter 6.

5.3.2.4 Updated Marker Wadden Models

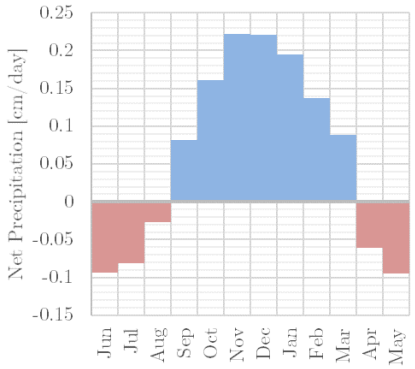

Figure 5-20: Updated Marker Wadden atmospheric conditions (summer start)

Including an update of material parameters, the new baseline models, including the average net model which serves as the "updated" model, have an initial start month in the summer, as this was suggested by Boskalis to be the most likely initial surface exposure period. This shift in initial starting month produces the average monthly net precipitation value timeline which can be seen in Figure 5-20.

Based on this timeline, new baseline models –including net precipitation, precipitation only, and evaporation only– were run in order to get a sense of the ranges experienced. In addition, the general model runtime has been extended to 5 years in order to get a full understanding of both the short and long-term results. The precipitation only model serves to estimate settlement due to consolidation only and will be used against other model to estimate and isolate settlements due to crust formation.

Figure 5-21 shows the water content profiles of these three basic atmospheric condition simulations. All three had a starting date of June, in order to keep the variations to a minimum. The models perform as expected, with the precipitation only case showing no crust formation and only slight increases in the surface water content. When comparing the net conditions to those of evaporation only, one can see that the crust develops earlier in time in the evaporation only case, as expected. An additional note is that these variations in crust development equalize over time, with the water content profiles at 4 and 5 years showing about the same results for both cases.

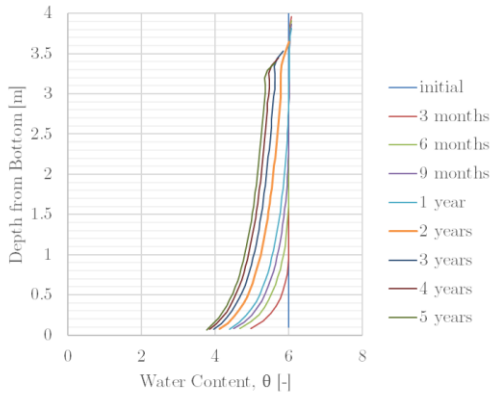

(a) precipitation only

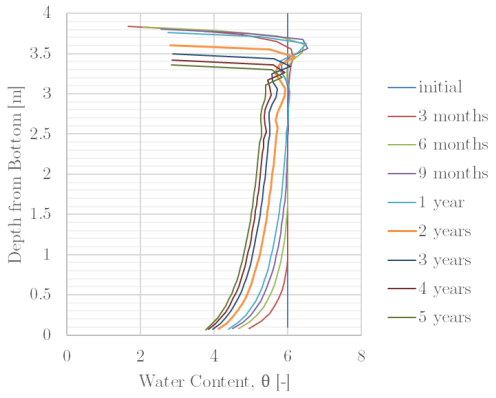

(b) evaporation only

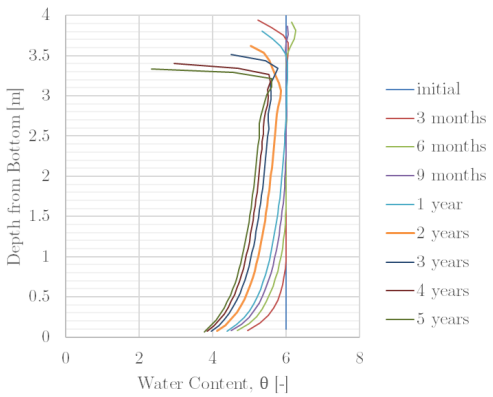

(c) average net

Figure 5-21(a)(b)(c): Baseline (summer) model water content profiles

5.3.2.5 Initial Seasonal Variations

Building off of the observations made from the baseline models, the next aspect assessed was the effect of initial seasonal start date variations. By "seasonal start", one is referring to the initial time of year when the free surface water is removed completely and the soil surface is initially exposed to atmospheric conditions for the first time. Initial exposure to varying evaporation and precipitation averages will influence the desiccation process. The seasonal start months for summer, fall, winter, and spring were designated as June, September, December, and March, respectively.

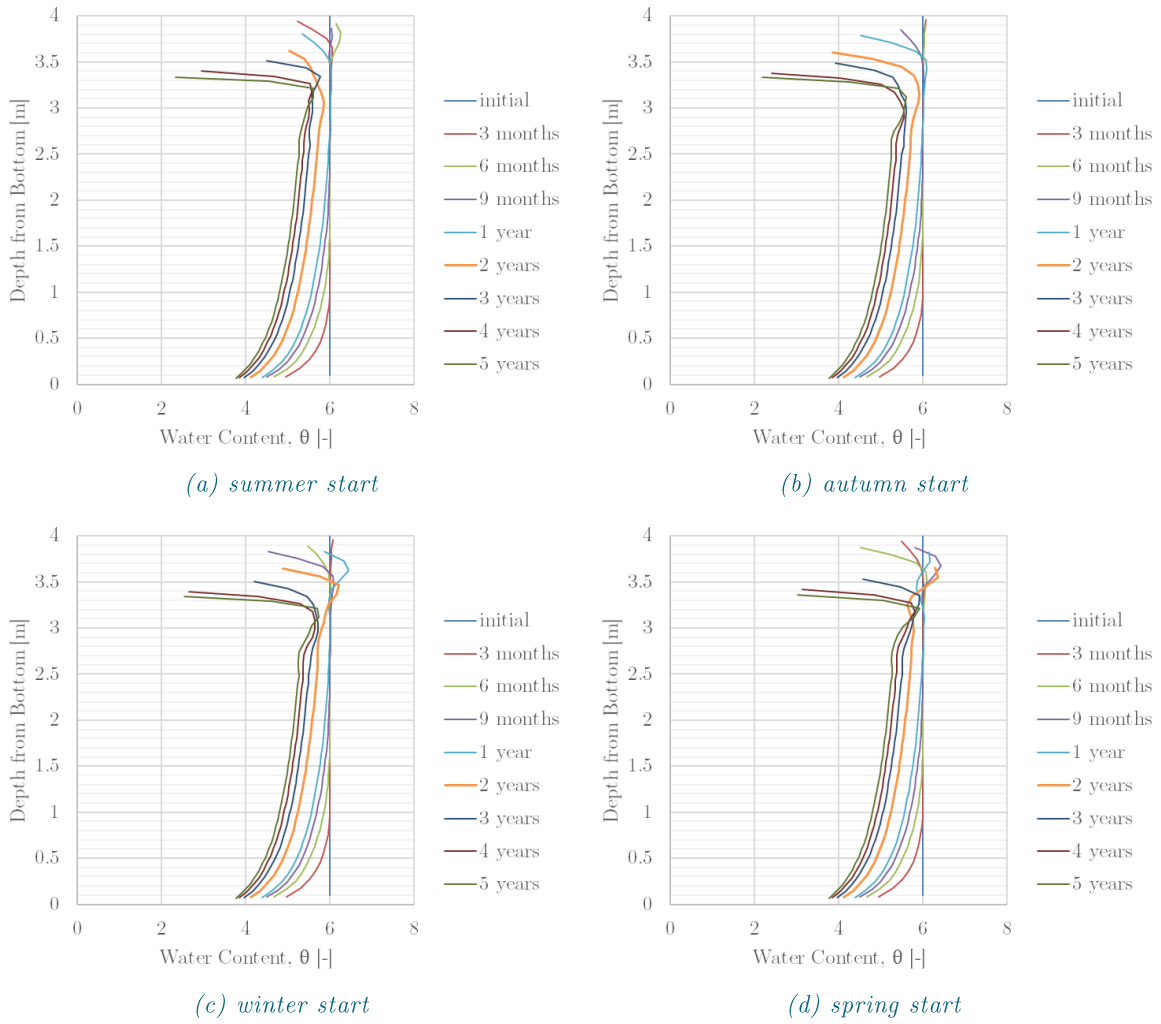

(a) summer start *(b) autumn start*

(c) winter start *(d) spring start*

Figure 5-22(a)(b)(c)(d): Initial seasonal "start" variations model water content profiles

Figure 5-22 shows that all of the water contents equalize by the fourth/fifth year mark, as with the baseline models. However, it is important to note the variations experienced in the first years, especially when looking at the variation in the profiles at the end of the second year. Also, observed in these graphs is that the desiccation process only heavily influences the material in the top meter of the 4-meter layer, besides the general reduction in the water content profile which takes place.

5.3.2.6 Surface Water Mitigation

As with the large-scale containers, emphasis was placed upon the active aspect of mitigating atmospheric conditions in order to facilitate the desiccation and crust formation process. Realistically, this can be done to either assist or inhibit the desiccation process. In terms of actively assisting the desiccation process, surface drainage measures must be put in place. There are two types of surface drainage measures that can be utilized. One includes constructing trenches through which rain water will travel to and be dispersed. The other method would be to utilize pumps to control the water level. However,

this is primarily something which would be done for only the initial stages of development. In terms of inhibitive effects of surface water activities, is it possible that during the initial spring months, the surface will be submerged once again. This is typically done in order to prevent unwanted seeds which arrive due to wind dispersal from taking root on the islands.

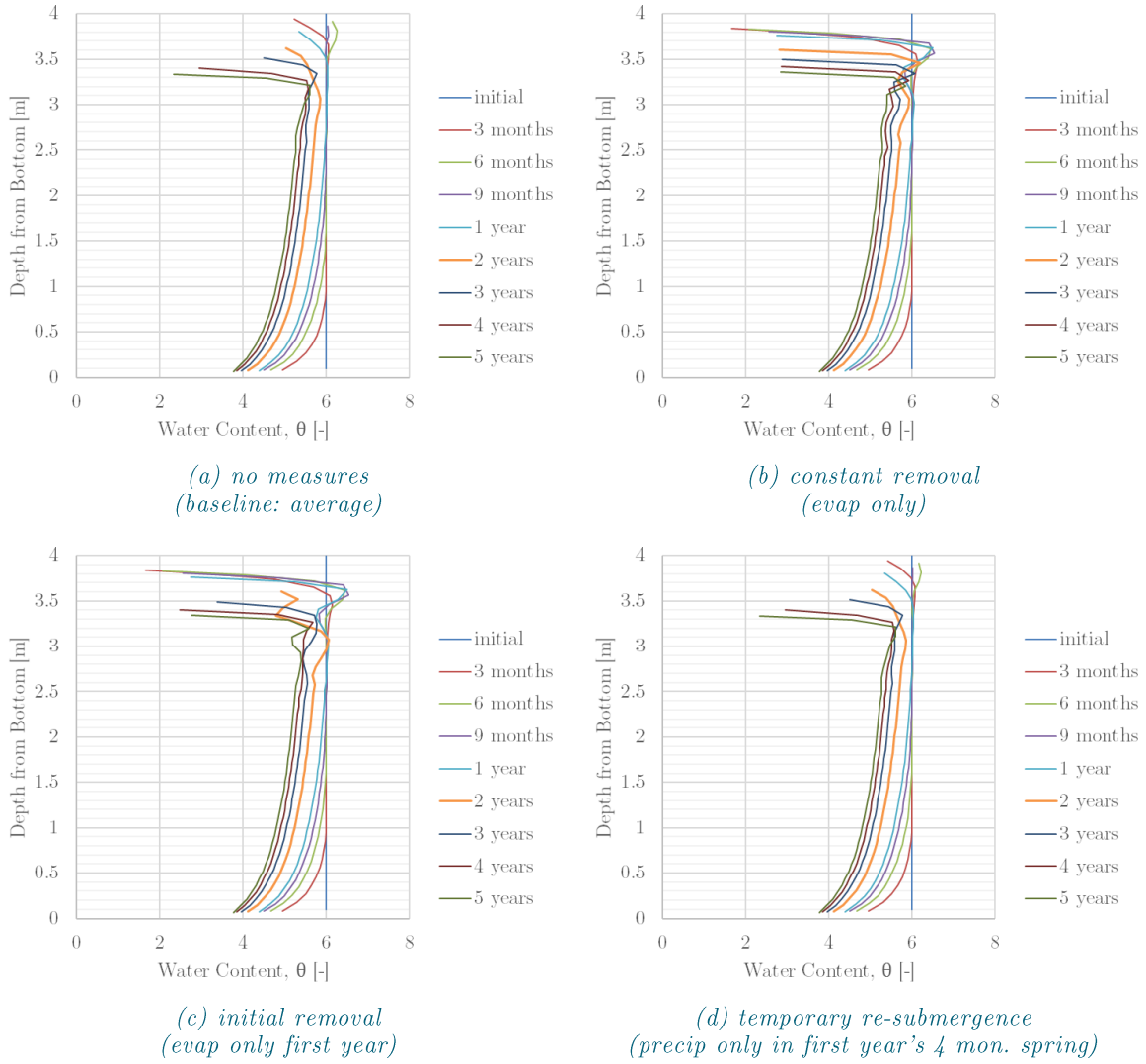

(a) no measures (baseline: average)

(b) constant removal (evap only)

(c) initial removal (evap only first year)

(d) temporary re-submergence (precip only in first year's 4 mon. spring)

Figure 5-23(a)(b)(c)(d): Surface water conditions model water content profiles

Based upon these different surface water mitigation scenarios, the following results have been obtained, shown in Figure 5-23. It should be noted that each of these models have an initial seasonal start set as the summer season, as this was proposed by Boskalis to be the most likely initial surface exposure time period.

6 Further Analysis & Discussion

Some preliminary observations of the results have been proposed in Chapter 5. However, this chapter will provide a more conclusive and comprehensive analysis of both the large-scale test and numerical modelling aspects of this research and how they relate to one another in a larger scope.

6.1 Large-Scale Test Analysis

The large-scale tests, in addition to serving as a direct comparison of atmospheric and surface water conditions, were also performed in order to validate and assess the trends observed to those proposed by the conceptual model. Furthermore, the in-situ measured results can then be compared to those predicted by the numerical model, in order to ascertain the viability of the model as a prediction tool for the Marker Wadden as well as potentially other soil and atmospheric conditions.

6.1.1 Conceptual Model Validation

One of the main motives for conducting large-scale tests was to validate the conceptual model formed at the start of this research. As no time scale was theorized before the start of the large-scale modelling, the hope was that the material within the containers would go through both stages of the desiccation and crust formation process. However, it soon became evident that due to the restrictions in time and manual labor required in order to maintain representative surface water conditions, that the testing duration was too short for the material to really have significant developments in terms of settlement, crust, and shear strength development. An additional factor is this decision was that the winter season would result in minimal desiccation in comparison to the earlier seasons, which average higher evaporation rates and overall lower daily net precipitation averages.

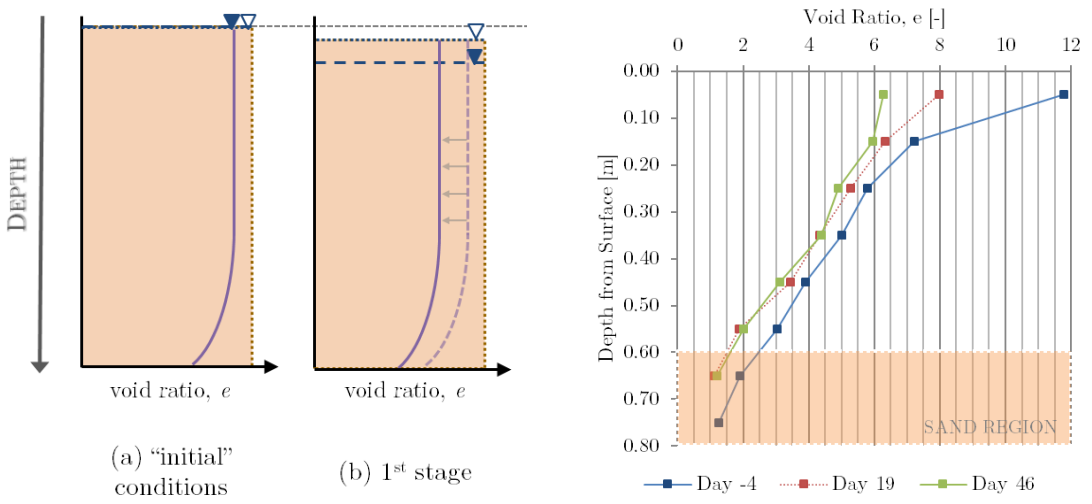

(a) *(b)*

Figure 6-1(a)(b): Conceptual vs measured void ratio profile changes

That being said, there were still some general trends in both the water content and void ratio which aligned with the developments predicted within the profile for the first stage of desiccation. Figure 6-1 shows a direct comparison between the conceptualized void ratio profile and the measured development of the void ratio profile over time in C1. Some deviation between the general form of the profile may be attributed to the presence of sand which gradually settled at the bottom of the container, in comparison to the conceptualized model which has uniform fractions. In addition, the large deviation in the surface

value of Day -4 can be attributed to the sampling method utilized and the fact that some water remained atop the material at this point which was incorporated into the water content check of the soil sample. Overall, the leftward shifting trend can be seen in both, validating not only the reduction of the void ratio over the complete depth, but also as a result the overall reduction in water contents throughout the profile due to the water being drawn up from within the material as a whole layer.

Other aspects of the conceptual model, such as the evaporation efficiency and pore pressure profile, were much more difficult to validate. Changes in soil evaporation efficiency were not directly measured, but due to the oftentimes clear presence of some water atop the material, and the fact that significant crust formation did not occur, it is safe to assume that the evaporation which took place occurred close to its full (open-water) potential as water loss without crust formation would indicate that the material was within the first stage of desiccation. In the case of the pore pressure validation, due to the pre-established placement of the piezometers, there were no detailed readings taken at close to the surface of the material which could track any changes over time or during re-wetting events. However, the general pore pressure readings were generated for the specific testing days and have been provided in the section Complete Pore Pressure Readings in the Appendices for reference, as these were also initially used in an attempt to distinguish between the soil and water elevation.

Due to the failure in the attempts made to identify and track the soil elevation and any changes which may have taken place, no conclusive estimates on the amount of settlement which took place could be reached. However, based on general height readings taken from Beeker cores, it can be stated that minimal amounts of settlement did occur in C1 and C2, in the order of a few centimeters. This settlement, as stated in the conceptual model, is attributed directly to the water loss taking place during the first stage of drying.

Furthermore, no significant increases in the surface shear strength were observed, further indicating the fact that the none of the containers entered the second stage of desiccation and drying, where significant reduction in the void ratio and water content at the surface would result in more significant deviation in the shear strength at the surface in relation to the rest of the profile. However, what small development did occur can be attributed to the water loss, and slight strengthening of the soil due to the reduction in void ratio.

6.1.2 Numerical Model Validation

Additionally, the obtained measurements were meant to serve as a way to compare and validate to the results determined using the numerical model. As can be seen in Figure 6-2, the measured and modelled results for the large-scale tests were not directly comparable. While the physical and modelled results cannot be directly compared due to the issues mentioned earlier in this section, the trends within each of the containers in terms of water content, void ratio, density, and shear strength could be assessed in order to determine whether it was an irregular development or whether the development fell in line with what was to be expected.

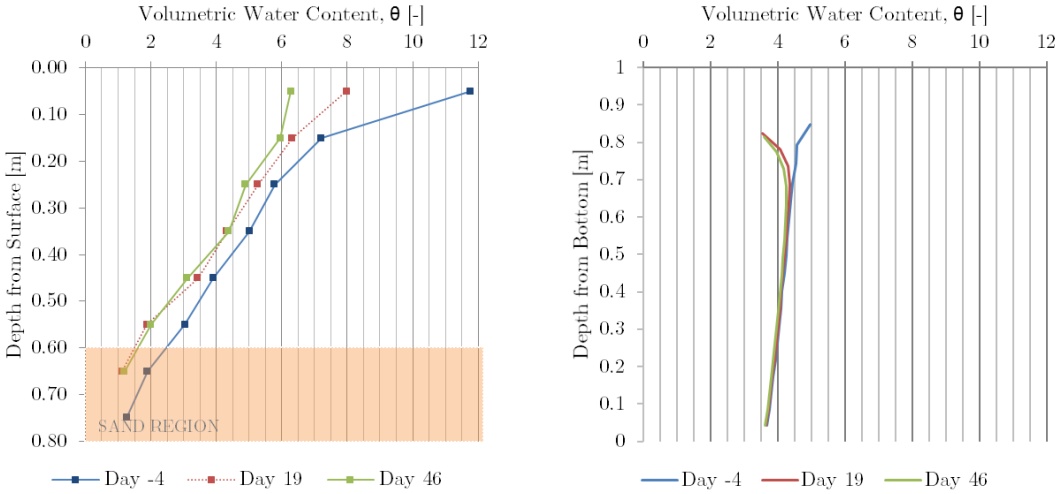

(a) measured *(b) modelled*

Figure 6-2(a)(b): Measured vs modelled water content profiles for C1 conditions

In general, both the physical and the modelled results exhibit similar trends for each of the container conditions. However, due to the lower initial water content after the pre-run, the model results predict crust formation which did not occur within the containers and that the physical results do not show. This also resulted in drastically elevated shear strength estimations, which also did not reflect those measured in-situ.

The main reasoning for the modelling difficulties experienced in relation to the large-scale test were that efforts to reproduce the initial conditions of the containers at the conclusion of the settlement and self-weight consolidation phase and the initial conditions of the desiccation phase were not completely successful. This could have been due either to one or a combination of various factors, the primary ones including the following:

(a) Modelling limitations
(b) Uncertain initial material properties
(c) Discrepancies in Hyprop testing

One of the primary limitations of the numerical model is that it assumes the layer to be homogenous throughout the vertical profile. This became an issue in terms of modelling the containers for two main reasons:

1. The initial density of the filling slurry for the containers was unknown, and variation range of 1260-1150 kg/m^3 was estimated by van Olphen, with 1150 kg/m^3 suggested to be the closest in accuracy based on additional research and DELCON modeling (van Olphen, 2016).
2. The presence of sand within the initial slurry mixture resulted in a creation of semi-distinct sand layers at the bottom (as well as the middle of C2 and C3) of each of the containers during the settlement stage.

The first point effects the initial profile of the material, and errors in this value made it hard to generate an optimal pre-run which would result in a similar modelled profile output in comparison to the profile determined at the start of this research. The second issue regarding the elevated sand contents effects the overall consolidation and depth readings, resulting in high deviations between measured profiles and the modelled profiles. This can be most easily seen when comparing C2 measured and modelled conditions. In addition, the SWRCs were determined using disturbed material collected from the surface of the previously settled and consolidated material within C1 and C2. Not only does this not represent the lower sand regions, but the material makeup is presumed to be different than of the initial filling slurry, especially based on the difference between the top layers in the containers and the initial slurry mix shown in Figure 5-1 and Figure 5-2, respectively. Because of this, the calculated SWRC parameters from the top layer material does not reflect the conditions of the complete layer, and in addition, have a lower maximum saturated water content, based on the highest initial water content which was measured during the Hyprop testing. Inputting these SWRC parameters along with the assumed initial

water content for the layer resulted in a model error, as the model does not know how to incorporate water contents which are significantly higher than that stated in the SWRC input parameters.

After plotting both the Hyprop results and the rough effective stress and water contents (in reference to depth profiles) within C1, a high deviation was identified between the plotted strength/stress and water content relations. While the deviation at higher water contents was anticipated, it was theorized that the initial lower portions of both the Hyprop and effective stress points should approximately line up (not evident in Figure 6-3). Because of the restriction in the allowable SWRC input, the model underestimates the initial water content profile at the end of the pre-run by almost double.

In addition to this significant deviation in initial water contents, the modifications of the net precipitation conditions within each container may not accurately reflect what the container actually experienced, as modifications were made on a very general basis. For instance, at times, the cover would not keep 100% of the water from entering the container, however the cover was implemented in the model modifications as either on (and 100% blocking water) or off (0% blocking). Based on this alone, it is expected that the model would overestimate the conditions experienced in the container and the progression of the desiccation process. Additionally, the model is best for longer term, general predictions of the soil profile, rather than modelling the minute and small deviations in atmospheric conditions over a short time. It is for this reason -as well as the presence of the sand layers and higher density variations within the profile- that the modelling of the containers could not be directly compared to the physical results.

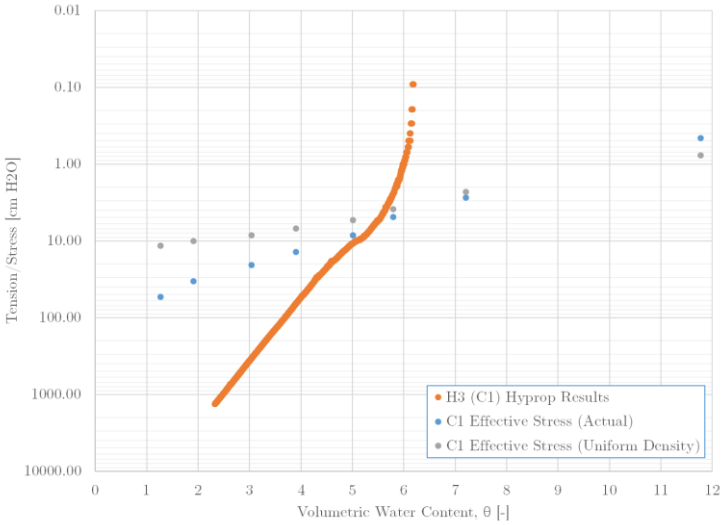

Figure 6-3: Hyprop vs effective stress SWRC estimation

However, many of the major issues faced when modelling the large-scale containers are not the same issues faced when utilizing the model as a prediction tool for the Marker Wadden. The large-scale testing required a backwards extrapolation of current data to estimate the initial soil properties and conditions within the containers after initial filling. While this could be done in part, the actual material used in the Hyprop test had already experienced the initial settlement, self-weight consolidation, as well as some stresses. This makes the generated SWRC unviable for properly outlining the strength vs water content behavior between initial deposition and end of initial self-weight consolidation. However, the material used in the SWRC determination in regards to the Marker Wadden was taken much earlier in the complete consolidation process, and therefore has less deviation from its initial conditions just after deposition. This, coupled with the fact that much more precise information regarding the initial conditions and properties is available makes modeling of the Marker Wadden much more optimal. Therefore, there is still confidence in the model and its results when assessing the Marker Wadden. Although, there are new issues and limitations which will be discussed in relation to the Marker Wadden, and will be discussed in a later section.

6.1.3 Additional Findings

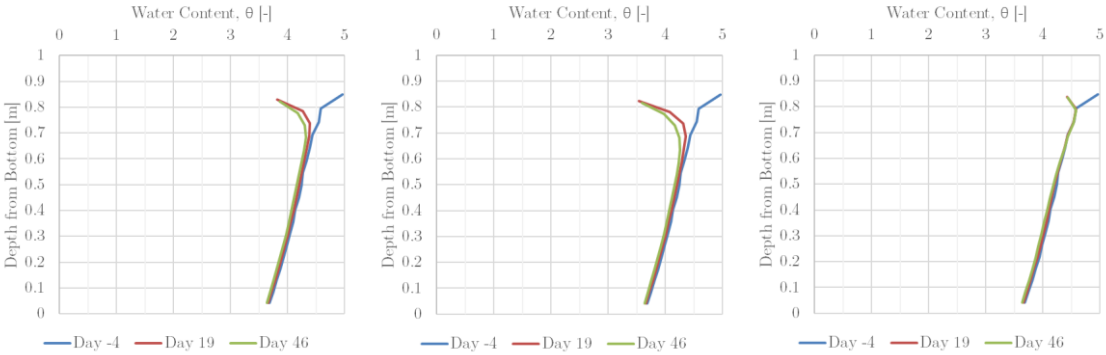

(a) C1 net precipitation *(b) C2 net precipitation* *(c) C3 net precipitation*

Figure 6-4(a)(b)(c): Modelled water content profiles of C1 material with varying net conditions

Although the measured and modelled results are not directly comparable, there are still some aspects which can be extracted from the modelling of the large-scale conditions. In order to make a more direct and clear assessment of the effect of varying atmospheric conditions, and compare the trends found in the measured results, modelling of C1 material with C1, C2, and C3 atmospheric conditions was performed. As can be seen in Figure 6-4, there is no significant difference between the C1 and C2 net conditions. This is attributed to the fact that although it was theorized that the ventilator would significantly increase the windspeed and airflow within C1, this did not occur in reality, especially once the windspeed within all of the containers was corrected to account for the container walls. Implementation of these representative conditions was minimally different in relation to one another. However, it is important to note the differences between C1/2 and C3 conditions. Due to the restricted evaporation and water buildup on the surface of the material in C3 after the initial water removal, the desiccation process was hindered significantly. When looking at the physical results, shown in Figure 5-8, the deviation which occurs at the surface over time follows the levels of mitigation measures put in place, although this cannot be 100% confirmed, as the active surface water removal within C2 was terminated midway through the scheduled project timeline. The effects of surface water mitigation measures —as well as seasons atmospheric variations— was assessed in more detail using the Marker Wadden modelling, and is discussed in the next section.

6.1.4 Remarks on Measured Results

As always, in-situ testing comes with its own set of issues and inconsistencies. Three of the main issues will be discussed in this section. One general potential source of error was the time delay between sampling and testing. Because of this, the 'in-situ' water contents should be considered critically, as the time between sampling and oven drying could be extensive at times. It can be assumed that even during this time, evaporation took place even though the samples were kept in a cool refrigerated storage area.

6.1.4.1 Depth & Settlement Inconsistency

In an ideal reference measurement setup, all depth measurements would be referenced from the bottom of the container to the height at the point being measured within each of the containers. However, due to the method of measurements, both the densimeter and vane rheometer were initially measured from first entry into the soil and then the additional centimeters to each subsequent measurement point. By using the same equipment setup height, the distance of the measured point from the bottom of the container could then be back-calculated. However, variations in the equipment setup (in order to properly secure it), restrictions in the deepest measurable depth, and general measurement deviations between the mobile scaffolding to the container, lowered the confidence in the accuracy of the depths being calculated. This is an issue when comparing the progression of various soil profile properties over time, as the measured values at a certain calculated "depth" may not truly be from the same height in the container. Additional issues with the settlement and material surface measurement method also made it hard to track the exact height changes within each of the containers, making it hard to establish settlement progression over time.

6.1.4.2 Densimeter Inconsistency

Theoretically (with complete and optimum calibration of densimeter) density measurements should be 1:1 with those of the Beeker core. However, Figure 6-5 shows clear deviations from this 1:1 line as the density increases, which can reasonably be assumed as the data points which fell within the higher sand content regions. This has been determined based on the fact that as the densimeter was not properly calibrated for the sandier regions, a higher deviation between the densimeter readings and straightforward Beeker core averages would be exhibited.

Furthermore, there is a concerning overall increasing deviation from the equivalency line between the data collection times, as indicated by the reduction in the coefficient of determination values between subsequent testing periods. While some error can be incurred due to the actual date variations between Beeker core and densimeter testing, it may also possibly show the deterioration of the densimeter accuracy (which could be attributed to a later discovery of a lose receptor wire).

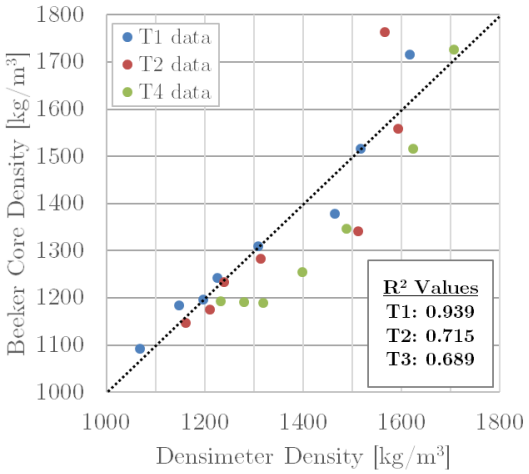

Figure 6-5: C1 density variance (densimeter vs Beeker core)

6.2 Marker Wadden Predictions

The Marker Wadden was modeled numerous times based on different atmospheric conditions and material input parameters. Many of the varying input parameters were eliminated during the initial sensitivity analysis and during the "optimal" model determination process.

6.2.1 Updated Estimates

Initial ideas for modelling and assessing the Marker Wadden was to implement the updated SIC parameters which had been determined after the initial modelling had already taken place. However, as expressed earlier in both Chapter 5 and in sections prior to this, it was established that this relation does not realistically relate the void ratio and hydraulic conductivity, especially when comparing it to existing clay mineral data. Because of this, the "updated" Marker Wadden run consisted primarily of new Hyprop SWRC inputs, as this reduced the model oscillations exhibited. This minor change emphasizes the sensitivity of the model in relation to the SWRC inputs utilized, and also shows the importance of properly defining the permeability relation utilized within the model.

Additionally, the initial seasonal start was taken to be summer, as this was proposed by Boskalis to be the most likely period of initial surface water removal. The final results of the "updated" run can be seen in Figure 6-6. Some important aspects to note is the delayed development of surface shear strength. The model predicts that significant surface shear strength will not develop until after four years; however, the requirement of 5 kPa will be met around two years based on average weather data in the Netherlands. Total settlements —including consolidation and additional consolidation due to the crust— of a little more than half a meter is expected, with a crust starting to develop significantly after three years. At the five-year mark, the crust is expected to have a thickness of around 15 cm (from 3.35 m to 3.20 m from the bottom of a 4m layer). These values, in addition to more, have also been provided in Table 6-1(a)(b) and Table 6-2(a)(b) to serve as a comparison for the other variations modelled.

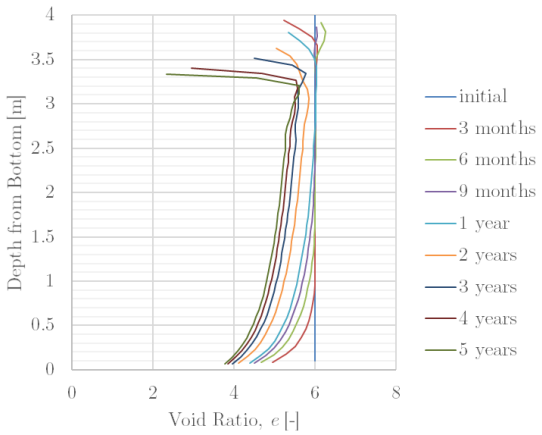

(a) void ratio profile

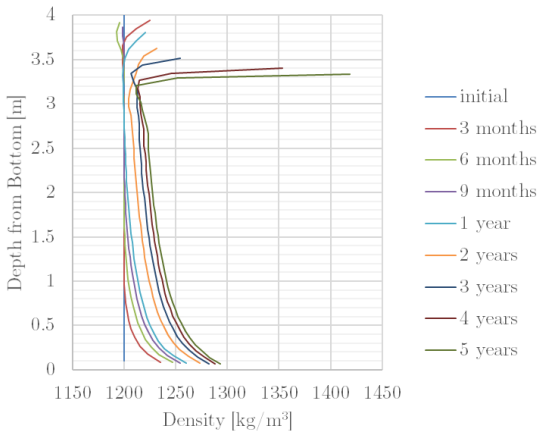

(b) density profile

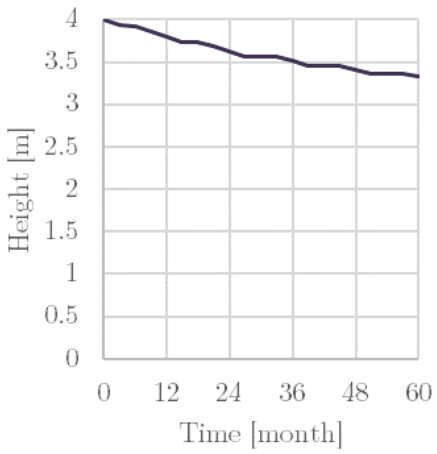

(c) layer height over time

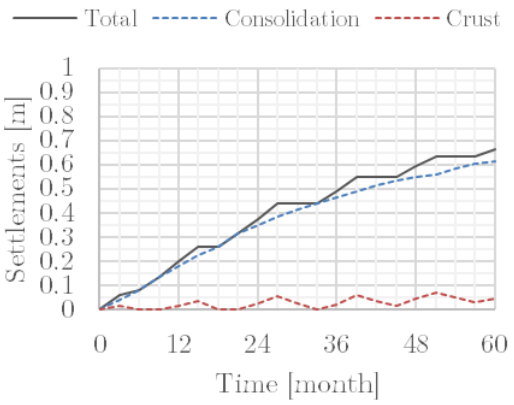

(d) settlement breakdown

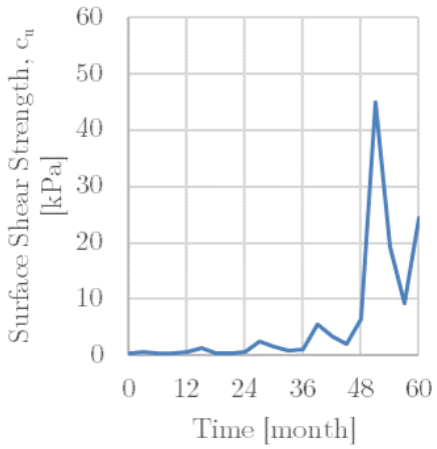

(e) surface shear strength

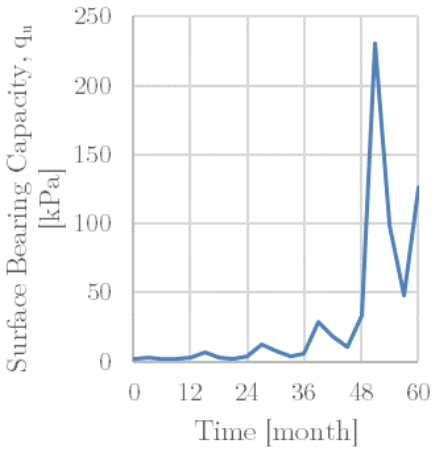

(f) surface bearing capacity

Figure 6-6(a)(b)(c)(d)(e)(f): Results of the "updated" Marker Wadden model

6.2.1 Impact of Initial Seasonal Effects

The next major consideration to be modelled in regards to the Marker Wadden were the initial seasonal effects. The void ratio profiles over time for each of these seasonal variations can be seen in Figure 6-7, with all of the different initial seasons showing around the same crust stabilization by the fourth year. The first two years of the Marker Wadden, however, vary substantially based on the initial season. Surprisingly, the autumn start season shows the earliest and most significant desiccation and crust development, however summer is not that far off. Most importantly, spring as the start season shows the most delayed development, with very limited crust development until the third year. As this is also the least likely start season[1], it is of minimal concern for the Marker Wadden project. But these observations and fluctuations can be important when ascertaining in the field whether the development is on track with meeting the design requirements by the specified deadline. The exact value breakdowns in both the short and long-term (one and five years, respectively) in Table 6-1.

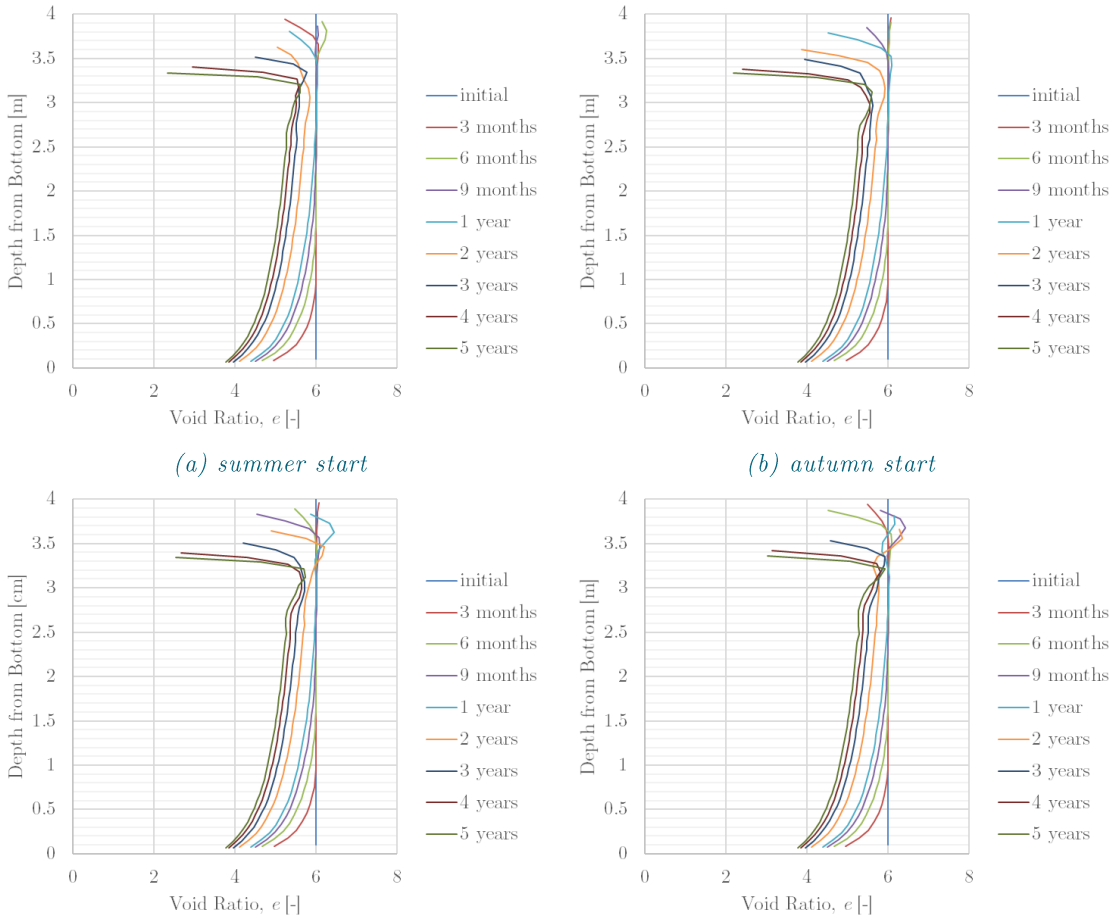

(a) summer start *(b) autumn start*

(c) winter start *(d) spring start*

Figure 6-7(a)(b)(c)(d): Initial seasonal variations model void ratio profiles

Also included is a breakdown of the total settlements due to consolidation and crust. These can be seen in Figure 6-8, although each look generally similar in trends to one another. This is due to the cyclic nature of the atmospheric conditions in advancing crust formation and hindering its development. Table 6-1 also includes a calculation of the total settlement due to the crust, in both the short and long-term timeline.

[1] Spring was designated as the least likely season for initial dewatering due to higher anticipated precipitation averages during this season. In addition, unwanted vegetation growth has an increased probability of occurring, due to the wind transport of seeds from other areas within the Netherlands.

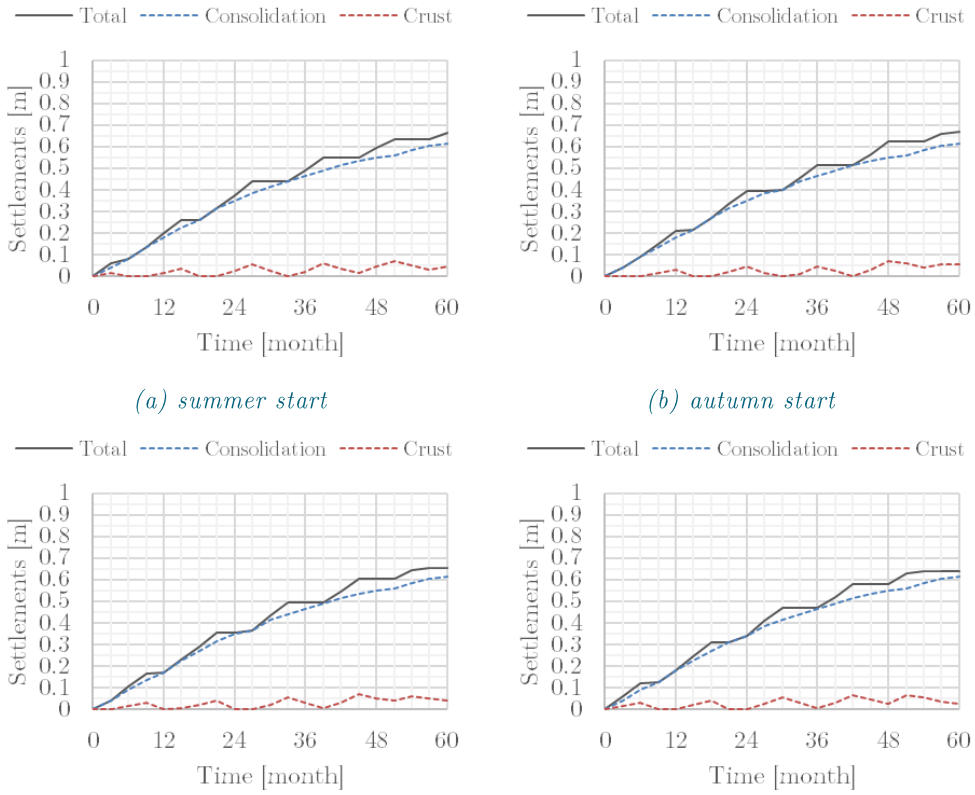

(a) summer start *(b) autumn start*

(c) winter start *(d) spring start*

Figure 6-8(a)(b)(c)(d): Initial seasonal variations settlement components

Just as with the updated Marker Wadden model run, the surface shear strength is slow to develop regardless of the initial season. While each of them meet the design requirement after the second year, the maximum shear strength exhibited by the fourth and fifth years vary considerably. This can be seen in Figure 6-9. It is through the graphs in Figure 6-9 that the limitations of modelling with a consistent daily average per month can be seen. The shear strength values obtained and shown in Table 6-1 are unrealistic in the sense that real climate conditions often do not allow for 30-day uninterrupted evaporation or precipitation, which would account for the significant increases and decreases of shear strength seen in the later months.

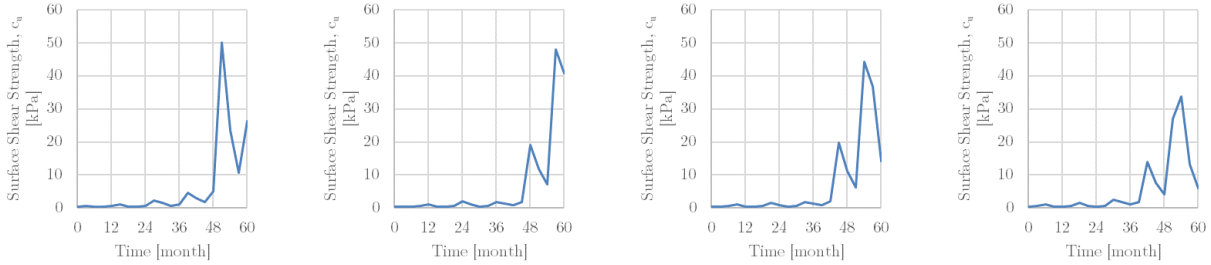

(a) summer *(a) autumn* *(a) winter* *(a) spring*

Figure 6-9(a)(b)(c)(d): Initial seasonal variations surface shear strength development

	Height [m]	Total Settlement [m]	Crust Thickness [m]	Settlement due to Crust [m]	Shear Strength [kPa]
Summer	3.80	0.20	0.48	0.001	0.63
Autumn	3.79	0.21	0.37	0.031	1.11
Winter	3.83	0.17	0.41	0.000	0.46
Spring	3.82	0.18	0.31	0.000	0.39

(a) one year

	Height [m]	Total Settlement [m]	Crust Thickness [m]	Settlement due to Crust [m]	Shear Strength [kPa]
Summer	3.34	0.66	0.22	0.049	24.52
Autumn	3.33	0.67	0.21	0.055	39.74
Winter	3.35	0.65	0.23	0.041	14.69
Spring	3.36	0.64	0.14	0.025	5.75

(b) five years

Table 6-1(a)(b): Initial seasonal variations settlement, crust, & strength values

6.2.2 Impact of Surface Water Conditions

Some simplistic atmospheric input modifications were modelled in order to determine the general effects of surface water measures on both the long and short-term desiccation and crust formation. The general water content profiles for these different representations can be seen in Figure 5-23.

The three main representations were the following:

- Complete surface water removal: evaporation only
- Initial surface water removal: evaporation only the first year
- Temporary re-submergence: first year's spring season (4 months) precipitation only

The changes made in the surface water conditions —although minor in timescale— in comparison to the longer five-year endpoint, does show some differences in the desiccation and crust formation development. For instance, Figure 6-10 shows the faster settlement which takes place initially when just one year of active surface water removal is incorporated. This is opposed to the observations made between the net conditions in which no measures are put in place and the situation of re-submergence, which could be done in the spring months to prevent unwanted plant growth; there seems to be no major difference or delays in progression.

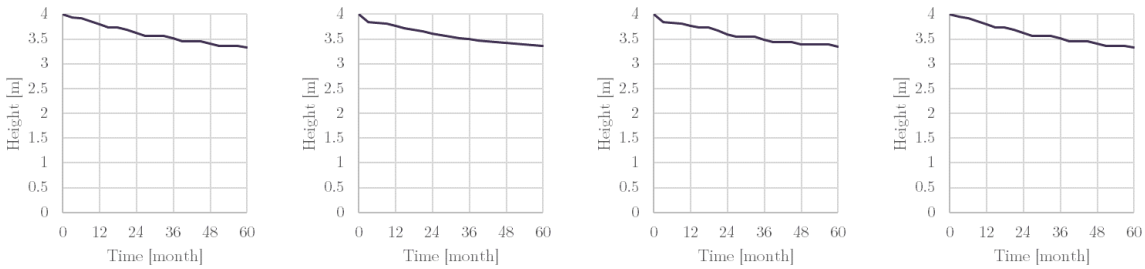

(a) net conditions (no measures) *(b) complete removal* *(c) initial removal* *(d) temporary re-submergence*

Figure 6-10(a)(b)(c)(d): Surface water measures layer heights over time

Table 6-2 shows the consolidation and crust factors of the total settlements after both one and five years. However, the effect of the crust is more cyclic in significance, based on the seasonal conditions, and these cyclic effects over time can be seen in Figure 6-11. Furthermore, there are additional factors which should still be consider and applied to these estimates, including aspects such as how effective any surface water removal methods are in terms of removing and preventing surface water build up,

varying timeframes of active surface water mitigation, and the sudden re-introduction of water atop the surface material.

	Height [m]	Total Settlement [m]	Crust Thickness [m]	Settlement due to Crust [m]	Shear Strength [kPa]
Summer (average)	3.80	0.200	0.48	0.001	0.63
Constant Removal	3.76	0.235	0.14	0.053	9.32
Initial (first year) Removal	3.76	0.235	0.14	0.053	9.32
Temporary (4mo) Resubmergence	3.80	0.198	0.48	0.016	0.63

(a) one year

	Height [m]	Total Settlement [m]	Crust Thickness [m]	Settlement due to Crust [m]	Shear Strength [kPa]
Summer (average)	3.34	0.663	0.22	0.049	24.52
Constant Removal	3.36	0.643	0.15	0.029	7.86
Initial (first year) Removal	3.34	0.659	0.14	0.045	9.12
Temporary (4mo) Resubmergence	3.34	0.663	0.22	0.049	24.46

(b) five years

Table 6-2(a)(b): Surface water measures settlement, crust, & strength values

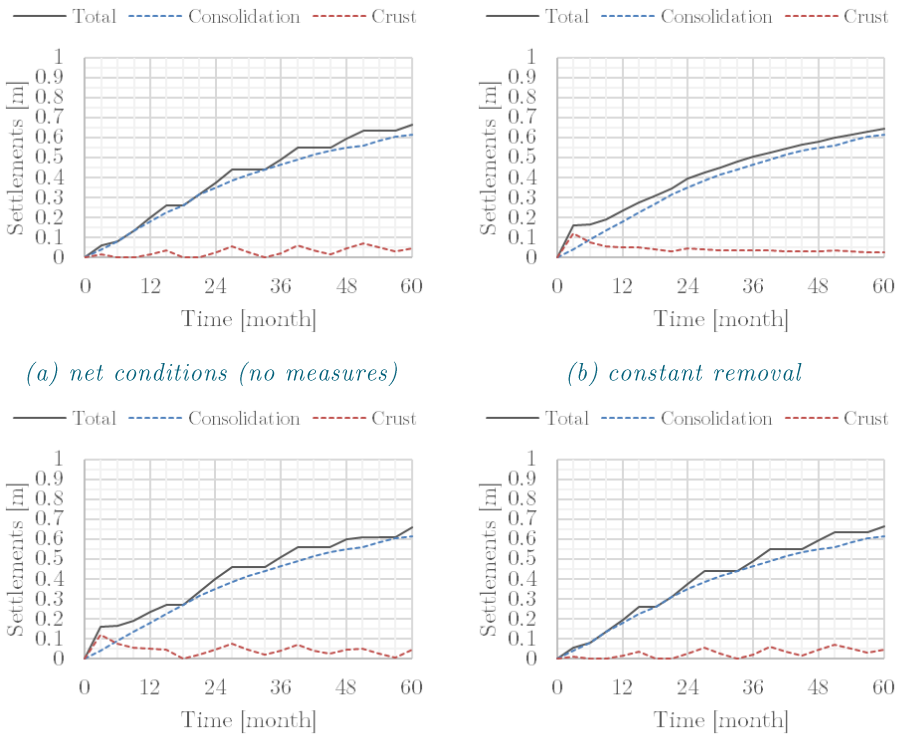

(a) net conditions (no measures)

(b) constant removal

(c) initial removal

(d) temporary re-submergence

Figure 6-11(a)(b)(c)(d): Surface water measures settlement components

6.3 Material Parameter Variability

Before comparing physical and numerical modelling methods and results, it is important to also assess the inherent variability which can occur when classifying and determining material properties and relations. For this research, the two main material parameters with high variability and impact on results included the SWRC, as well as the permeability (i.e. hydraulic conductivity) relations.

6.3.1 SWRC Determination

The SWRC can be estimated through a number of tests and methods. While the main method investigated in this research was the Hyprop, other methods also include the oedometer relation (as used in the original Marker Wadden estimations), as well as a general check using the effective stress and water content profiles.

6.3.1.1 Sample Collection & Preparation

There is also an issue of the collection method utilized for all of the Hyprop tests. Unfortunately, all the material taken from the both the containers and the Marker Wadden were obtained by heavily disturbing the material, and because it was assumed to already be disturbed, was further mixed before being poured into the Hyprop testing piece in order to obtain homogenous samples. This could have had an effect on the output, as ideally one would take a relatively undisturbed sample of the soil and test directly with it.

Finally, there were also some issues with the tensiometer readings, even with corrections being applied. However, this does not rule out the validity of the Hyprop or negate its usefulness. With the proper modifications, such as those done by Chin A Moei in his thesis entitled “Effects of Organic Matter on Shrinkage and Water Retention Behaviour of Organic Dredged Sediment”, one can also successfully implement a second tensiometer which can then be used to determine the unsaturated hydraulic conductivity, a helpful parameter to identify in this situation (Chin A Moei, 2016).

6.3.1.2 Oedometer vs Hyprop

As stated multiple times throughout this research, there are multiple methods which can be used to obtain an approximate SWRC. This can include using an oedometer and constructing a normal consolidation line (NCL), or using a Hyprop and determining an intrinsic consolidation line (ICL). Differences in the estimated soil water retention curve take place dependent upon the type of consolidation which takes place during the testing methods. This occurs due to the fact that the oedometer induces anisotropic consolidation of the soil, while suction-based evaporation tests —such as the Hyprop— induce isotropic consolidation of the soil. Isotropic consolidation conditions more closely emulate the consolidation experienced due to evaporation and transpiration conditions, due to the reduced shear stresses experienced between the soil particles, which allows for increased condition to occur. Deviation between the two tests also occurs at lower water contents at and below the plastic limit, probably due to the addition of air into the soil system (Fredlund, 1967).

While it is believed that a SWRC generated through a Hyprop can be more accurate than that produced by an oedometer, there is still variability present in these tests, especially as the Hyprop is designed as an element test and has inherent difficulties in measuring higher water contents with low suction.

6.3.1.1 Hyprop Variance

Figure 6-12 shows all of the corrected SWRC data points for all six of the Hyprop tests performed on various samples. As outlined in Figure 4-13, consideration was put into checking the natural variance of both the material and the Hyprop test itself. Surprisingly, there was a large variation between both the container material (H3 and H4) as well as the Marker Wadden samples (H1 and H2). The variation between the Marker Wadden samples could be expected, as they were from two different collection batches; however, the samples from C1 were both samples from the same remixed batch collected from one location in C1. H3 actually best matches H6, which was performed using completely separate material collected from the surface layer of C2.

The fitting of the van Genuchten could also play a role in the precision of the parameters used within the model, however all of the coefficients of determination (R^2 values) were above 0.99. However, the

fitting of the van Genuchten equation to the SWRC data points have been provided in the Appendices in the section SWRC Calculations.

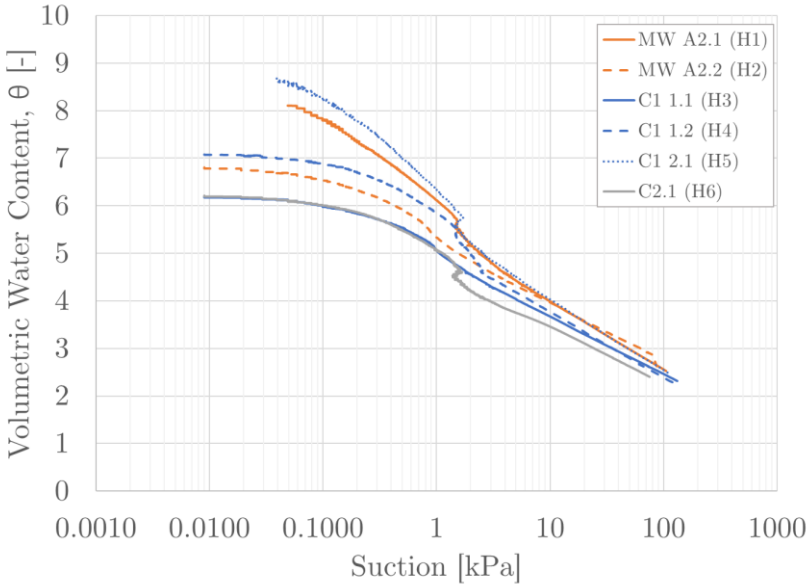

Figure 6-12: All Hyprop generated SWRC data plots

6.3.2 Hydraulic Conductivity Relations

The proposed and utilized permeability relations and inputs varied significantly in terms of estimating the hydraulic conductivity as specific void ratios. All of the investigated relations have been plotted in Figure 6-13. Based upon a mineralogy analysis conducted for the Marker Wadden, the clay material was identified to be made up of primarily illite and smectite clay minerals, with approximately 84% of the total mineralogy comprising of illite and smectite (Hendriks, 2016). Based on this, previous illite and smectite experimental data relating the void ratio and coefficient of permeability were also plotted in order to compare these values to those which would be estimated by the various relations (U.S. Army Corps of Engineers, 1993).

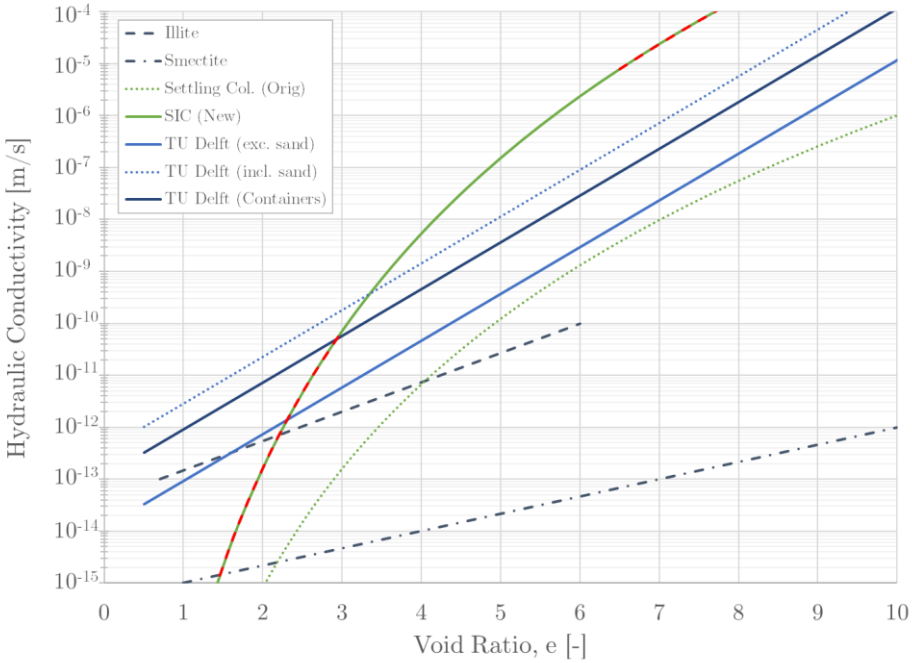

Figure 6-13: Permeability vs void ratio relations & estimates

6.3.2.1 TU Delft Log-Linear Relation

Unfortunately, when permeability relations which fell between the experimentally determined illite and smectite ranges, the model would not compute an output. Therefore, only slight modifications were made to the originally proposed log-linear relations. This included using solely the relation meant to represent the pure clay sample, while a reduced version of the relation meant to represent sandier samples was utilized when modeling the containers (due to the presence of sand within them).

6.3.2.2 Power-Log Relation

As can be seen in Figure 6-13, the power-log relation tends to estimate extremely low hydraulic conductivities for lower water contents, and higher values for the water contents which fall in range of the model. Updates to this power-log relation only increased the predicted settlement by a significant amount, and seemed unrealistic, especially in comparison to the values predicted for the involved clay minerals. Also shown in Figure 6-13 in dotted red lines are the regions in which the relation is extrapolated to and where no experimental data exists to validate the permeabilities estimated at those void ratios.

6.4 Model Sensitivity Analysis

The model was sensitive to both the SWRC and permeability input parameters, but for very different reasons. The SWRC curve, while relatively easily determined through oedometer and Hyprop testing, was not easily incorporated into the model for soils with high initial water contents (i.e. above 10). Furthermore, modifying the SWRC curve one parameter at a time is not always the most efficient, as there is no clear correlation between a fitting parameter and its exact influence on the shape of the curve. For instance, slight changes in the n parameter resulted in either major curve changes, or in the model crashing.

The model and its output was also highly sensitive to the permeability relation and relevant input parameters. However, in this instance, it was found that the relations themselves were quite varied in the predicted permeability for certain void ratios. Careful study must be given to finding the proper A and B input parameters regardless of the relation, as slight changes in these values will result in drastic increases in model computation time, and often generating unrealistic outputs.

7 Conclusions

The purpose of this section is to summarize all the major key findings of this research, both in terms of theoretical understanding as well as practical implications in relation to the Marker Wadden. Furthermore, recommendations for improved testing methodology as well as additional research will be proposed.

At the beginning of this research, the following main research question was proposed:

What are the effects of evaporation & precipitation conditions on desiccation and crust development of soft, fine-grained soil in terms of time, strength, and consolidation?

This was to be addressed using the following three sub-questions:

- What is the evolution of desiccation and crust formation in soft, cohesive, fine-grained soil material?
- How can this process be modelled, and which parameters significantly affect the model's output prediction —and therefore the desiccation, crust formation, and consolidation of the soil?
- What is the effect of atmospheric & surface water conditions on desiccation, crust development, and consolidation?

The responses to these questions are discussed in detail in the following three sub-sections.

7.1 Evolution of Desiccation & Crust Formation

The desiccation and crust formation process for soft, cohesive, fine-grained soil has been described in detail in the conceptual model detailed in Chapter 3. The desiccation process can be characterized by two distinct stages of drying. The first stage takes place under the assumption that the material remains saturated even as water is being transported from within the soil profile and the ground water table lowers. The material above the ground water table remains saturated due to capillarity, and in this zone negative pore pressures begin to develop. With regular soils, this region would be minimal, however due to the higher clay and silt fractions (and therefore reduction in pore size), the thickness of the capillary region can be quite substantial, and an important consideration in terms of the desiccation process. Due to the water loss taking place throughout the complete profile, the initial void ratio profile after the self-weight consolidation phase has taken place reduces. Additionally, it is assumed that during this first stage any settlement which occurs is directly related to the water loss taking place, as evaporation occurs close to its full potential. However, after a certain point —usually at a point near the liquid limit of the soil— the water being drawn from within the soil profile can no longer sustain the full evaporation potential can no longer be maintained by the water being transported from within the complete soil profile.

It is after this point that the second stage of drying is assumed to take place. During this stage, the soil begins to lose saturation from the surface downwards and a dense crust begins to form with significant void ratio reduction whose values deviate from the initial profile form. The crust can be quantified as the region from the surface downwards which exhibits significantly reduced void ratio values up until the first major inflection point, after which the void ratio generally resumes its natural distribution profile form. In addition, as this crust layer is no longer considered to be completely saturated (and therefore buoyant), it acts as an additional surcharge load atop the softer deeper material, causing additional surcharge consolidation. It is also during this stage that a significant crack network will form as a result in a build up of lateral stresses imposed upon the surface material due to horizontal shrinkage. Eventually, the effects of the second stage of drying reaches a depth limit within the soil, typically either the natural surrounding ground water table or a desiccation limit based on the plastic limit of the material.

In addition to the type of material going through the desiccation and crust formation process, there are other factors which have a significant influence upon the time and extent of desiccation. These include the climate and atmospheric conditions of the site, including the potential evaporation rate, average precipitation, sun exposure, and wind speed; any surface drainage measures put in place onsite to assist in the removal of any surface water buildup due to rain events; and finally, the presence of vegetation,

which can help draw up water from within the soil profile or hinder evaporation by shading the soil surface.

This model was validated in part through the measured results obtained by large-scale testing. This includes validation of the reduction in both water content and void ratio profiles stated to take place during the first stage. This leftward shifting indicates that the water loss due to evaporation is being supplied by the complete material profile. Other aspects of the conceptual model, such as the evaporation efficiency were not directly measured, but due to the oftentimes clear presence of some water atop the material, and the fact that significant crust formation did not occur, it is safe to assume that the evaporation which took place was able to occur close to its full (open-water) potential.

In addition, minimal amounts of settlement were observed within two of the containers, in the order of a few centimeters. This settlement, as stated in the conceptual model, is attributed directly to the water loss taking place during the first stage of drying. Furthermore, no significant increases in the surface shear strength were observed; however, what small development did occur can be attributed to the water loss, and slight strengthening of the soil due to the reduction in void ratio, and resultant increase in density.

7.2 Modelling of Desiccation & Crust Formation

During the modelling process of both the large-scale test containers as well as the Marker Wadden, certain parameters and relations were identified as critical to the "optimal" modelling of the material and atmospheric conditions. The main driving equations behind the modelling of desiccation and crust formation include the shrinkage characteristic curve, soil water characteristic curve, and the permeability relation utilized. Of these three, two were identified to be considerably critical to the model and its output. The first critical aspect of the modelling was the SWRC, including how it is determined. The second critical modelling input was the permeability relation and estimated parameters, of which two relations were assessed. Careful determination and/or estimation should be made not only when determining which relation to use, but which function values to set. Small changes in these values results in order of magnitude variations in estimated hydraulic conductivity values for certain void ratios. In terms of pure modelling, slight variations of these parameters also resulted in varying degrees of numerical oscillations within the model and its results, which is another important aspect to consider when assessing the results.

Additionally, the model limitations and its inherent differences in comparison to the actual soil profile pose challenges in properly assessing the validity of results. This was especially seen when attempting to re-create the conditions and measured results from the containers using the model. Previously identified variations in the vertical profile made directly comparing it to a model which assumes a single homogenous layer near to impossible. However, some of these difficulties can be attributed to incorrect initial values and Hyprop sampling. Because of this, it is assumed the model is still valid for the predicting the behavior, desiccation, and crust formation within the Marker Wadden.

7.2.1 Material Parameter Determination

The SWRC has inherent variations based on the type of method/estimation used to determine it, as seen in the general variation exhibited by the Hyprop SWRC results. While it is believed that a SWRC generated through a Hyprop can be more accurate than that produced by an oedometer, there is still variability present in these tests, especially as the Hyprop is designed as an element test and has inherent difficulties in measuring higher water contents with low suction. However, an additional benefit of the Hyprop is that, if modified slightly, it can also approximate the soil's unsaturated hydraulic conductivity.

In terms of the permeability relation, it was found that the log-linear relation proposed by Kim, Diels, and Feyen (1992) best represented the material within the Marker Wadden, based on the clay mineral present and experimental data found in literature. Careful consideration should be made when assessing which relation to use in which situation, as the power-log relation estimates extremely low permeabilities when the void ratio range is low in comparison to the log-linear relation. One would infer from this that the SIC relation is best used of the initial phases while the material is well above its liquid limit, while the log-linear relation would be best utilized when assessing the desiccation process, where lower void ratios are expect to be encountered. In addition, the power-log relation commonly used in DELCON

modelling may in some cases be a better representation of the behavior of the soil, especially while it is in fluid state.

7.3 Effect of Atmospheric & Surface Water Conditions

On a practical level, this research emphasizes the importance of atmospheric conditions on the desiccation and crust formation process. This includes not only the impact of "uncontrollable" atmospheric conditions, such as seasonal variations, but also the influence of active surface water measures on the acceleration or hindering of the desiccation process. Atmospheric conditions play a significant role in the desiccation and crust formation process, as this process is driven by evaporation, which is in turn determined by the atmospheric and climate conditions. Although this study was limited in its capacity, it clearly showed that while these variations can heavily influence the short-term effects of desiccation, stabilization will occur in the long-term.

The effects of variations in atmospheric conditions was assessed even further when modelling variations in Marker Wadden conditions and properties. This included an assessment of the short and long-term effects of initial seasonal variations in which initial surface water was removed, assuming that any excess precipitation would runoff automatically. Findings from this assessment include significant short-term variations during the first two years after initial exposure, but generally equalized results by the fourth and fifth years. Additional observations include the delay in significant shear strength development within any of the variations until the third or fourth year, with maximum shear strength ranging between 50 and 35 kPa, dependent upon the initial season. These shear strength values should be considered carefully however, due to the use of continuous 30-day evaporation or precipitation atmospheric condition. These considerable —and typically unrealistic— long uninterrupted periods allows for significant strengthening or weakening of the soil. In reality, fluctuations between evaporation and precipitation will occur at much smaller intervals, hindering the soil from exhibiting such extreme strengthening and weakening cycles.

In addition to the uncontrollable atmospheric condition variations, the effect of various surface water measures of the Marker Wadden was investigated. The first simulation modelled the desiccation process assuming complete and constant surface water removal, or in atmospherically modified terms, evaporation only. This results in the quick formation of the crust layer early on, in as early as three months. The next simulation modelled was the use of initial surface water removal (i.e. only evaporation in the first year). This resulted in accelerated settlements early on in the desiccation process as the crust layer forms quickly and acts as a surcharge load on the lower material. Finally, the last surface water simulated represented the possibility of purposeful, temporary, re-submergence of the material surface, performed in the spring season in order to prevent unwanted vegetation from taking root and growing. Results of this simulation —which was atmospherically represented by having precipitation only during the first year's four months in the spring— show a delay in crust formation and settlement. However, it should again be noted that all three of the simulations once again exhibited stabilization in terms of settlement and crust formation by the fourth and fifth years.

In the case of the containers, although hard to completely validate, the variations in the net precipitation conditions resulted in identifiable trend extent variations in each of the profiles —or in the case of C3, a lack thereof. Modelled results show that the assisted measures in C1 and C2 (while similar in extent) aided the desiccation process in comparison to the lesser desiccated material under general atmospheric conditions and C3 in which minimal desiccation took place due to the significant surface water build up during the project timeline.

7.4 Implications for the Marker Wadden

Based on the results of the various model simulations and the requirements set forth for the Marker Wadden, it is proposed that the optimal seasons to start the desiccation process is summer or fall, when there is less precipitation and more evaporation. While all of the model results show similar profiles by the end of the fourth and fifth years, summer and autumn as initial seasons show the most consistent development of the crust and shear strength over time.

Additionally, careful monitoring of the material surface and excess surface water should be put in place. If there is a consistent layer of surface water atop the material, the desiccation process and crust development will be significantly hindered. This leads into the idea of establishing either active or passive means of surface drainage in the form of pumps or trenches, to ensure there is no water buildup.

An additional advantage of active surface water removal in the first year is that the settlement will occur at a faster rate. This may be helpful in that if an additional layer is needed, it will be known sooner rather than later and can be added in time to also be allowed to desiccate and develop strength within the required time.

Total settlements are not expected to exceed half a meter; however, if this occurs (or is at risk of occurring), the best measure to take would be to re-submerge the surface as soon as possible, and add an additional fill layer to meet the elevation requirements. However, this additional fill load being placed after desiccation of the lower layer(s) has already begun to take place will influence the profile exhibited by the material.

The modelling has shown that the development of the shear strength will be slow in the initial first year, however it should at times meet the required design shear strength of 3 kPa, before developing higher shear strengths in the subsequent years. So, extended lower initial readings of the shear strength does not automatically mean that the strength will not develop later.

It is important to note the although the model can help predict the behavior of a soil, it is still beneficial to monitor the development of the crust layer and progression of desiccation through in-situ testing. This is due to the inherent inhomogeneity and spatial variability out in the field.

A possible estimation tool for assessing the shear strength of the soil includes a determination of the target water content required in order to achieve the desired strength, which can be done through either oedometer NCL or the Hyprop ICL. In-situ shear strengths as determined by field vanes can then also back-calculate the estimated water content, and can be corroborated with lab testing to make sure the assumed material relations match the in-field conditions.

Furthermore, just as with the containers and the variations present at the edges of the container vs in the middle, this may also occur at full-scale, with the middle of the site exhibiting different conditions than that of the edges. Other factors which may influence these estimations and advisements include the presence of vegetation, significant weather events, any type of surface water measure in place, and the effects of the surrounding ground water table on limiting the desiccation process.

7.5 Recommendations

As with any project of this scope and magnitude, there are aspects which in hindsight could have been done differently or more efficiently, as well as additional expansion questions which are brought about as a result of the project's limitations. Some of these aspects have been covered below, in the hopes that any further research will take the challenges and issues faced in this project and learn from it when planning new research projects. Furthermore, additional research aspects which could be used to form the basis of new projects are proposed.

7.5.1 Test Methods & Modelling

There are many testing methods utilized in this research which can be improved upon or further modified. Just as in the main section of this research, this has been separated into three distinct aspects, the large-scale testing, Hyprop testing, and modelling.

7.5.1.1 Large-Scale Test Setup

First, keeping the large-scale containers indoors in a climate controlled room would have been more ideal. This would allow for more direct control over the various atmospheric conditions experienced within each of the containers. However, as the containers had already been placed outside and the material left to consolidate prior to this research, this was not possible. Additional changes to this setup include the following:

1. Improved surface water removal techniques & representations

This suggestion is due in part to the fact that the utilized pump and vacuum methods were not 100% effective, with some surface water remaining atop the material within the containers. Furthermore, better representative water removal measures, such as trenches or a sloped surface for better runoff conditions, could be implemented in future setups.

2. Detailed surface settlement monitoring

The only manual setup used to monitor settlements was a measurement stick attached to the inner sidewall of each container, which had been setup during van Olphen's thesis. However, surface changes within the containers were expected to deviate from one another based on the distance from the walls. Because of this, a more extensive setup was designed in order to pick up the surface changes throughout the complete container, as well as be able to track changes within the order of millimeters. However, this setup was incidentally abandoned due to difficulties in obtaining valid data in the containers, and more thought should be given to future monitoring of the settlements which take place.

3. Consistent in-situ depth location measurement markers

As remarked upon earlier, one high source or error was due to the inconsistencies in noting accurate reference depth locations during the in-situ testing of density and shear strength. Some of this was due in part to limitations and restrictions on equipment setup and space requirements, but also due to the fact that depths were referenced based on the surface of the material, which is a changing reference point. A more consistent depth measuring system from multiple reference points should be considered in the future.

4. Detailed surface monitoring

Crust formation plays a critical role in the desiccation process. As such, this crust formation should be more closely monitored and observed. This can include more detailed pore pressure readings within the surface material, additional monitoring of crack formation, as well as careful observation setup to monitor the swelling effects during re-wetting events. Additionally, a setup which allows for a visual assessment of the crust thickening process (i.e. a "window") would be quite beneficial in further studies of the desiccation and crust formation process.

5. Soil evaporation measurement system

It is noted that open-water evaporation is not the same thing as soil evaporation. This is due to the fact that the surface of the material itself and its resistance to evaporation should be taken into consideration. One method used in agricultural settings is to implement a system which allows for direct weight check of the soil. Typically, this is done by filling a porous bucket with material and placing it within the main soil so that the surfaces are flush. This bucket can then be lifted and weighed periodically in order to get a more accurate estimation of the water loss which occurred.

7.5.1.2 Hyprop Test Setup

Additional tests utilizing the Hyprop should be modified to include both tensiometers, in order to be able to determine the unsaturated hydraulic conductivity and compare it to that determined through the model equations without potentially damaging the tensiometer, as would have occurred in the current setup. Other modifications to this setup could also include a volume change monitoring system. With this, the SCC could then also be estimated for the material.

Other potential improvements include more careful sampling and preparation methods, as many corrections had to be applied to the recorded data points in order to obtain viable SWRC data points to fit the van Genuchten equation.

7.5.1.3 Modelling Modifications

Models such as these are essentially always a work in progress and can always be improved upon. Stated limitations of the model include that fact that as the model is currently one-dimensional, no assessment of lateral deformations (and therefore cracking) can be taken into account (Vardon et al., 2015). This also includes other aspects which could play a role in the crust formation and desiccation process such as chemical and biological effects. Furthermore, the model assumes that all water which does not infiltrate into the soil becomes runoff, which was not the case in the large-scale containers, and may not be realistic in terms of the Marker Wadden in situations where significant re-submergence is required. These conditions could only be implemented by modifying and forcing the atmospheric conditions.

The main limitations of the model which were repeatedly encountered during this research was constraints of initial conditions. For instance, in terms of the large-scale modelling, a pre-run had to be implemented due to the fact that the model assumes a single initial water content value along the complete depth of the layer and begins to run on the basis that settlement and initial self-weight

consolidation must still occur. In addition, the initial conditions are restrained to the assumption that all layers deposited will be homogeneous not only in terms of depth, but also in respect to one another. This is not a realistic assumption in terms of the Marker Wadden, where due to filling process variability in terms of density is present.

7.5.2 Further Research

There were many limitations due to the scope of this research. Because of this some of the following research is proposed to address the gaps within this research, as well as new questions which arise from the conclusion of this research:

- Variation of initial densities and its impact on the desiccation and crust process in terms of settlement, strength, and time. Is there an "optimal density" which can be used in order to achieve a strong enough crust in a shorter amount of time?
- The impact of significant weather events as well as external influences (i.e. strong storm events, removal of top layer while desiccation is ongoing, addition of new layer atop desiccated material)
- The effects of natural crackage (manmade vertical drains) on the desiccation process and how it changes predicted settlements, desiccation, and strength.
- The influence of additives such as bamboo fibers or bentonite on shear strength development and final conditions
- Effects of vegetation on the desiccation process
- A detailed study of the effects of obtaining SWRCs with material in different stages of the overall settlement, consolidation, and desiccation processes.

8 References

Boskalis, 2015. EMVI 2 - landschappelijke kwaliteit vogelparadijs.

Budhu, M., 2011. Soil mechanics and foundations. Wiley.

Cargill, K.W., 1985. Mathematical model of the consolidation/desiccation processes in dredged material (Technical Report No. 0-85–4). U.S. Army Engineer Waterways Experiment Station, Vicksburg, Mississippi (USA).

Chin A Moei, S.A., 2016. Effects of organic matter on shrinkage and water retention behaviour of organic dredged sediment (MSc). Delft University of Technology.

de Lucas Pardo, M.A., 2014. Effect of biota on fine sediment transport processes. A study of Lake Markermeer (Ph.D.). Delft University of Technology.

Elsharief, A.M., Abdelaziz, O.A., Dafallaa, M.A., 2015. The influence of matric suction on the shear strength of highly plastic compacted swelling clays. The Electronic Journal of Geotechnical Engineering 20, 12555–12568.

European Commission, 2016. The natura 2000 biogeographical regions [WWW Document]. European Commission- Environment. URL http://ec.europa.eu/environment/nature/natura2000/biogeog_regions/ (accessed 8.20.16).

European Environment Agency, 2011. Natura 2000 - standard data form: Markermeer & Ijmeer (NL9803029) [WWW Document]. Natura 2000. URL http://natura2000.eea.europa.eu/Natura2000/SDF.aspx?site=NL9803029#3 (accessed 8.20.16).

Fredlund, D.G., 2006. Unsaturated soil mechanics in engineering practice. Journal of geotechnical and geoenvironmental engineering 132, 286–321.

Fredlund, D.G., 1967. Comparison of soil suction and one-dimensional consolidation characteristics of a highly plastic clay (Technical Report No. 245). Divsion of Building Research, National Research Council, Ottawa, Ontario (Canada).

Fredlund, D.G., Rahardjo, H., 1993. Soil mechanics for unsaturated soils. Wiley, New York.

Fredlund, M.D., Wilson, G.W., Fredlund, D.G., 2002. Representation and estimation of the shrinkage curve. Presented at the Third International Conference on Unsaturated Soils, Swets & Zeitlinger, Recife, Brazil.

Haliburton, T.A., 1978. Guidelines for dewatering/densifying confined dredged material (Technical Report No. DS-78-11). U.S. Army Engineer Waterways Experiment Station, Vicksburg, Mississippi (USA).

Hendriks, H.C.M., 2016. The effect of pH and the solids composition on the settling and self-weight consolidation of mud (MSc). Delft University of Technology.

KNMI, 2017a. Daggegevens van het weer in Nederland [WWW Document]. KNMI - Koninklijk Nederlands Meteorologisch Instituut. URL https://www.knmi.nl/nederland-nu/klimatologie/daggegevens (accessed 2.20.17).

KNMI, 2017b. Klimaatatlas: Klimaattabel, LH15 [WWW Document]. KNMI - Koninklijk Nederlands Meteorologisch Instituut. URL http://www.klimaatatlas.nl/klimaatatlas.php?wel=stationsdata&ws=tabel&wom=Klimaattabel,%20LH15 (accessed 2.20.17).

Luxemburg, W.M.J., Coenders, A.M.J., 2015. Lecture notes CIE4440: hydrological processes and measurements.

Merckelbach, L.M., Kranenburg, C., 2004. Determining effective stress and permeability equations for soft mud from simple laboratory experiments. Geotechnique 54, 581–591.

Murthy, V.N.S., 2003. Geotechnical engineering: principles and practices of soil mechanics and foundation engineering. Marcel Dekker, New York, NY (USA).

Natuurmonumenten, 2014. Unique project: nature islands in the markermeer - Marker Wadden [WWW Document]. Natuurmonumenten. URL https://www.natuurmonumenten.nl/marker-wadden/english/present-situation (accessed 8.20.16).

Roels, A., 2015. Consolidatie Marker Wadden - Finaal (MEMO No. 13084–03–M08–AROE–0b). Boskalis Hydronamic.

Roels, A., Jacobs, W., 2015. Numerieke simulatie van eigengewicht consolidatie Marker Wadden (MEMO No. 130844-01-M02- AROE-2). Boskalis Hydronamic.

Seki, K., 2007. SWRC fit- a nonlinear fitting program with a water retention curve for soils having unimodal and bimodal pore structure. Hydrology and Earth System Sciences Discussions 4, 407–437.

Stark, T.D., Choi, H., Schroeder, P.R., 2005a. Settlement of dredged and contaminated material placement areas. I: Theory and use of primary consolidation, secondary compression, and desiccation of dredged fill. Journal of waterway, port, coastal, and ocean engineering 131, 43–51.

Stark, T.D., Choi, H., Schroeder, P.R., 2005b. Settlement of dredged and contaminated material placement areas. II: Primary consolidation, secondary compression, and desiccation of dredged fill input parameters. Journal of Waterway, port, coastal, and ocean engineering 131, 52–61.

Tuller, M., Or, D., 2003. Retention of water in soil and the soil water characteristic curve.

Turnhout, P., 2016. MEMO: Draagkracht plas-dras, Marker Wadden (MEMO). Boskalis.

U.S. Army Corps of Engineers, 1993. Seepage analysis and control for dams (Engineer Manual No. EM 1110-2-1901).

van Olphen, E.J.C., 2016. Consolidation behaviour of soft cohesive soils, the correlation between different scale model tests: case study of the Marker Wadden (MSc). Delft University of Technology.

Vardon, P.J., van Paassen, L., van Tol, A.F., 2015. Sludge depot modelling for self-weight consolidation and atmospheric drying. Delft University of Technology.

Vardon, P.J., van Tol, A.F., 2014. Sludge ripening model - documentation and user manual (rev 1). (Manual). Delft University of Technology.

Vijverberg, T., Jacobs, W., Lievens, R., Roels, A., 2016. On the beneficial use of soft mud - case study Marker Wadden project.

Winterwerp, J.C., van Kesteren, W.G.M., 2004. Introduction to the physics of cohesive sediment in the marine environment. Elsevier.

Wroth, C.P., Wood, D.M., 1978. The correlation of index properties with some basic engineering properties of soils. Canadian Geotechnical Journal 15, 137–145.

9 Appendices

A Evaporation Calculations

A.1 General Evaporation Calculations

This appendix includes the additional values, formulas, and equations needed to calculate evaporation using the Penman evaporation equation (see [2-1]), which has also been restated below for convenience.

$$E_p \approx E_o = \frac{\frac{sR_n}{\rho\lambda} + \frac{c_p\rho_a}{\rho\lambda}\frac{(e_s - e_a)}{r_a}}{s + \gamma} \qquad [\ 9\text{-}1\ ]$$

In which,

R_n	net radiation on the earth's surface [J d^{-1} m^{-2}]
λ	latent heat of vaporization≈ $2.45*10^6$ [J/kg]
s	slope of saturation vapor pressure-temperature curve [kPa/°C]
c_p	specific heat of air at constant pressure≈ 1004 [J kg^{-1} K^{-1}]
ϱ_a	density of air≈ 1.205 [kg/m^3]
ϱ	density of water≈ 1000 [kg/m^3]
e_a	actual vapor pressure in the air at 2 m height [kPa]
e_s	saturation vapor pressure for the air at 2 m height [kPa]
γ	psychrometer constant≈ 0.066 [kPa/°C]
r_a	aerodynamic resistance [d/m]

e_s is the maximum vapor pressure of water particles at a certain temperature which can be present before condensation occurs and can be determined using the following formula, in which T is the temperature in Celsius:

$$e_s(T) = 0.61\exp\left(\frac{19.9T}{273 + T}\right) \qquad [\ 9\text{-}2\ ]$$

This value, along with the relative humidity (h), can then be used to calculate the actual vapor pressure at the actual current temperature using the following derived relation:

$$e_a = he_s(T) \qquad [\ 9\text{-}3\ ]$$

The slope of the saturation vapor pressure curve, or s, can be determined using the following derived formula:

$$s = \frac{5430e_s}{(273 + T)^2} \qquad [\ 9\text{-}4\ ]$$

Once those values have been calculated, the net solar radiation must be determined. This can be achieved using the following formula:

$$R_n = (1 - r)R_{s,in} - R_{l,in} \qquad [\ 9\text{-}5\ ]$$

In which r is the surface albedo which has a typical range between 0.10 - 0.30 for bare soil surfaces, and $R_{s,in}$ and $R_{l,in}$ is the incoming short and long wave radiation, respectively.

$R_{s,in}$ within the Netherlands can be computed using the following empirical relation, in which n/N is the ratio of actual and possible sunlight hours and R_a is the short wave radiation energy:

$$R_{s,in} = \left(0.20 - 0.48\tfrac{n}{N}\right)R_a \qquad [\ 9\text{-}6\ ]$$

R_a can be determined using Table 9-1, which gives the R_a/λ values depending on global location.

	Lat	Jan	Feb	Mar	Apr	May	Jun	Jul	Aug	Sept	Oct	Nov	Dec
	NORTHERN HEMISPHERE												
Equator	60	1.4	3.6	7.0	11.1	14.6	16.4	15.6	12.6	8.5	4.7	2.0	0.9
	52	3.2	5.5	8.8	12.5	15.4	16.6	16.0	13.6	10.2	6.7	3.9	2.6
	50	3.7	6.0	9.2	12.7	15.5	16.6	16.1	13.7	10.4	7.1	4.4	3.1
	40	6.2	8.4	11.1	13.8	15.9	16.7	16.3	14.7	12.1	9.3	6.8	5.6
	30	8.1	10.5	12.8	14.7	16.1	16.5	16.2	15.2	13.5	11.2	9.1	7.9
	20	10.8	12.4	14.0	15.2	15.7	15.8	15.8	15.4	14.4	12.9	11.3	10.4
	10	12.8	13.9	14.8	15.2	15.0	14.8	14.9	15.0	14.8	14.2	13.1	12.5
	0	14.6	15.0	15.2	14.7	13.9	13.4	13.6	14.3	14.9	15.0	14.6	14.3
	10	15.9	15.7	15.1	13.9	12.5	11.7	12.0	13.1	14.4	15.4	15.7	15.8
	20	16.8	16.0	14.5	12.5	10.7	9.7	10.1	11.6	13.6	15.3	16.4	16.9
	30	17.2	15.8	13.5	10.9	8.6	7.5	7.9	9.7	12.3	14.8	16.7	17.5
	40	17.3	15.1	12.2	8.9	6.4	5.2	5.6	7.6	10.7	13.8	16.5	17.8
	50	16.9	14.1	10.4	6.7	4.1	2.9	3.4	5.4	8.7	12.5	16.0	17.6
	60	16.5	12.6	8.3	4.3	1.8	0.9	1.3	3.1	6.5	10.8	15.1	17.5
	SOUTHERN HEMISPHERE												

Table 9-1: Short wave radiation in terms of R_a/λ (kg m $^{-2}$ d^{-1}) (Luxemburg and Coenders 2015)

$R_{l,in}$ can be computed using the following empirical formula, in which σ is the Stefan-Boltzmann constant ($4.9\text{x}10^3$ J d^{-1} m^{-2} K^{-4}), T is the air temperature in Celsius:

$$R_{l,in} = \sigma(273+T)^4(0.47 - 0.21\sqrt{e_a})(0.2 + 0.8\frac{n}{N}) \quad [\ 9\text{-}7\ ]$$

Finally, the aerodynamic resistance can be calculated using the wind speed in m/s, u, recorded from 2 meters above the surface and using the following equation (Luxemburg and Coenders, 2015):

$$r_a = \frac{245}{86400(0.5u + 0.5)} \quad [\ 9\text{-}8\ ]$$

Furthermore, reduced windspeeds were utilized as a majority of the wind is blocked due to the container walls. This means a significant reduction between the wind speeds recorded at the elevated point above the container and the actual windspeed which passes across the surface of the material.

A.2 Modifications for Container Variations

Modification of the calculated evaporation and net precipitation took place for all of the containers, based on the type of conditions present in each of them. For all of the containers, the windspeed used in the calculations for the evaporation were reduced significantly due to the container walls serving as a wind barrier. Table 9-2 shows how the modification were generated based on the physical changes performed within each of the containers.

Container	Physical Condition/Modification	Representative Precipitation/Evaporation Modification
C1, C2, C3	Initial water removal	Precip. = 0 Evap. = regular
C1, C2	Water removal (instances)	Precip. = 0 (3 previous days) Evap. = regular
C1	Container cover (tarp)	Precip. = 0 Evap. = regular (unless ventilated)
C1	Ventilator (air blower)	Precip. = regular (unless covered) Evap. = windspeed is taken to be ventilator airflow/container cross section

Table 9-2: Modifications for large-scale net precipitation

B Container Testing

This Appendix includes additional information and data regarding the large-scale testing.

B.1 Detailed Large-Scale Testing Log

Table 9-3 and Table 9-4 include a more detailed record of the large-scale test conditions and the modifications implemented during the stated dates.

Date	Day	Rain	Cover	Vent	Acitivty	Remarks
Monday, September 12, 2016	-4				T1* Beeker Core	had to take 2 samples in C2 because first one didn't reach the bottom
Tuesday, September 13, 2016	-3				Echosounder	3 points in a longitudinal cross section within each container, including the 4th
Friday, September 16, 2016	0				Initial Pumping I	started pumping inside subcompartments for C3 and C1 (with some issues of water flowing from main in to subcompartments)
Monday, September 19, 2016	3				Initial Pumping II & Deltares Tutorial	installed pumps in main compartments of all to completel "initial" water removal; first calibration of densimeter using material from container 4
Tuesday, September 20, 2016	4				T1 Deltares Testing	removal of C3 floater; dropped clamp in C3 (retrieved)
Wednesday, September 21, 2016	5					
Thursday, September 22, 2016	6					
Friday, September 23, 2016	7					
Monday, September 26, 2016	10				T2 Deltares Testing	vaccuumed leftover excess water from all 3 containers; good testing
Tuesday, September 27, 2016	11					
Wednesday, September 28, 2016	12					
Thursday, September 29, 2016	13					
Friday, September 30, 2016	14					
Monday, October 03, 2016	17				evaporation pan installed	from the start to record (started level); webcam images fixed (except not really), backup of images on server from this date
Tuesday, October 04, 2016	18					
Wednesday, October 05, 2016	19				T2* Beeker core	dropped probe shielding in C3 (NOT retrieved); also gather 1 additional sample from C2 (not used)
Thursday, October 06, 2016	20				tried to install in-situ evap	not achieved, disturbed area in C3
Friday, October 07, 2016	21				Leica scan	issue with scan to get complete image (slowed the pt/s rate and seemed to help)
Monday, October 10, 2016	24					
Tuesday, October 11, 2016	25				blower installed in C1	not programmed for autorun
Wednesday, October 12, 2016	26				T3 Deltares Testing	dropped a screw in C3 (retrieved); only 1 V and 1 D was performed in C1 due to time; dropped connector of V into C1 (fixed)
Thursday, October 13, 2016	27					
Friday, October 14, 2016	28					rain
Monday, October 17, 2016	31				vaccuum C2 and C1	
Tuesday, October 18, 2016	32	x	x		installation of tarp cover	significant storm at night
Wednesday, October 19, 2016	33	x	x		tarp	removal of some of the water buildup (no noticeable touching of tarp to mud surface); resecuring of tarp
Thursday, October 20, 2016	34	x	x	x		ventilator turned on (and kept on overnight)
Friday, October 21, 2016	35		x*	x	removal of tarp	removed tarp by 16; vaccumed C2 and a little bit in C1; ventilator turned off around 16
Monday, October 24, 2016	38			x	ventilator on	left on overnight (not sure if scheduled operation yet)
Tuesday, October 25, 2016	39			x	MW visit	beeker core samples taken (see map printout for locations
Wednesday, October 26, 2016	40	x		x		
Thursday, October 27, 2016	41			x		
Friday, October 28, 2016	42			x		
Monday, October 31, 2016	45			x		ventilator outlet was found above container (rather than above soil)…unsure how long it was placed this way…check pictures
Tuesday, November 01, 2016	46	x	x*	x*	T4 Deltares Testing	beeker samples for calibration and chem analysis; vent turned off from 07.00-16.00, cover put on at 16.30

Table 9-3: Detailed large-scale test logbook (I)

Date	Day	Rain	Cover	Vent	Acitivty	Remarks
Wednesday, November 02, 2016	**47**		x	x		
Thursday, November 03, 2016	**48**		x	x		
Friday, November 04, 2016	**49**		x	x		
Monday, November 07, 2016	**52**		x	x		
Tuesday, November 08, 2016	**53**		x	x		
Wednesday, November 09, 2016	**54**		x	x		
Thursday, November 10, 2016	**55**		x	x	water sucking	removed water from top of C1 tarp, and in C2
Friday, November 11, 2016	**56**		x*	x	Leica scan	water built up in C2 due to previous night's rain;however water sucker was unavailable. C2 and C3 both have water in them for scan; main cover removed briefly at 14 for scan
Monday, November 14, 2016	**59**		x	x		
Tuesday, November 15, 2016	**60**		x	x		
Wednesday, November 16, 2016	**61**		x	x		
Thursday, November 17, 2016	**62**		x	x		
Friday, November 18, 2016	**63**	x	x	x		significant wind and rain event over the weekend
Monday, November 21, 2016	**66**	x	x*	x*		Thomas remarked that a cable broke, and water was released into the container, had also stated that he turned off the vent (but unknown for how long)
Tuesday, November 22, 2016	**67**		x			
Wednesday, November 23, 2016	**68**		x	x		
Thursday, November 24, 2016	**69**		x	x		
Friday, November 25, 2016	**70**		x	x		
Monday, November 28, 2016	**73**		x*	x	water sucking, cover	Roeland sucked water out and removed tarp
Tuesday, November 29, 2016	**74**					
Wednesday, November 30, 2016	**75**					containers frozen
Thursday, December 01, 2016	**76**					
Friday, December 02, 2016	**77**					
Monday, December 05, 2016	**80**					
Tuesday, December 06, 2016	**81**					
Wednesday, December 07, 2016	**82**					
Thursday, December 08, 2016	**83**		x	x		
Friday, December 09, 2016	**84**		x	x		
Monday, December 12, 2016	**87**		x	x		
Tuesday, December 13, 2016	**88**		x	x		
Wednesday, December 14, 2016	**89**		x	x		
Thursday, December 15, 2016	**90**		x	x		
Friday, December 16, 2016	**91**		x	x		
Monday, December 19, 2016	**94**		x	x		
Tuesday, December 20, 2016	**95**		x	x		
Wednesday, December 21, 2016	**96**		x	x		
Thursday, December 22, 2016	**97**		x	x		
Friday, December 23, 2016	**98**		x	x		
Monday, December 26, 2016	**101**		x	x		
Tuesday, December 27, 2016	**102**		x	x		
Wednesday, December 28, 2016	**103**		x	x		
Thursday, December 29, 2016	**104**		x	x		
Friday, December 30, 2016	**105**		x	x		
Monday, January 02, 2017	**108**		x	x		

Table 9-4: Detailed large-scale test logbook (II)

B.2 Densimeter Measurement Calibration

	density (kg/l)	voltage
water	**1**	
surface water (1)	1	0.57
surface water (2)	1	0.68
	average	0.63
	deviation	0.06
bucket	**1.2**	
1 cm		3.84
2 cm		3.88
3 cm		4.16
4 cm		3.76
5 cm		4.40
6 cm		4.04
7 cm		3.90
8 cm		4.07
9 cm		4.13
10 cm		3.90
	average	4.01
	deviation	0.19

Table 9-5: Densimeter calibration readings

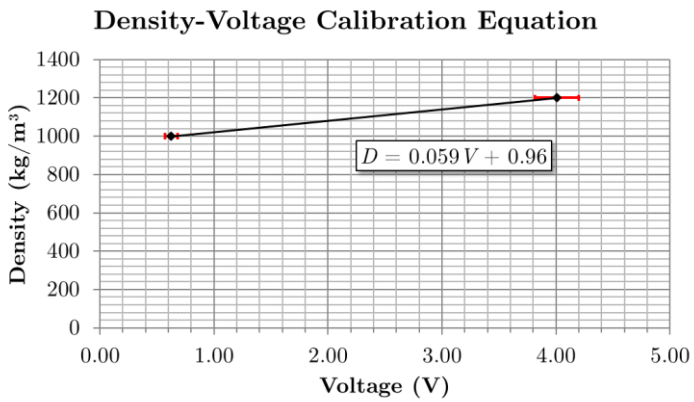

Figure 9-1: Density-voltage calibration equation (densimeter)

Figure 9-1 shows the calibration equation utilized for the densimeter output readings in order to convert them into their respective density values. This calibration equation is based on the values shown in Table 9-5, and consists of a voltage reading of the natural water present in the material, with an assumed known density of 100 kg/m3, in addition to a value taken from a bucket filled with the material with a "known" density. In this case, the bucket filled with the material had varied voltage output readings based on depth, and therefore error bands exist, and it is factored into the equation with the red error bands shown in Figure 9-1. Please note that this equation is only valid for the region with limited sand contents, as increasing sand content necessitates the need for an additional calibration equation. This additional calibration was not performed, and therefore the regions where elevated sand fractions are present do not have correct density values.

B.3 Complete Pore Pressure Readings

Figure 9-2 shows selected pore pressure readings on select testing dates compiled into depth profiles, including the elevated initial profile before initial surface water removal.

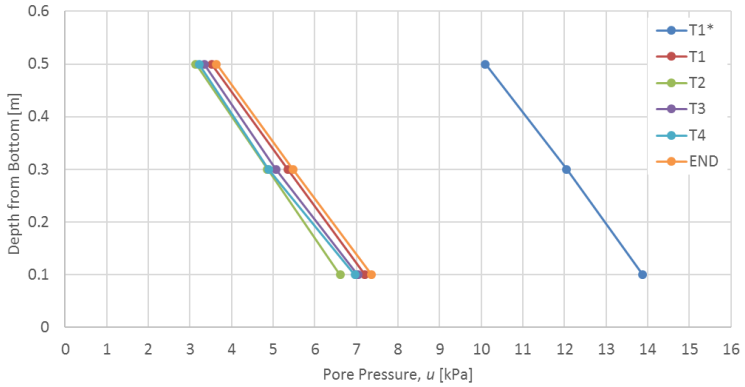

(a) C1

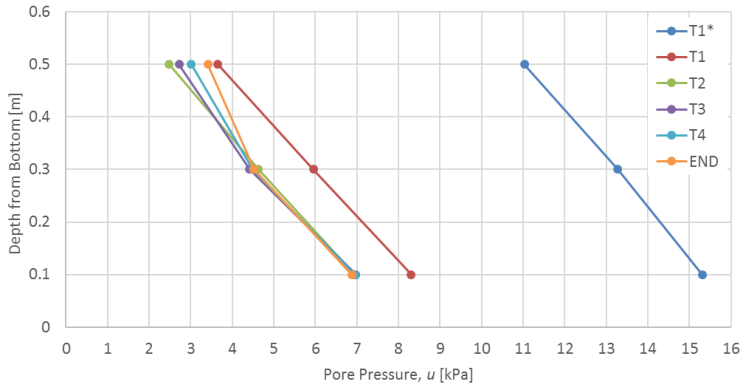

(b) C2

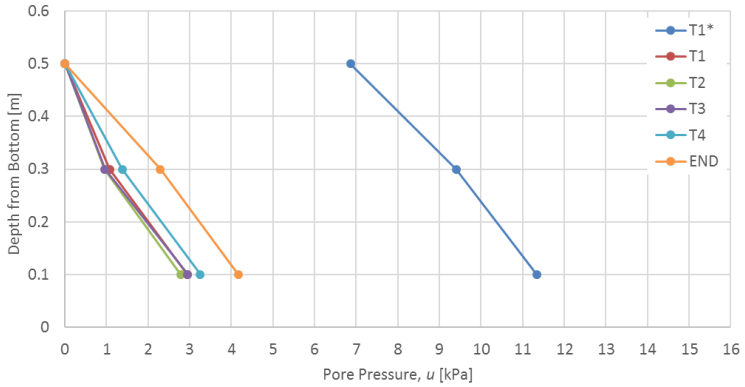

(c) C3

Figure 9-2(a)(b)(c): Recorded pore pressure profiles over time for C1, C2, C3

C SWRC Calculations

This appendix provides more detailed information about the calculation procedure utilized to develop the SWRC curves for each of the Hyprop samples tested.

The Hyprop test automatically collects data including the tensiometer readings, temperature, and gross weight at selected time intervals. For each of the tests, the time interval was set to once per minute for the first hour and then to one every ten minutes. Using this data —in addition to the oven dry data performed on each of the samples after the Hyprop testing had concluded— the gravimetric water contents could be determined. These gravimetric values were then converted into volumetric water contents for ease using the specific gravity values calculated previously. A sample of these values and calculations can be seen in Table 9-6.

Many of the initial tensiometer readings were negative and therefore not viable data in terms of plotting it logarithmically. Because of this, initial corrections were implemented based on the assumption that these negative values were due to hydrostatic pressures based on the location of the tensiometer tip within the sample profile. However, this did not negate all of the erroneous values, and the next step involved a minimal cut of this data out of the final data points used in SWRC generation. Additional data cuts included those data points which occurs after the initial drop in tension readings, which aligned tentatively to air entry.

Finally, these data points were inputted into a fitting model in order to determine the van Genuchten fitting parameters, which were then used for the modelling. While the numerical outputs of these fitting were included in the main section in Table 5-5, the raw graphical fitting outputs have been provided in Figure 9-3 for each of the Hyprop samples tested.

Constant Values					H1					
					Tension [kPa]	Gross wgt [g]	M_W [g]	Corrected Tension [kPa]	θ [-]	w [-]
positive pore pres		0.499	kPa		-0.38	289.06	223.58	0.12	8.23	3.41
					-0.39	289.04	223.56	0.11	8.23	3.41
	M_S [g]	Max Gross wg	Initial M_W [g]	G_S	-0.39	289	223.52	0.11	8.23	3.41
H1	65.48	289.06	223.58	2.41	-0.39	288.98	223.5	0.11	8.23	3.41
H2	73.88	303.82	229.94	2.41	-0.4	288.95	223.47	0.10	8.22	3.41
H3	72.69	291.78	219.09	2.39	-0.4	288.93	223.45	0.10	8.22	3.41
H4	69.68	304.53	234.85	2.39	-0.41	288.92	223.44	0.09	8.22	3.41
H5	62.41	294.91	232.5	2.39	-0.41	288.9	223.42	0.09	8.22	3.41
H6	80.28	306.35	226.07	2.4	-0.4	288.88	223.4	0.10	8.22	3.41
					-0.41	288.87	223.39	0.09	8.22	3.41
					-0.4	288.85	223.37	0.10	8.22	3.41
					-0.41	288.84	223.36	0.09	8.22	3.41
					-0.41	288.82	223.34	0.09	8.22	3.41
					-0.41	288.8	223.32	0.09	8.22	3.41
					-0.4	288.79	223.31	0.10	8.22	3.41
					-0.41	288.76	223.28	0.09	8.22	3.41
					-0.41	288.75	223.27	0.09	8.22	3.41
					-0.42	288.73	223.25	0.08	8.22	3.41
					-0.42	288.71	223.23	0.08	8.22	3.41
					-0.41	288.7	223.22	0.09	8.22	3.41
					-0.42	288.68	223.2	0.08	8.21	3.41
					-0.42	288.66	223.18	0.08	8.21	3.41
					-0.42	288.64	223.16	0.08	8.21	3.41
					-0.42	288.63	223.15	0.08	8.21	3.41

Table 9-6: Sample of raw and corrected Hyprop data

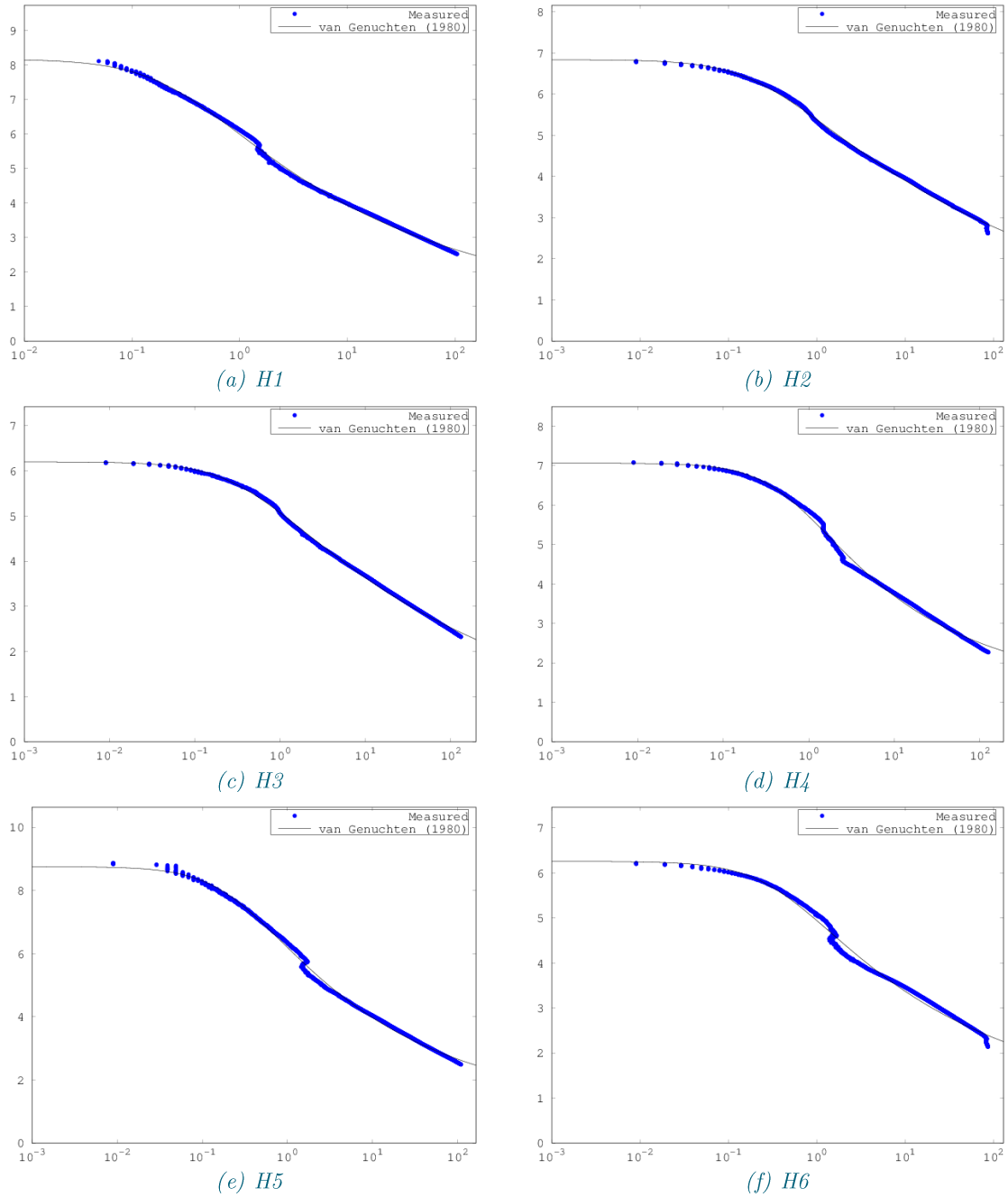

(a) H1 (b) H2

(c) H3 (d) H4

(e) H5 (f) H6

Figure 9-3(a)(b)(c)(d)(e)(f): Fitted SWRC curve to Hyprop data for all samples

D Modelling Data

This appendix includes main data relevant to the modelling, including a sample of the input windows, the large-scale conditions input parameters per model run, and the main Marker Wadden updated input parameters.

D.1 Model Input & Output Sample Views

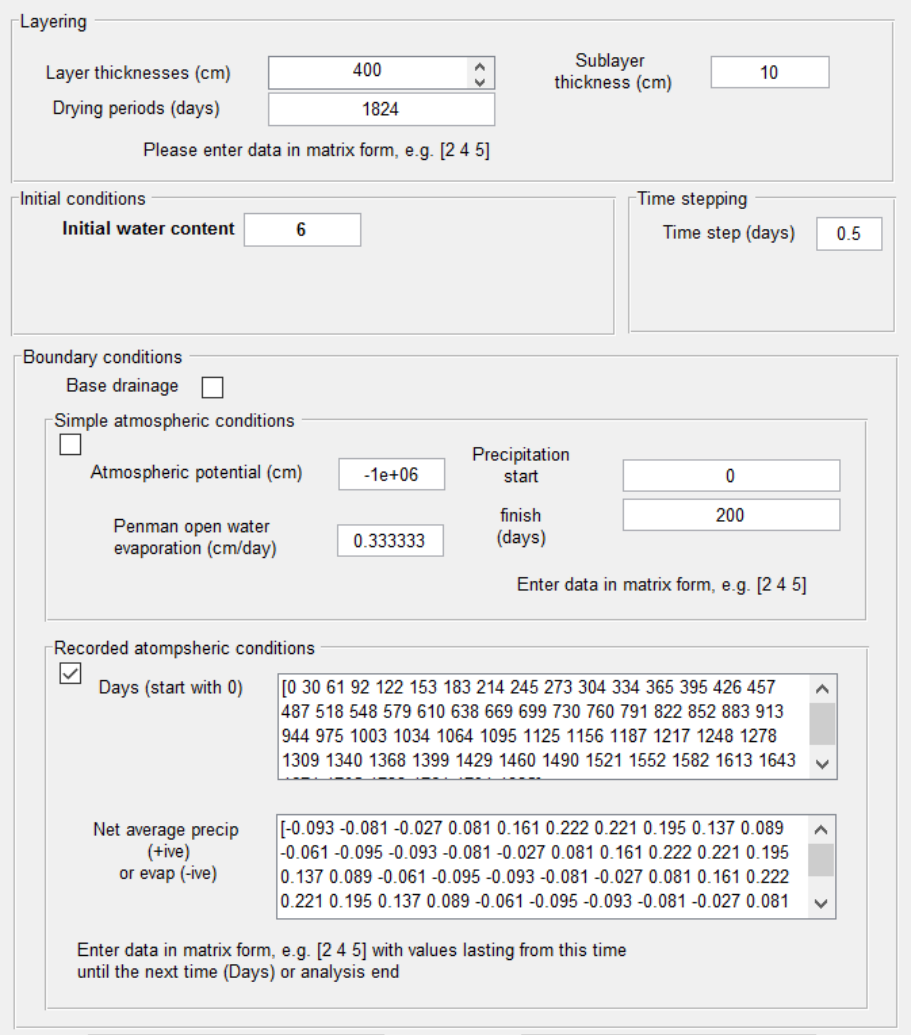

Figure 9-4: Sample of model simulation settings input screen

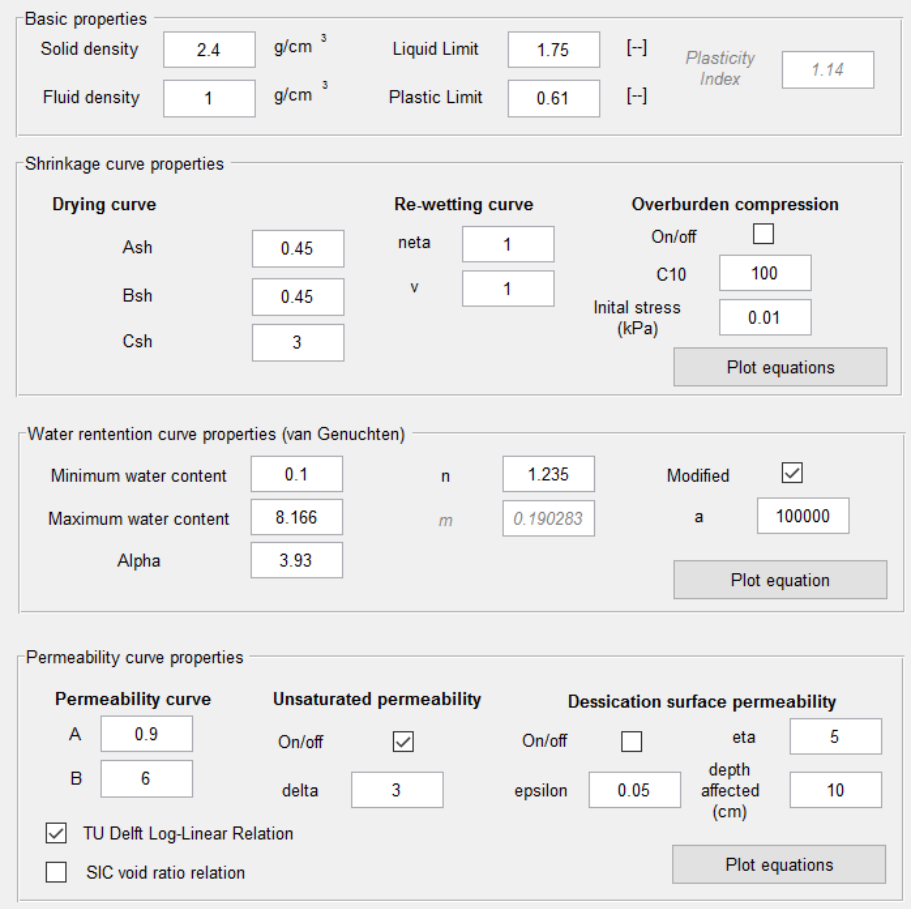

Figure 9-5: Sample of model simulation settings input screen

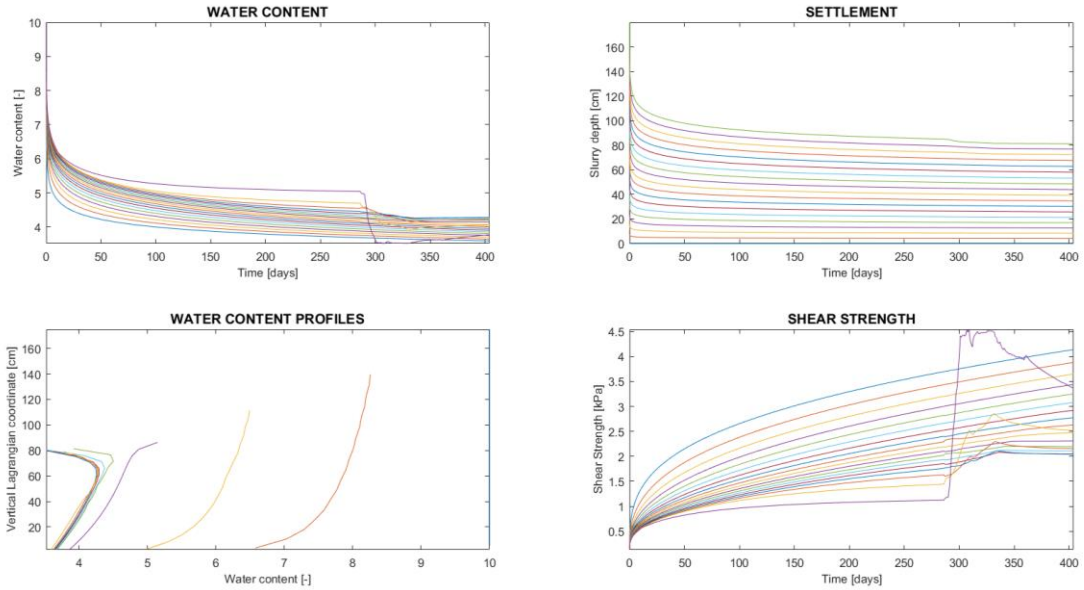

Figure 9-6: Sample of raw model results

D.2 Large-Scale Testing Inputs

Table 9-7 shows the model input settings for each of the main model runs used in the large-scale testing analysis.

Simulation Settings		M1_C1_v1 C1 (with C1_Net)	M2_C2_v1 C2 (with C2_net)	M3_C3_v1 C3 (with C3_net)	M4_C1N_v1 C1 with C_Net	M5_C12_v1 C1 with C2_Net	M6_C13_v1 C1 with C3_Net
Material Type	**[-]**	**C1**	**C2**	**C3**	**C1**	**C1**	**C1**
Chosen Hyprop SWRC	**[-]**	**H3**	**H6**	**H6**	**H3**	**H3**	**H3**
Chosen Timeline	**[-]**	**C_Prerun_290**	**C_Prerun_290**	**C_Prerun_290**	**C_Prerun_290**	**C_Prerun_290**	**C_Prerun_290**
Chosen Weather	**[-]**	**C1_Net**	**C2_Net**	**C3_Net**	**C_Net**	**C2_Net**	**C3_Net**
Chosen Initial Water Content Profile	**[-]**	**C1_initial**	**C2_initial**	**C3_initial**	**C1_initial**	**C1_initial**	**C1_initial**
Chosen K Relation	**[-]**	**TUD_NEW**	**TUD_NEW**	**TUD_NEW**	**TUD_NEW**	**TUD_NEW**	**TUD_NEW**
Layering							
Layer Thickness	[cm]	[180]	[180]	[100]	[180]	[180]	[180]
Drying Periods	[days]	[404]	[404]	[404]	[404]	[404]	[404]
Sublayer Thickness	[cm]	10	10	10	10	10	10
Measured Height at T_0	[cm]	83	82	46	83	83	83
Initial Conditions							
Initial Water Content (Single Value)	**[--]**	**10**	**10**	**10**	**10**	**10**	**10**
Find Initial Water Content Profile	Y/N	Y	Y	Y	Y	Y	Y
Initial Water Content/Profile	--	[11.77 7.21 5.79 5	[9.44 7.88 4.91 5.!	[8.21 2.7 4.63 3.4!	[11.77 7.21 5.79 5	[11.77 7.21 5.79 5	[11.77 7.21 5.79 5
Water Content Profile Section Thickness	[cm]	10	10	10	10	10	10
Time Stepping							
Time Stepping	days	1	1	1	1	1	1
Boundary Conditions							
Base Drainage	Y/N	N	N	N	N	N	N
Simple Atmospheric Conditions	**Y/N**	N	N	N	N	N	N
Atmospheric Potential	**cm**	--	--	--	--	--	--
Atmospheric pressure	Pa	--	--	--	--	--	--
Penman Open Water Evaporation	cm/day	--	--	--	--	--	--
Precipitation Start	{days}	--	--	--	--	--	--
Precipitation End	{day}	--	--	--	--	--	--
Recorded Boundary Conditions	**Y/N**	Y	Y	Y	Y	Y	Y
Days (start with 0)	[day]	[0 290 291 292 29	[0 290 291 292 29	[0 290 291 292 29	[0 290 291 292 29	[0 290 291 292 29	[0 290 291 292 29
Net Average precip (+ive) or evap (-ive)	[cm/day]	[0 -0.221 -0.261 -(	[0 -0.221 -0.261 -(	[0 -0.221 -0.261 -(	[0 -0.221 -0.261 -(	[0 -0.221 -0.261 -(	[0 -0.221 -0.261 -(
Material Properties							
Basic Properties							
Solid Density	g/cm3	2.39	2.40	2.40	2.39	2.39	2.39
Fluid Density	g/cm3	1	1	1	1	1	1
Liquid Limit	[--]	1.96	1.55	1.67	1.96	1.96	1.96
Plastic Limit	[--]	0.64	0.62	0.63	0.64	0.64	0.64
Plasticity Index	*[--]*	*1.32*	*0.92*	*1.04*	*1.32*	*1.32*	*1.32*
Shrinkage Curve Properties							
Drying Curve							
Ash (initial minimum void ratio)	--	0.30	0.30	0.30	0.30	0.30	0.30
Bsh	--	0.30	0.30	0.30	0.30	0.30	0.30
Csh	--	3	3	3	3	3	3
Re-Wetting Curve							
neta	--	1	1	1	1	1	1
v	--	1	1	1	1	1	1
Overburden Compression		--	--	--	--	--	--
On/Off	Y/N	N	N	N	N	N	N
C10		--	--	--	--	--	--
Initial Stress	kPa	--	--	--	--	--	--
Water Retention Curve Properties		--	--	--	--	--	--
Minimum Water Content		0.100	0.100	0.100	0.100	0.100	0.100
Maximum Water Content		6.200	6.256	6.256	6.200	6.200	6.200
Alpha		2.83E+00	2.74E+00	2.74E+00	2.83E+00	2.83E+00	2.83E+00
n		1.159	1.230	1.230	1.159	1.159	1.159
m		*0.137*	*0.187*	*0.187*	*0.137*	*0.137*	*0.137*
Modified	Y/N	Y	Y	Y	Y	Y	Y
a		100000	100000	100000	100000	100000	100000
Permeability Curve Properties							
Chosen K Relation		TUD_NEW	TUD_NEW	TUD_NEW	TUD_NEW	TUD_NEW	TUD_NEW
Permeability Curve							
A		0.9	0.9	0.9	0.9	0.9	0.9
B		5	5	5	5	5	5
Unsaturated Permeability							
On/Off	Y/N	Y	Y	Y	Y	Y	Y
delta		3	3	3	3	3	3
Desiccation Surface Permeability							
On/Off	Y/N	N	N	N	N	N	N

Table 9-7: Input settings for large-scale model runs

D.3 Marker Wadden Updated Main Run Input

There were numerous model runs which were performed for the Marker Wadden analysis; however, most of these variations involved the atmospheric conditions or the relation variables which have been provided earlier in the main section of this research. Table 9-8 shows the complete inputs for the main updated model run for the Marker Wadden.

Simulation Settings		Summer_Net
Material Type	**[-]**	**MW_new**
Chosen Hyprop SWRC	**[-]**	**H1**
Chosen Timeline	**[-]**	**NL_Summer_5yr**
Chosen Weather	**[-]**	**NL_Summer**
Chosen Initial Water Content Profile	**[-]**	**none**
Chosen K Relation	**[-]**	**TUD2_OLD**
Layering		
Layer Thickness	[cm]	[400]
Drying Periods	[days]	[1824]
Sublayer Thickness	[cm]	10
Measured Height at T_0	[cm]	--
Initial Conditions		
Initial Water Content (Single Value)	**[--]**	**6**
Find Initial Water Content Profile	Y/N	N
Initial Water Content/Profile	--	--
Water Content Profile Section Thickness	[cm]	--
Time Stepping		
Time Stepping	days	0.5
Boundary Conditions		
Base Drainage	Y/N	N
Simple Atmospheric Conditions	**Y/N**	N
Atmospheric Potential	**cm**	--
Atmospheric pressure	Pa	--
Penman Open Water Evaporation	cm/day	--
Precipitation Start	{days}	--
Precipitation End	{day}	--
Recorded Boundary Conditions	**Y/N**	Y
Days (start with 0)	[day]	[0 30 61 92 122 1
Net Average precip (+ive) or evap (-ive)	[cm/day]	[-0.093 -0.081 -0.(
Material Properties		
Basic Properties		
Solid Density	g/cm3	2.40
Fluid Density	g/cm3	1
Liquid Limit	[--]	1.75
Plastic Limit	[--]	0.61
Plasticity Index	*[--]*	*1.14*
Shrinkage Curve Properties		
Drying Curve		
Ash (initial minimum void ratio)	--	0.45
Bsh	--	0.45
Csh	--	3
Re-Wetting Curve		
neta	--	1
v	--	1
Overburden Compression		--
On/Off	Y/N	N
C10		--
Initial Stress	kPa	--
Water Retention Curve Properties		--
Minimum Water Content		0.100
Maximum Water Content		8.166
Alpha		3.93E+00
n		1.235
m		*0.190*
Modified	Y/N	Y
a		100000
Permeability Curve Properties		
Chosen K Relation		TUD2_OLD
Permeability Curve		
A		0.9
B		6
Unsaturated Permeability		
On/Off	Y/N	Y
delta		3
Desiccation Surface Permeability		
On/Off	Y/N	N

Table 9-8: Input settings for main updated Marker Wadden model run

Page purposefully left blank